NAWI Graz
Natural Sciences

OMV

Master´s Thesis

Title of the Master´s Thesis

“The Evolution of the Paleo-Danube Deltas of the Lower Pannonian in the Vienna Basin”

Submitted by

Arthur Borzi

In partial fulfillment of the requirements for the degree of

Master of Science (MSc)

Graz 2021

Supervisors: Werner E. Piller, Mathias Harzhauser

In cooperation with OMV: Philipp Strauss, Wolfgang Siedl

Abstract

The Vienna Basin is a rhombohedral SSW-NNE oriented Neogene extensional basin that formed along sinistral fault systems during Miocene lateral extrusion of the Eastern Alps. The basin fill consists of shallow marine and terrestrial sediments of early to late Miocene age reaching a thickness of 5500 m in the central part of the basin. The early Pannonian is a crucial time in the development of the Vienna Basin, and is marked by the formation of Lake Pannon. The lake formed at 11.6 Ma when a significant regressive event isolated Lake Pannon from the Paratethys Sea, giving rise to lacustrine environments. At that time the delta of the Paleo-Danube started shedding its sediments into the central Vienna Basin. Based on the age model of Harzhauser et al. (2004), delta deposition commenced around 11.5 Ma and persisted until 11.1 Ma. The subsurface deltaic deposits can be linked with the Hollabrunn-Mistelbach Formation, which represents the coeval fluvial deposits of the Paleo-Danube in the eastern fluvial plains of the North Alpine Foreland Basin. Therefore, the Paleo-Danube represents an extraordinary case in which coeval riverine and deltaic deposits of a Miocene river are continuously captured.

Herein we present an interpretation of depositional architecture and depositional environments of this delta in the Austrian part of the central Vienna Basin based on the integration of 3D seismic surveys and well data. The mapped delta has an area of about 580 km^2, and solely based on the geometry we classify the delta as a mostly river–dominated delta with significant influence of wave–reworking processes. Seven paleogeographic maps were created, showing the interplay between lacustrine environments of Lake Pannon, delta evolution and riverine systems incising in the abandoned deltaplain. Delta evolution commences with the deposition of the Gr. Engersdorf lobe, before the Aderklaa and Matzen region are covered by a south -eastward prograding deltaic structure. Between the Matzen lobe and the Zistersdorf structure, which is the uppermost observable lobe, a major depositional gap occurs. Onlaps between single deltalobes indicate a northward-movement of the main distributary channel. Rough water-depth estimates are carried out with in-seismic measurements of the true vertical depth between the topset deposits of the delta and the base of the bottomset deposits. These data suggest a decrease of lake water depth from about 170 m during the initial phase of delta formation at 11.5 Ma to about 100 m during its terminal phase at 11.1 Ma.

A major lake level rise of Lake Pannon around 11.1 Ma caused a flooding of the margins of the Vienna Basin, resulting in a back stepping of riverine deposits and termination of delta deposition in the investigation area.

Content

1. Introduction

The aim of the study is to investigate the lower Pannon subsurface deltaic structures deposited by the Paleo-Danube at around 11.6 Ma, marking the onset of these structures in the central Vienna Basin, which were already recognized by Suess (1866), but never studied in high resolution and by means of seismic interpretation. The Vienna Basin situated between the Eastern Alps, the Western Carpathians and the Western Pannonian Basin, is one of the best documented extentional basins worldwide. Its research history began around 200 years ago and persisted until recent. Since the 1930ies, the Vienna Basin was systematically drilled and continuously explored for over 60 years, leading to a comprehensive knowledge of basin geometry, facies and tectonic architecture (e.g. Seifert 1993; Brix and Schulz 1993, Wessely 1993, Decker 2005 et al., Strauss et al. 2006, Siedl et al. 2020). During the early Miocene the Alpine - Carpathian thrust front reached the European forelands leading to the formation of the Vienna Basin. Three stages of development are recognized in the evolution of the Vienna Basin (Arzmüller, 1988): The Pre-, Proto- and Neo–Vienna Basin. The Pre-Vienna Basin was formed in the middle Jurassic as a rift basin on top of the crystalline basement of the Bohemian Massif in the area of today`s Vienna Basin until the Alpine – Carpathian units were thrust over the European passive continental margin and the overlying North Alpine Foreland Basin (NAFB) (Wessely 2000), forming the Vienna Basin in the early Miocene as an E-W trending piggyback basin on top of the Alpine thrust sheets. In general, the formation of the Vienna Basin can be divided into four stages: the formation of a piggyback basin in the early Miocene, development of the pull apart basin in middle to late Miocene, E-W compression and basin inversion during the late Miocene and E-W extension ranging from Pleistocene to recent (e.g. Royden 1985, Decker 1996, Decker et al. 2005). The sedimentary basin fill of the Vienna Basin was described profoundly by many authors (e.g. Tollmann 1985, Jiricek 1988, Kreutzer 1993, Wessely 2000, Siedl et al. 2020) and is related to the Paratethyan realm and Lake Pannon respectively. Marine sedimentation prevailed until late Badenian when the connections of the Paratethys to the open ocean were restricted, leading to the formation of the Sarmatian sea, which turned to changing salinity conditions and an endemic fauna (Rögl 1999). This restricted aquatic realm was further reduced during the Pannonian, when increasing continentalization and tectonic uplift in the Carpathians isolated the Pannonian Basin from the reduced salinity realms of the Eastern Paratethys and led to the formation of Lake Pannon (Rögl 1999). The formation of Lake Pannon can be separated into three intervals: An initial stage with low water levels, resulting in the isolation of the Paratethys Sea at around 12 Ma, a stage of gradual transgression which lasted until 9.5 Ma and a long interval of shrinking and filling of the Lake, persisting into the early Pliocene (Magyar 1999). A forerunner of the Danube (Paleo-Danube) flowed across the NAFB during the early Pannonian, depositing the Hollabrunn-Mistelbach alluvial fan (Nehyba & Roetzel 2004). This structure prograded towards the east and deposited most of the coarse-grained material west of the Steinberg-fault, before building up deltaic complexes and distributing sands across the basin in a southeastern direction. The base of the Pannonian corresponds to a relative sea-level fall at the Sarmatian/Pannonian boundary and marks a type 1 sequence boundary which is related to the glacio-eustatic sea-level lowstand of cycle TB 3.1 of Haq et al. (1988). A sequence stratigraphic interpretation for the upper Pannonian deposits is problematic, due the retreat of Lake Pannon. Due to this reason our investigation is focused solely on the lower Pannonian deltaic deposits. Specifically, the identification of the lower Pannonian deltaic complexes was achieved with the tools of seismic interpretation, where a 3D-seismic block with a length of 45 km, a width of 25 km and a maximum depth of 2500 m was investigated. To display the seismic data the program Petrel E&P Software Platform was used. To define the seismic bodies as of deltaic nature, stratal patterns and general deltaic depositional features like foreset, topset and bottomset accommodations were identified and highlighted. Stratal termination patterns were used as a tool to identify the relation between the distinct deltaic lobes and argue their depositional development. Furthermore, well-log data was used

to correlate the identified deltaic structures to an existing age model after Harzhauser et al. (2004), and to also define a sequence stratigraphic frame for the lower Pannonian delta. Seven paleogeographic maps were created to show the dynamic development of the deltaic deposits through time, but also to illustrate two major channels, identified before and after the inception and the end of the deltaic deposition. All the above-mentioned features were used to show the exact distribution of the lower Pannonian deltas, which were shed into the central Vienna Basin by the Paleo-Danube at around 11.6 Ma, revealing the shape, area, thickness and dynamic development of the delta, with so far unreached spatial and temporal resolution.

2. Geographic and Geological Overview

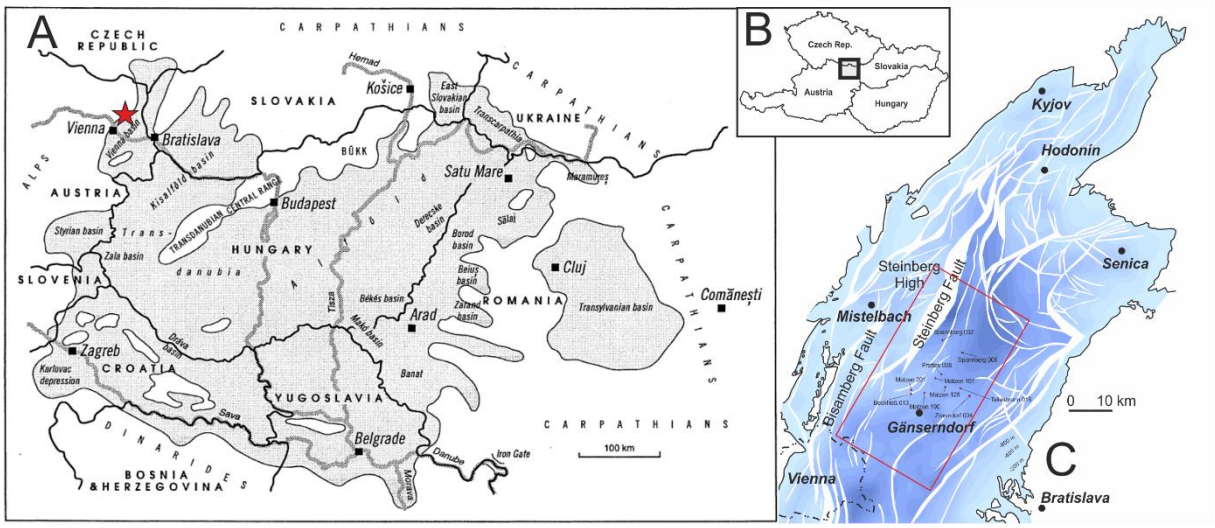

Figure 1: (A) Location of the Vienna Basin in the Pannonian Basin (red star) modified after Magyar (1999). (B) Geographic position of the Vienna Basin in Central Europe. (C) Geological map of the Vienna Basin. The red rectangle (45 x 25 km) marks the outline of the studied seismic block.

2.1 Geographic Overview

The Vienna Basin is situated between the Czech Republic, Slovakia, Austria and Hungary. It is about 200 km long and 60 km wide and strikes roughly NE-SW. It developed along sinistral fault systems during Miocene lateral extrusion of the Eastern Alps (Strauss et al. 2006), and is located northeast of a bend in the Alpine chain, where the east-west strike of East Alpine units changes into the SW-NE strike of Carpathian units (Wessely 1988). The studied 3D seismic block is located in the central part of the Vienna Basin in Austria (Fig 1C). On the surface this rectangle reaches from the Vienna city limits in the south-west to the Zistersdorf-area in the north-east, and from Gr. Engersdorf in the north-west to Zwerndorf in the south-east. This area amounts to approximately 1125 km^2 with a maximum depth of 2500 m.

2.2 Geological Overview.

The Vienna Basin is one of the most intensively studied Neogene basins and serves as a classic example for a pull–apart basin (e.g. Strauss et.al. 2006, Royden 1985, Wessely 1988). It is a regional depression between the Eastern Alps and the Western Carpathians located along the Vienna Basin Transfer fault (Hinsch et al. 2005) and formed along sinistral fault systems during Miocene lateral extrusion of the Eastern Alps (e.g. Royden 1985, Strauss et al. 2006). The basin fill consists of shallow marine and terrestrial sediments of early to late Miocene age and can reach a thickness of 5500 m in the central parts of the basin (e.g. Wessely 1988). Many authors contributed to a better understanding of the Vienna Basin and a lot of research was done in the last two centuries, but it was not until seismic

surveys brought a new powerful tool, that the Vienna Basin was explored in much more detail. Strauss et al. (2006) presented an improved sequence stratigraphic framework for the southern and central Vienna Basin (Fig. 3), based on the integration of 3D seismic reflection data, well data, surface outcrops and refined biostratigraphy which considerably improved the understanding of age and timing of the sedimentary and kinematic evolution of the Vienna Basin.

2.2.1 The Vienna Basin

The Vienna Basin is situated above the thin-skinned nappes of the Alpine – Carpathian thrustbelt, which were thrust over the European continental margin before the middle Miocene (Decker 1996). In general, the Vienna Basin shows three crustal sections (Wessely 1993). The uppermost Neogene basin fill, which consists of lower Miocene (Eggenburgian) to upper Miocene (Pannonian) clastic sediments and shallow water limestones, which can reach a thickness of 5,5 km. The Alpine-Carpathian thrust sheets, reaching a maximum thickness of 8 km, composed of nappes of the Silesian and Penninic Flysch units, Mesozoic and Paleozoic cover nappes of the Austroalpine nappe complex, and the Austroalpine basement nappes. The lowermost section is the Bohemian crystalline basement with Palezoic sediments and a Jurassic to Cenozoic sedimentary cover. (Fig 2).

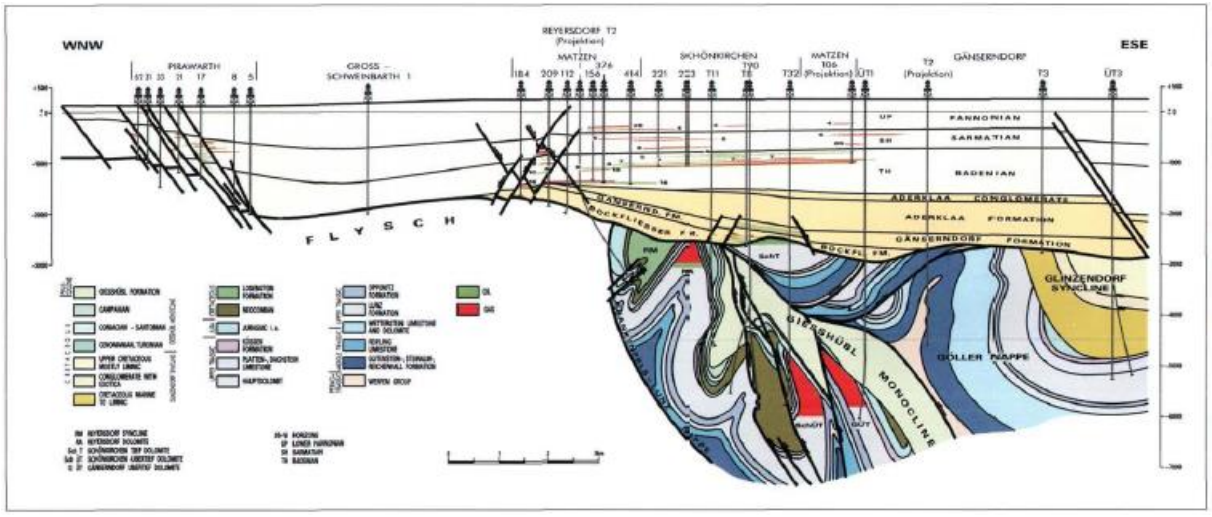

Figure 2: Cross–section along the Pirawarth-Matzen-Gänserndorf area (Wessely 1993). The Neogene fill starts with the deposition of the Bockfließ Fm., the colored section (e.g. Giesshübl Monocline) represents the Alpine - Carpathian thrust sheets. Not shown here is the Bohemian crystalline (Basement)

2.2.2 Evolution of the Vienna Basin.

The formation of the Vienna Basin can be divided into four major stages (e.g. Royden 1985, Decker 1996, Decker et al. 2005). Here is just a brief summary presented which follows the work of Strauss et al (2006) and Decker (1996, 2005)

1- Formation of a piggyback basin in the early Miocene
2- Pull apart basin from middle to late Miocene
3- E-W compression and basin inversion in the late Miocene
4- E-W extension from Pleistocene to recent.

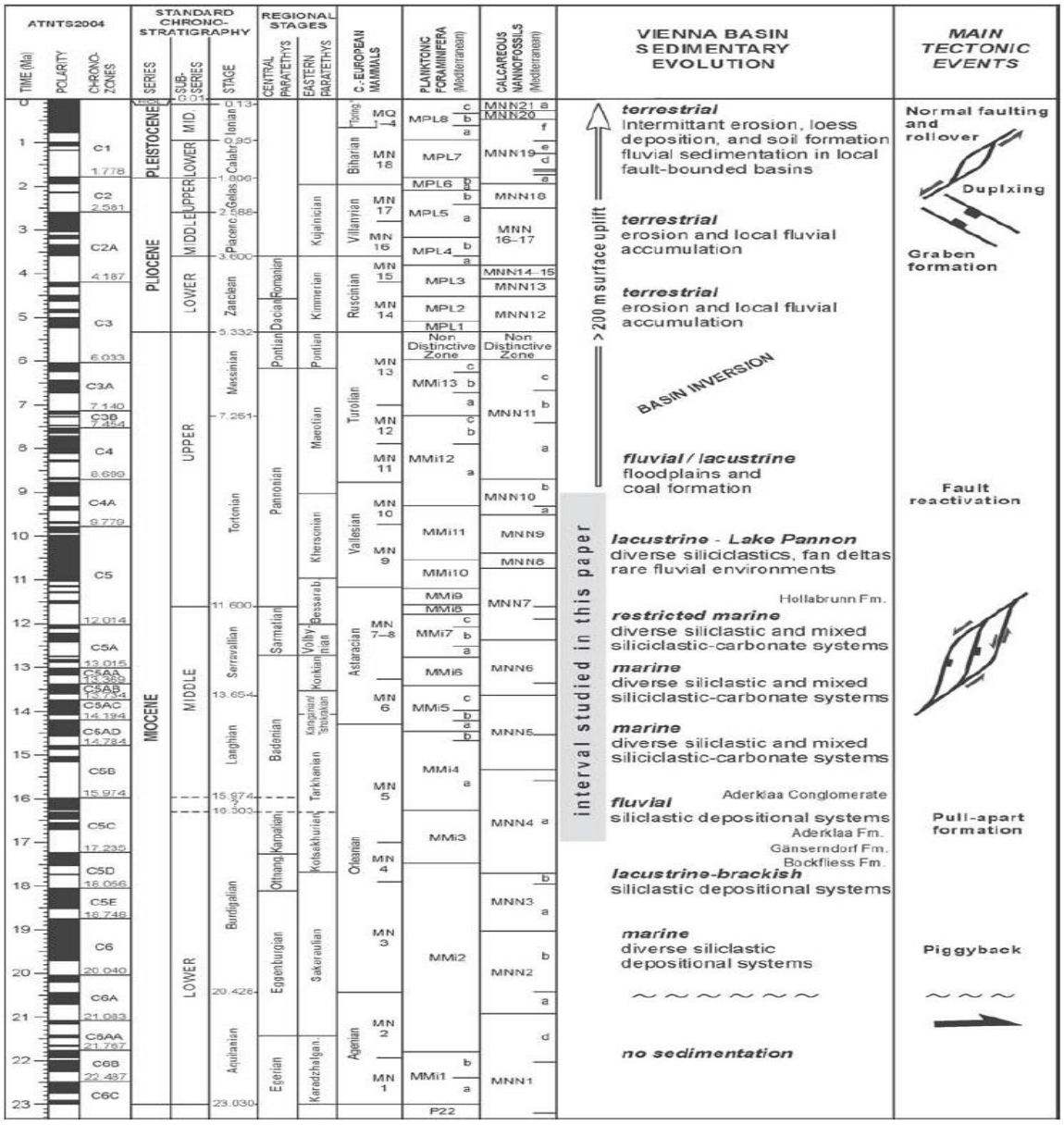

Figure 3: Stratigraphy and evolution of the Vienna Basin from the early Miocene to the present correlated with main tectonic events (table 1 in Strauss et al. 2006)

Formation of a piggyback basin:

In the early Miocene the Vienna basin formed as an E-W trending piggyback basin on top of the Alpine thrust belt, which was active from the Eggenburgian to the early Karpatian (Fig 3). During the Ottnangian and early Karpatian, the Bockfließ Formation was deposited, initiating a phase of lacustrine to brackish-littoral sedimentation. This formation is covered by the lacustrine-terrestrial deposits of the Gänserndorf Formation, which grades into the overlying fluvial Aderklaa Formation.

Pull-apart basin:

Thrusting developed into lateral extrusion during the late Karpatian, causing a change from the piggyback basin into a rhombic pull-apart basin (Fig 3). This change in regime marked the onset of a major regressive event at the Karpatian/Badenian boundary. In the southern Vienna Basin, the Aderklaa Conglomerate was deposited in a braided river system during the early Badenian. Generally, sediments were transported northwards but also from the SSE across the future Leitha Mountains and the Eisenstadt-Sopron Basin, forming a drainage system which ceased with the onset of subsidence in

the Eisenstadt–Sopron Basin. This event is followed by a marine incursion 14. 5 Ma ago, which reached the Eisenstadt -Sopron Basin and set up the Leitha mountains as a peninsula (Strauss et al. 2006). In the central part of the basin sedimentation can be divided into proximal deltaic clastics and distal basinal facies (sand, marl, clay). In the east, the Leitha Mountains were completely drowned during a sea-level highstand in the Badenian (Strauss et al. 2006). The sea-level dropped at the Badenian/Sarmatian boundary, exposing the Leitha Mountains and their Badenian sedimentary cover, forming an island again until the Pannonian Lake was filled during the late Pannonian (Harzhauser et al. 2004). During the Sarmatian, topographically lower situated parts of the Badenian sedimentary cover were eroded (Harzhauser & Piller 2004), resulting in detrital Leitha limestone, channel deposits and autochthonous bryozoan/serpulid limestone, which represent the uppermost Miocene sediments of the Leitha Mountains. In most parts of the Vienna Basin deposition continued throughout the Sarmatian and the general tectonic regime of SW-NE extension continued from the Badenian to the Sarmatian. A major regression marks the onset of the Pannonian, covering most of the Sarmatian deposits and depositing mainly sand and clay in the lacustrine environment of Lake Pannon during the early and middle Pannonian, while in the late Pannonian primarily alluvial sediments filled the basin.

E-W compression and basin inversion

In the latest Pannonian and Pliocene an E-W trending compressive stress field evolved, which resulted in basin inversion and sediment deformation (Fig 3).

SW-NE extension

A trans -tensional regime led to fault-controlled subsidence along the eastern limit of the Vienna Basin, indicating that faults along the Leitha Mountains are still active today (Fig 3)

2.2.3 Study related faults in the Vienna Basin

Four fault systems are important for this study: The Steinbergfault, the Markgrafneusiedlfault, the Matzen faults and the Aderklaa-Bockfliess fault. In general, several phases of faulting occurred in the Vienna Basin. The oldest event consists of lower Miocene synsedimentary faulting that has been transported with the moving thrust complex. The younger faults started when thrusting ended in Lower Austria in the Badenian, and mostly show growth fault patterns with large displacements. (Wessely 1988). The Steinbergfault is about 55 km in lateral extent and its maximum vertical displacement is close to 6000 m near Zistersdorf (Wessely 1988). It displays roll-over and growth strata geometries, which indicates listric fault geometries and flattening of the fault in depth (Decker 1996).

The Steinbergfault (as well as the Leopoldsdorffault) system probably root in the SE-dipping floor thrust of the Alpine-Carpathian nappes or in a detachment horizon within the autochthonous Jurassic sediments of the Bohemian crystalline basement. During the late Miocene lateral extrusion and eastward motion of wedges along the extentional faults ended, caused by a switch in far-field stresses to E-W directed compression which has been documented in the Eastern Alps, the Western Carpathians and in the Pannonian region, leading to the termination of basin subsidence in the Vienna Basin during the Pannonian (Decker 1996)

The Matzen fault system is of post-Pannonian age and shows only little displacements (10-80 m). This fault system may be related to tension caused by an updoming of a deeper situated basement which is also responsible for the Matzen - Spannberg elevation (Wessely 1988). The visible fault scarp coincides with the SE edge of the Pleistocene Gänserndorf terrace, which marks a large river terrace north of the Holocene floodplain consisting of coarse gravel in sandy matrix typical for braided river systems (Hintersberger et al. 2018).

The Markgrafneusiedlfault marks one of several normal splay faults that formed during the middle to upper Miocene and represents a SE dipping Neogene active normal fault (Hintersberger et al. 2018). It makes up the eastern margin of the Pleistocene Gänserndorf Terrace, while the NW dipping Aderklaa-Bockfließ fault makes up the western margin of the terrace and is characterized by a morphological fault scarp, which systematically decreases in height from SW to NE (Weissl et al. 2017).

2.3 The Pannonian

The Pannonian basin system is an integral part of the Alpine mountain belts of east-central Europe and is completely encircled by the Carpathian Mountains to the north and east, the Dinarides to the south, and the Southern and Eastern Alps to the west. The Pannonian area was deformed by Mesozoic thrusting and disrupted by a complex system of Cenozoic normal and wrench faults. The Pannonian basin is actually composed of small, deep basins separated by relatively shallow basement blocks. Neogene-Quaternary sedimentary rocks show more than 7 km in thickness in some areas and the basin system itself is about 400 km from north to south and 800 km from east to west. Currently, it is interpreted as a Mediterranean back arc extensional basin of middle Miocene age, and spans over ten different countries (Hungary, Slovakia, Poland, Ukraine, Romania, Slovakia, Serbia, Croatia, Slovenia and Austria). (Royden 1985) (Fig 1). Lake Pannon came into existence when increasing continentalization and tectonic uplift in the Carpathians isolated the Pannonian Basin from the Eastern Paratethys during the Tortonian (Fig 4). (Rögl 1999). Brackish conditions with occurrences of the molluscs *Congeria, Melanopsis* and *Lymnocardium* dominated the lake.

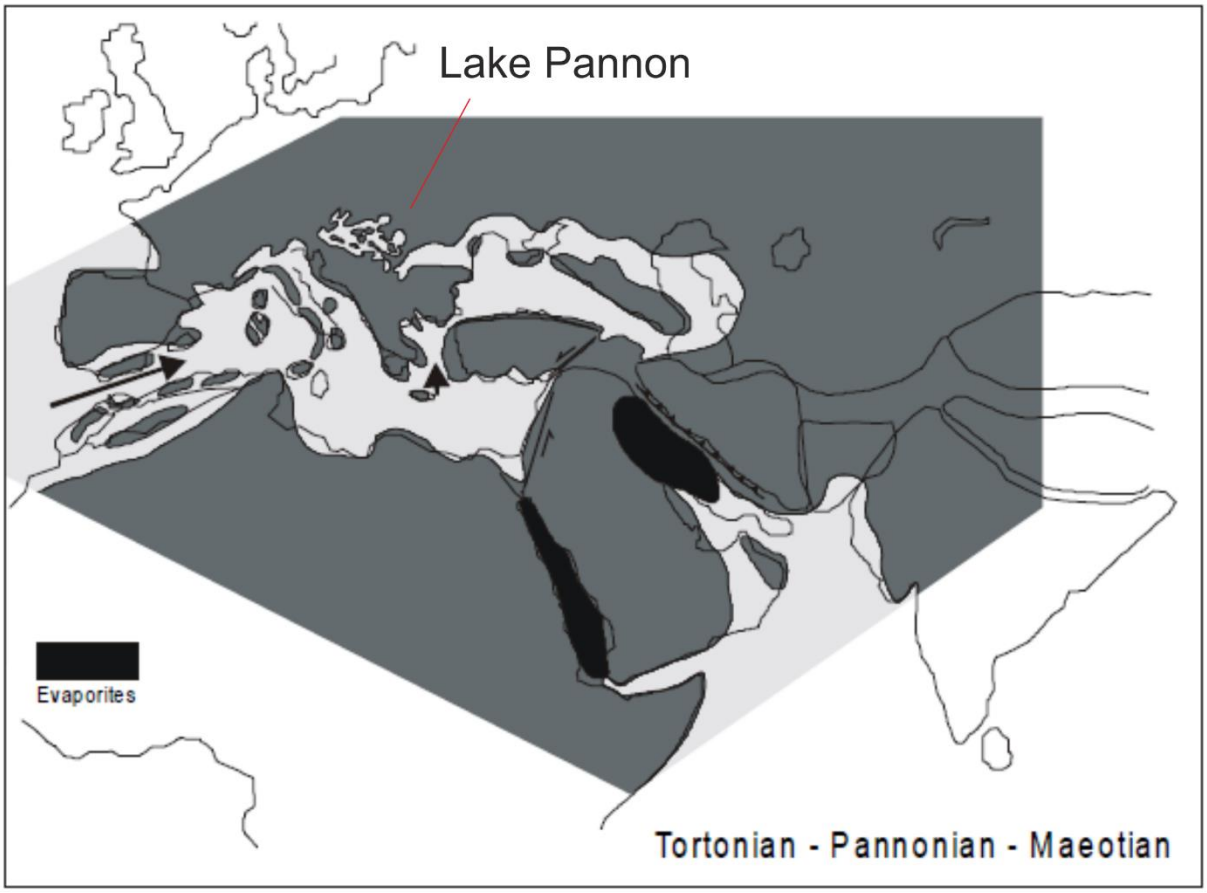

Figure 4: The Pannonian lake after its separation from the Paratethys. The red line points to the lake. After Rögl (1999)

The formation of Lake Pannon

Lake Pannon came into existence after a short regressive phase at the Sarmatian/Pannonian boundary, which corresponds to a worldwide regression (TB3.1 cycle of Haq et al. 1988) leading to the isolation of the Pannonian Basin from the Eastern Paratethys (Piller 1999) at around 12.0 Ma. This resulted in the isolation of the intra-Carpathian waters from the rest of the Paratethys, giving rise to the lake. Previously shallow water areas became dry land and only small areas of the Sarmatian deposits avoided complete erosion. The Styrian and Vienna Basin remained part of the lake, whereas the East Slovakian and Transylvanian basin where filled with sediments at this time and no deep-water environments can be found in the entire Pannonian Basin during the *Mecsekia ultima* Biochron ca. 12.0 Ma. At 10.8 Ma land areas where gradually flooded by Lake Pannon in the central part of the basin, depositing fine grained sediments, which left only little evidence of transgression in the sedimentary record. In the southern half of the basin (around the modern area of Croatia and Bosnia Herzegovina), carbonate precipitation was dominant while in the north, clastic sedimentation dominated. Deep sub-basins which formed at that time can be linked to the onset of rapid subsidence in several parts of the basin. At 9.5 Ma the lake reached its maximum extent, flooding the former dry western foreland of the Transdanubian Central Range (Magyar et al. 1999), marking a general transgressive trend for this time. However, the Vienna Basin became an alluvial plain at this time. This is followed by a sudden reduction of the lake to approximately half its size at 9.0 Ma. Deltas prograded from the northwest and northeast into the center of the basin and many alluvial plains formed during a time when the lake level dropped significantly. Another transgression took place at ca. 8.0 Ma, rising the overall water level and leaving only a few islands above lake level. This effect was balanced by high terrigenous influx in the northeastern and especially in the northwestern part where deltas prograded to the south (Juhász 1994). This progradation from the northwest nearly completely filled up the western part of modern Hungary at ca. 6.5 Ma, with only the Drava basin remaining subaqueous (Bakrač et al. 2012). During the early Pliocene the last vestige of Lake Pannon formed, as the basin continuously was filled from the north and the brackish endemic molluscs became extinct. To summarize, the evolution of Lake Pannon can be subdivided into three intervals: an initial regressive stage, isolating the Lake from the Paratethyan sea, a second interval, where gradual transgression took place and third long interval of shrinking and filling of the basin through prograding sedimentary systems. For a detailed overview and a paleogeographic reconstruction see Magyar (1999).

The Pannonian in the Vienna Basin

In the Vienna Basin the Pannonian Stage is represented by an up to 1200 m thick siliciclastic succession, comprising lacustrine and terrestrial deposits. It marks a crucial time in the evolution of the Vienna Basin, when Lake Pannon retreated and gave place to terrestrial – fluvial settings (Harzhauser et al. 2004). Papp (1951) applied a letter zonation to the biozones on the base of multiple units, characterized by several meters of sediment, separated by considerable gaps (Harzhauser et al. 2004). These zones are traditionally referred to as zones A-H (Papp-Zones), where A-C is correlated with the lower Pannonian, D-E with the middle Pannonian and F-H with the upper Pannonian. In the following an outline of lithostratigraphy and biostratigraphy of the Pannonian in the Vienna Basin is presented, based on the work of Harzhauser et al. (2004) who summarized the maze of Pannonian terms and managed to give a comprehensive overview of the Pannonian age in the Vienna Basin.

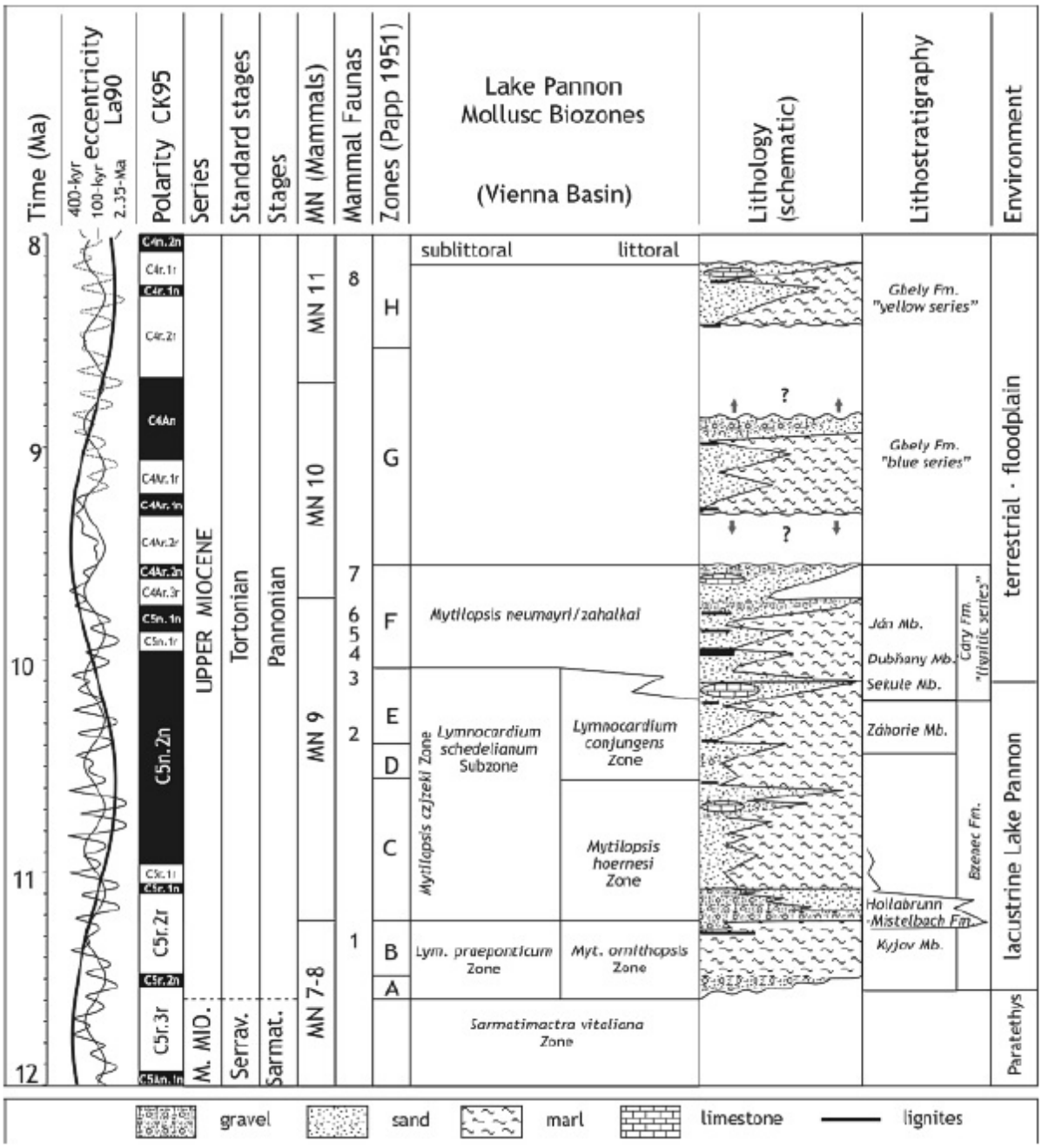

Figure 5: Chronostratigraphy, biostratigraphy and lithostratigraphy of the Pannonian in the Vienna Basin. Fig 1 in Harzhauser et al. (2004).

Lower Pannonian:

The lowermost sediments, which can be assigned to the Pannonian stage are only known from basinal settings, illustrating a phase when fluvial facies reached far out into the basin, depositing a 12-20 m thick unit of sand and gravel termed “Übergangsschichten” (= transitional beds), and reworking older Sarmatian strata (A in Fig 5). This phase corresponds to the zone A of Papp (1951) and in the northern part of the Basin represents the basal part of the *Bzenec Formation*, defined by Ctyroky (2000). Ostracods document a brackish-water environment (15-10 psu) (Kovac et al. 1998). This zone is followed by a 50-100 m thick unit of marl and sand which is overlain by a 20-50 m thick marker unit of ostracod-bearing, green-gray marly clay. This unit is correlated to *the Mytilopsis ornithopsis* Zone and corresponds to zone B of Papp (1951) (B in Fig 5). It shows a clear shale-line appearance in geophysical logs (Fig 6) and is comprised of prodelta and basinal facies, with a similar salinity as Zone A, indicating

a continuation of the brackish-water lake (Kovac et al. 1998). This prodelta and basinal facies is followed by the deltaic facies of the "großer unterpannoner Sand" (= big lower Pannonian Sand), which represents a sandy succession with scattered gravels up to 200 m thick, displaying a moderately serrated boxcar trend in geophysical logs. This unit is correlated with the *Mytilopsis hoernesi* Zone and with Zone C of Papp (1951), (C in Fig 5.). This succession is linked to a delta which was shed into the northwestern part of the Vienna Basin by the Paleo-Danube and the sediments correspond to the gravel of the Hollabrunn – Mistelbach - Formation. Brackish-water conditions still remain at this time (Kovac et al. 1998). Above the "big lower Pannonian sands" a characteristic but short shale-line pattern reflects a strong transgressional phase within the *Mytilopsis hoernesi* zone, pushing back the riverine systems and flooding the Mistelbach subbasin.

Middle Pannonian:

The basal zone of the middle Pannonian Zone D after Papp (1951) (D in Fig. 5) is represented by a thin unit of interbedded sand and marl, which shows similar geophysical log patterns (serrated, funnel-shaped curves, Fig 6) to the upper parts of the lower Pannonian deposits. Sediments of Zone D include marginal freshwater limestones and multilayered onkoids at the base of the *Lymnocardium schedalianum* Subzone at Leobersdorf. Salinity is slowly decreasing during this time (Kovac et al. 1998). Zone E after Papp (1951) (E in Fig 5) is composed of clay and sand and corresponds to the middle and upper *Lymnocardium schedalium* Subzone within the *Mytilopsis czjzeki* Zone. The salinity of this sedimentary environment can be determined with 3-15 psu on the basis of presence of the ostracods *Cyprideis heterostigma* (Reuss), *C. obesa* (Reuss) and a large number of *Candona unguicula* (Reuss) (Kovac et al. 1998). This unit depicts two characteristic coarsening upward cycles of approximately equal thickness indicating the development of fluvial channels in the former lacustrine environment.

Upper Pannonian:

In the late phase of the Pannonian, the margin of Lake Pannon had retreated from the Vienna Basin, giving place to floodplain deposits and freshwater lakes, which were separated from Lake Pannon. The upper Pannonian is represented by a uniform facies which can be found in the entire Vienna Basin and comprises zones F, G and H (Fig 5). Zone F is assigned to the lignite-bearing Cary Formation of the upper Pannonian and shows continued decreasing salinity of 0-15 psu documented by ostracods (Kovac et al. 1998). These sediments are overlain by a 450 m thick unit, consisting of marl, clay and silt with intercalations of sand, gravel, rare lignites and sporadic freshwater limestones in the top, which corresponds to zone G of Papp (1951) and the Gbely Formation, respectively. This formation represents freshwater sediments and marks the end of brackish-water conditions (Kovac et al. 1998). Above the Gbely Formation an up to 100 m thick succession, shows blue green clays, with layers of yellowish sand and very rare lignitic clay with occurrences of marl-concretions and scattered limestone, which was called "Bunte Serie" (= variegated series). This succession marks Zone H after Papp (1951).

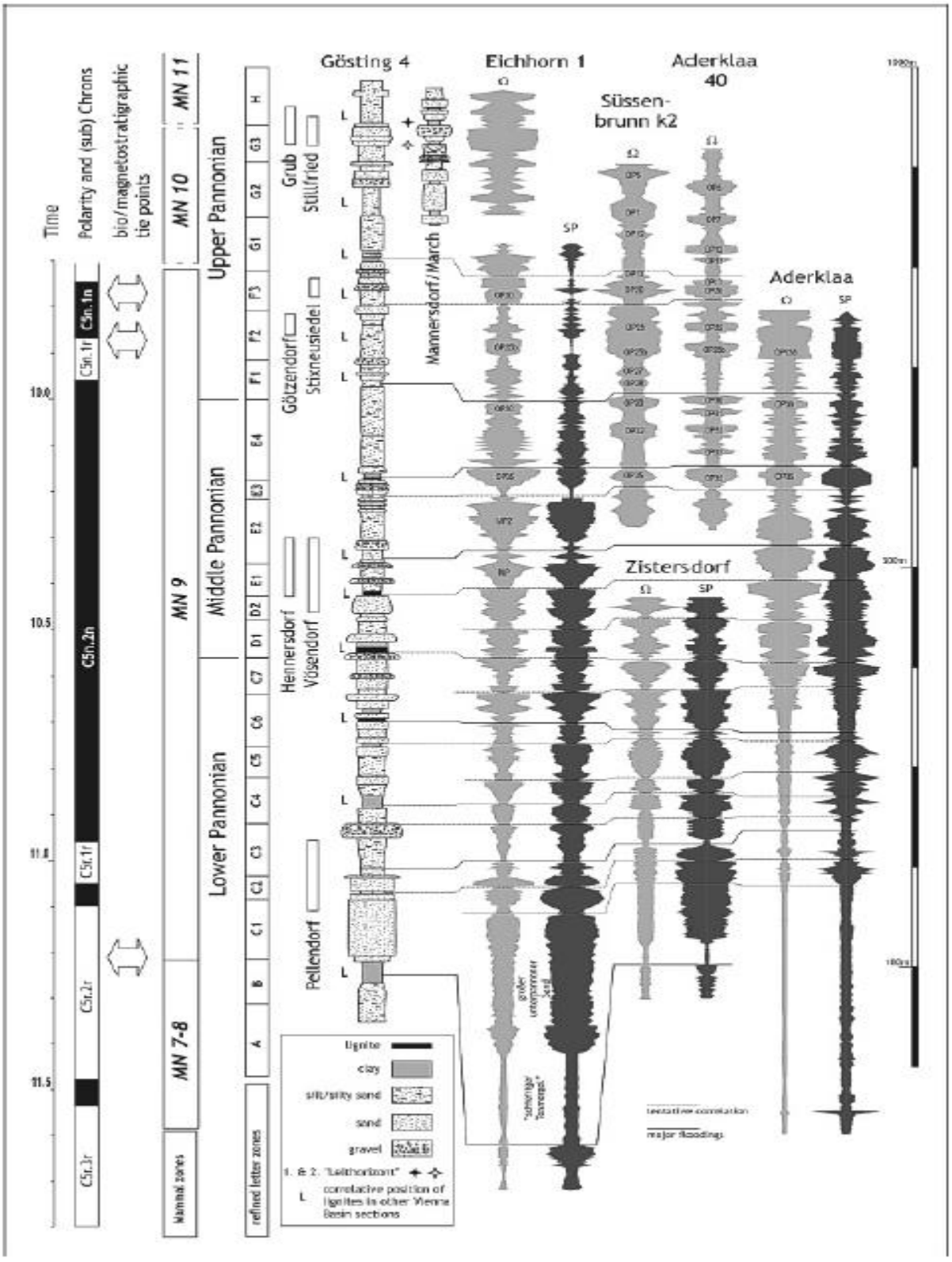

Figure 6: Tentative correlation of Pannonian deposits (Gösting 4 and Mannersdorf) and well-logs (Eichhorn 1, Süssenbrunn k2, Aderklaa 40, Zistersdorf, Aderklaa) within the Vienna Basin (Fig 3.in Harzhauser et al. (2004)

Pannonian Sequence stratigraphy:

In the latest Sarmatian a relative sea fall can be linked to the glacio-eustatic sea-level lowstand of the TB 3.1 cycle of Haq et al. (1998), which has been dated at around 11.5 – 11.6 Ma (Hilgen et al. 2000). Kosi et al (2003) defined the Sarmatian/Pannonian boundary as Type 1 sequence boundary which can

be linked to this relative sea level fall. This lowstand led to the emersion of many Sarmatian nearshore deposits along the Vienna Basin margins, while middle Miocene limestones of the vanished Paratethys became exposed, marking a time of intensive erosion as indicated by a strong discordance between Sarmatian and Pannonian deposits which is observable in surface outcrops and core-drillings respectively (Harzhauser et al. 2004). The lower Pannonian strata (A-$C_{1,2}$ in Fig 6) correspond to a 3rd order lowstand systems tract (LST), marking a time when fluvial facies penetrated far into the basin. This lowstand sediments can be assigned to the sand and gravel of the basal Bzenec Formation (Harzhauser et al., 2004). However, this 3rd order LST is modulated by a minimum of at least one higher order sequence, which is represented in geophysical logs as a characteristic shale-line pattern (schiefrige Tonmergel) and corresponds to Zone B after Papp (1951) (Fig 6). In the Styrian Basin, these deposits correspond to the Eisengraben Member, which was described as a transgressive systems tract (TST) by Kosi et al. (2003). Above this higher order TST, progradation of the deltaic bodies of the "großer unterpannoner Sand" and the Hollabrunn-Mistelbach-Formation takes place, which by Kosi et al. (2003) was described as the Vienna Basin counterpart of the Sieglegg Member in the Styrian Basin, which is described as a highstand systems tract by Kosi et al. (2003). Together, the Bzenec Formation, the Hollabrunn-Mistelbach Formation and the "großer unterpannoner Sand" are the equivalent to the LPa-1-Sequence defined by Kosi et al. (2003) in the Styrian Basin (Harzhauser et al. 2004). During the *Mytilopsis hoernesi* Zone, deltaic facies are transgressed by Lake Pannon marking the onset of the 3rd order TST (C_3 – E_1 in Fig 6), which can be subdivided into 4 higher order sequences (Harzhauser et al. 2004). The basal sequence illustrates characteristic funnel-shaped cycles in the Styrian Basin (Kosi et al. 2003) with similar counterparts in the upper Bzenec Formation and is correlated with the LPa-2 sequence defined by Kosi et al. (2003). Another higher order cycle is recognized by Harzhauser et al. (2004) in the Gösting 4 well (Fig 6) where synsedimentary intraclasts or gravel indicate such an interpretation. The third order TST culminates in a maximum flooding surface in the middle Pannonian within zone E in Fig 6. Progradation of sand and gravel into the Vienna Basin in the upper middle Pannonian (E_2-E_4 in Fig 6) is probably related to a third order highstand systems tract (HST), when floodplain conditions and isolated lakes developed (Harzhauser et al. 2004) and Lake Pannon retreated from the Vienna Basin, making a sequence stratigraphic approach for the upper Pannonian deposits problematic.

2.4 The Hollabrunn-Mistelbach Formation and the Paleo-Danube

The sediments of the Hollabrunn-Mistelbach Formation (HMF) were already recognized by e.g., Suess (1866) (Klien and Roetzel 2009). The fluviale nature of this formation was first described by Hassinger (1905b) who linked them to the Paleo-Danube. The mostly coarse-grained clastic fluvial to deltaic sediments of the HMF where studied intensely by Nehyba and Roetzel (2004) in 65 outcrops between Krems and Zistersdorf, discovering two genetically related environments: the dominant gravel-bed river depositional environment in the west which developed into a braid–delta environment towards the east. The formation spans on the surface in a WSW-ENE direction from Krems towards Hohenwarth, Ziersdorf, Hollabrunn and the Ernstbrunner Wald to the surroundings of Mistelbach and further to Zistersdorf over a length of ca. 86 km (Fig 8). This body is around 3 and 14 km in width, reaching a maximum of approximately 20 km in the Mistelbach-area. The prodelta-sediments cannot be traced on the surface, and extend subsurface, east of the Steinberg fault far to Slovakian territory (Fig 7) (Harzhauser et al. 2004).

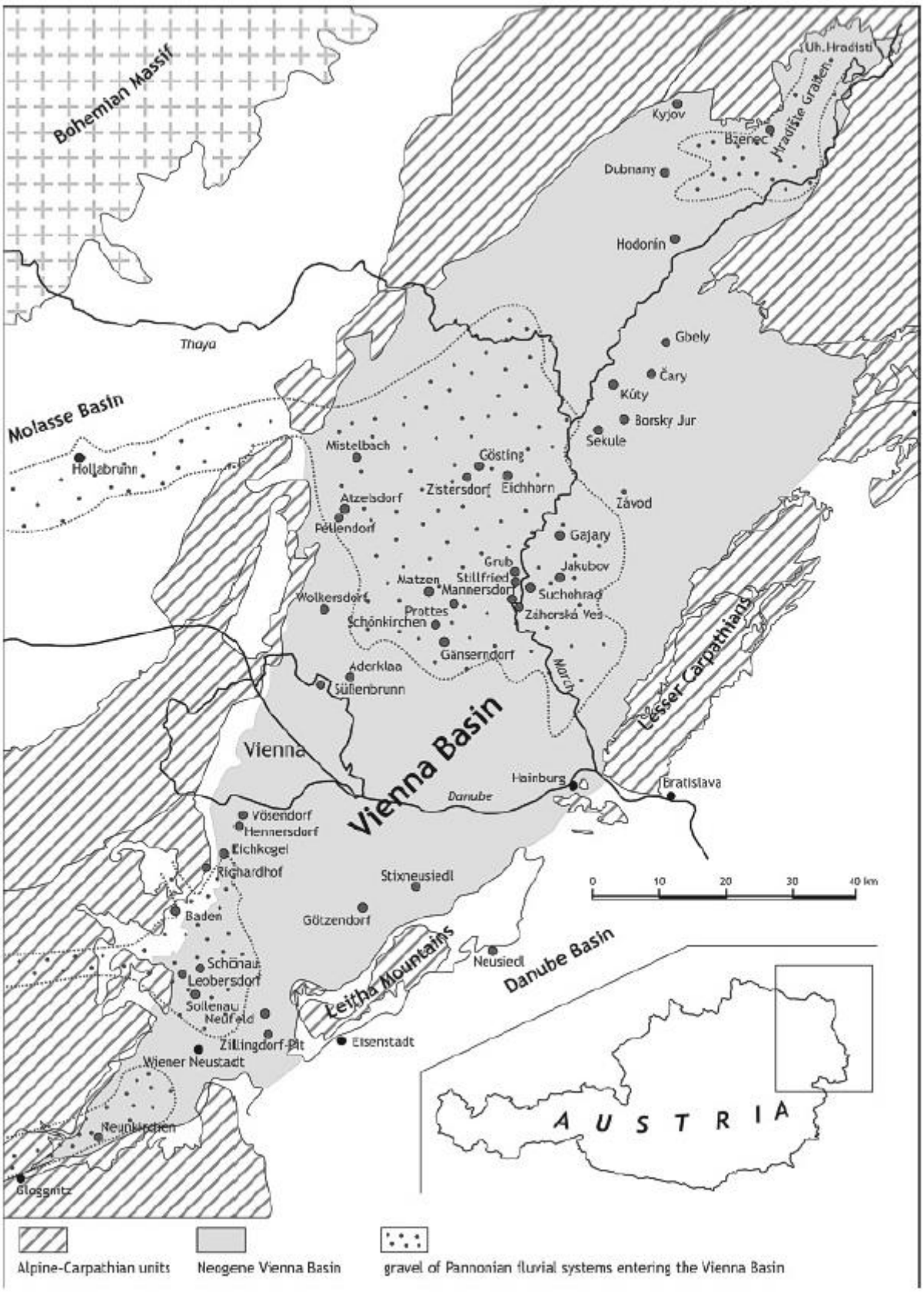

Figure 7: The Vienna Basin within the Alpine-Carpathian units. Small dots and dotted lines show the interpreted extent of the subsurface Pannonian delta lobes penetrating far into the Slovakian area (fig 2 in Harzhauser et al. 2004)

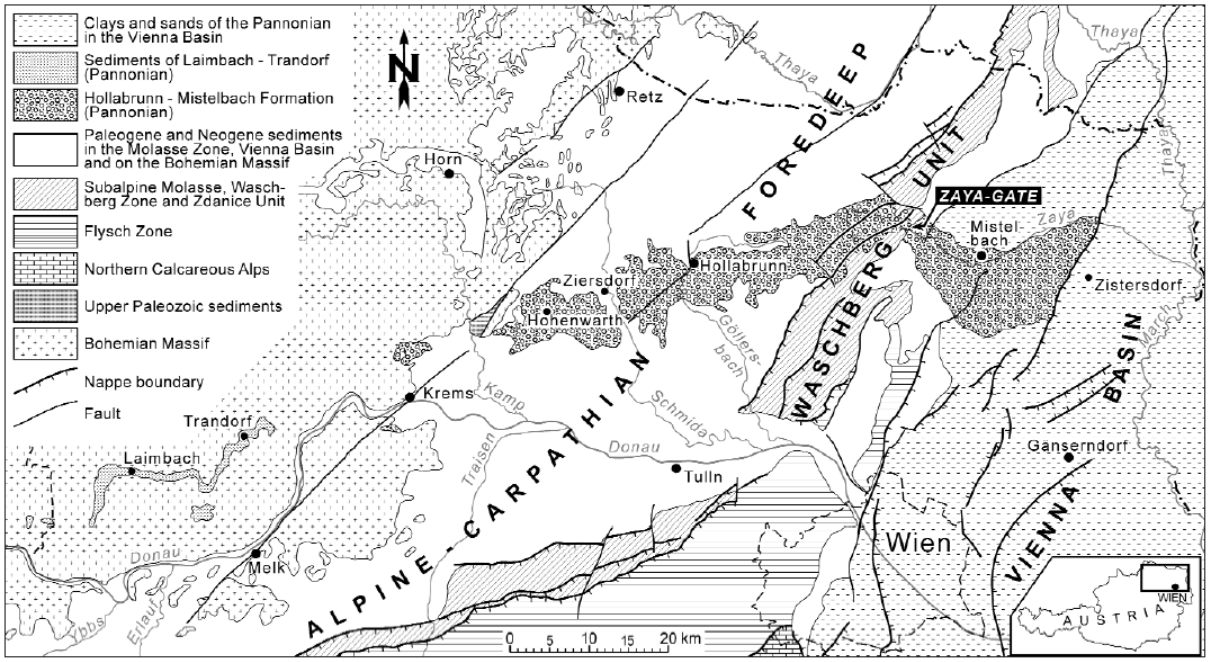

Figure 8: Simplified geological map of northeastern Austria with location and extent of the Hollabrunn-Mistelbach.Formation. (Fig. 1 in Nehyba & Roetzel 2004)

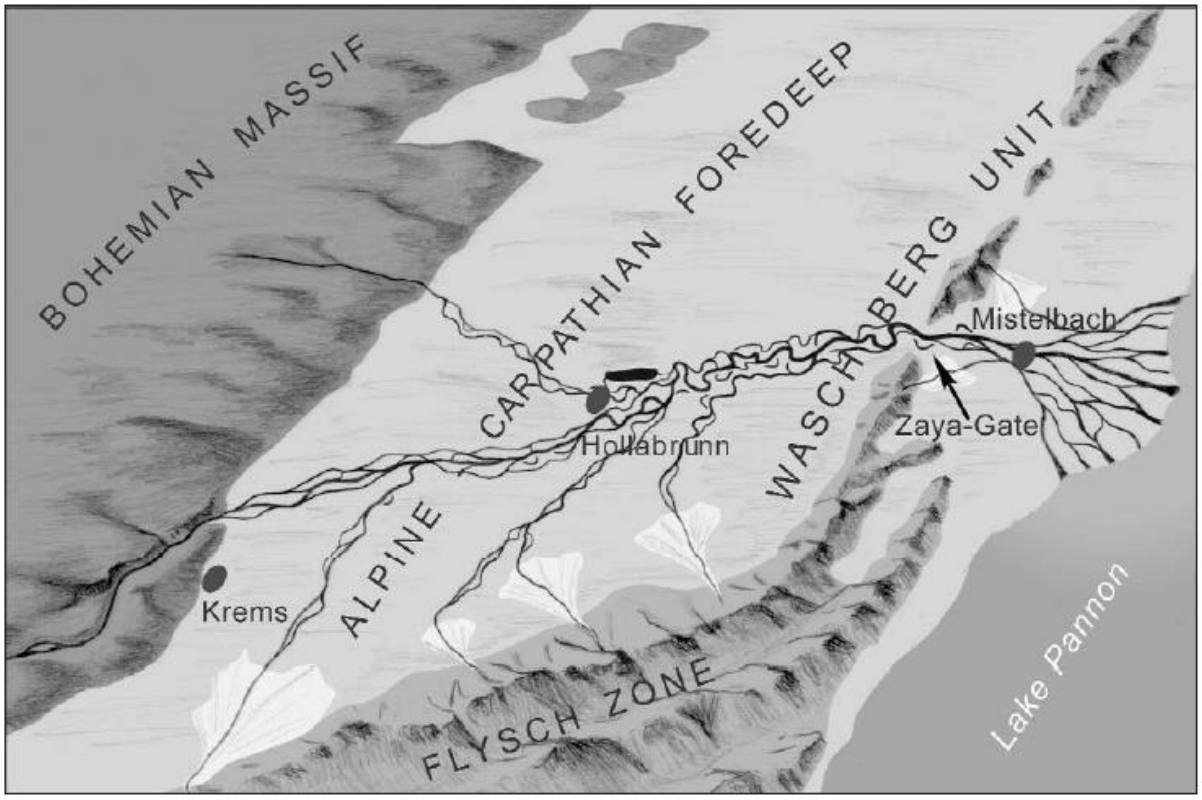

Figure 9: Hypothetical reconstruction of the depositional systems of the Hollabrunn-Mistelbach.Formation during the early Pannonian in the Alpine – Carpathian Foredeep and the Vienna Basin (Fig 21 in Nehyba & Roetzel 2004).

3. Deltas

3.1 Delta Definition

The concept of a delta dates back to c. 450 B.C when Herodotus observed the similarity between the alluvial plain of the Nile delta and the Greek letter Δ (Nemec 1990). Deltas form where rivers drain into a lake or ocean basin. River processes interact with ocean processes (waves and tides) to control the form of the delta, leading to the assumption that every delta is a unique result between the interplay of those processes. Deltas are discrete shoreline disturbances formed where alluvial system enters a basin and supplies sediment more rapidly than it can be redistributed by basinal processes (Orton & Reading 1993), resulting in a localized, often irregular progradation of the shoreline, controlled directly by a terrestrial feeder system, with possible modifications by basinal processes (Nemec 1990). A delta can be described as a three-dimensional stratigraphic unit, formed by many different delta lobes.

3.2 Delta Classification

Deltas can be broadly subdivided into two different categories: Clastic deltas and non-clastic deltas. Non-clastic deltas include pyroclastic deltas and lava deltas, which form in front of coasts when pyroclastic and lava flows enter the basin (Nemec 1990). This master`s thesis focuses exclusively on clastic deltas. For a detailed description of non-clastic deltas see Skilling (2002) and Smellie et al. (2013).

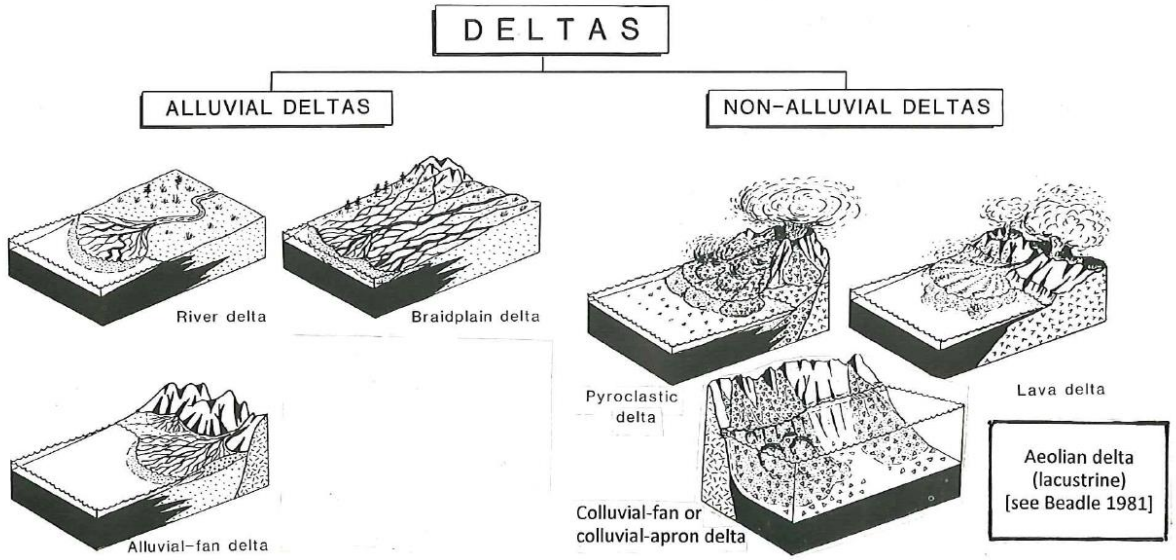

Figure 10: Division of deltas in alluvial and non-alluvial members. (Nemec 1990, Fig 1)

River formed deltas vary enormously in their characteristics and many deltas are not “delta-shaped” at all. Every delta, even though similar to others, is of unique shape and has special sedimentological characteristics which has led to the problem that the terminology and classification schemes are rather unsatisfying and often not applicable for a general description, because of the great number of criteria to be considered. However, many different approaches have been proposed in the literature to classify alluvial deltas. A brief overview is provided as follows:

- Classification over feeder system (Holmes 1966): Classification of deltas through their alluvial feeder systems. Feeder systems are very relevant to the character of the resulting delta body but considering that the same river or alluvial fan is able to produce different deltas. This classification should rather be considered as a higher-order secondary one (Fig 10) (Nemec 1990).

- Classification over thickness distribution (Coleman & Wright 1975): Classification of deltas through thickness distribution patterns, reflecting major controlling factors, from sediment-yield conditions to basinal regime. While being a serviceable classification, its requirement for quite detailed thickness data makes it rarely applicable (Nemec 1990).
- Classification over delta-front regime (Galloway 1975, Fig 14): Commonly used by sedimentologists, this classification focuses on the degree of reworking of the delta front by waves and tides, which led to the development of Galloway´s famous "triangular classification of deltaic depositional systems". He classified river deltas as "fluvial-dominated", "wave-dominated" or "tide-dominated" with a full range of mixed type varieties.
- Classification over tectono-physiographic settings (Ethridge & Wescott 1984): Three distinct delta categories to reflect different tectono-physiographic coastal settings were implemented: shelf-type, slope-type and Gilbert-type deltas. Being the first classification scheme for such deltaic systems, this concept found many followers. The problem is that the categories are way too broad and not enough attention is paid to the actual delta sediments (shelf-type deltas alone vary greatly as sedimentary deposits) (Nemec 1990).
- Classification over delta-front regime and grain size (Orton 1988): Extending the ternary diagram from Galloway (1975) in a fourth dimension to account for the dominant grain size delivered to the delta front. Reasoning is that the degree of reworking of a delta front is not independent of the grain size of the delta front material. For example, the same basinal wave regime will have a different impact on a fine-grained sandy delta compared to a coarse gravelly delta (Nemec 1990)
- Postma (1990) identified 12 prototype deltas. Those prototypes are classified on the basis of a unique combination of four different type of feeder systems and two ranges of basin depth (Fig. 11).

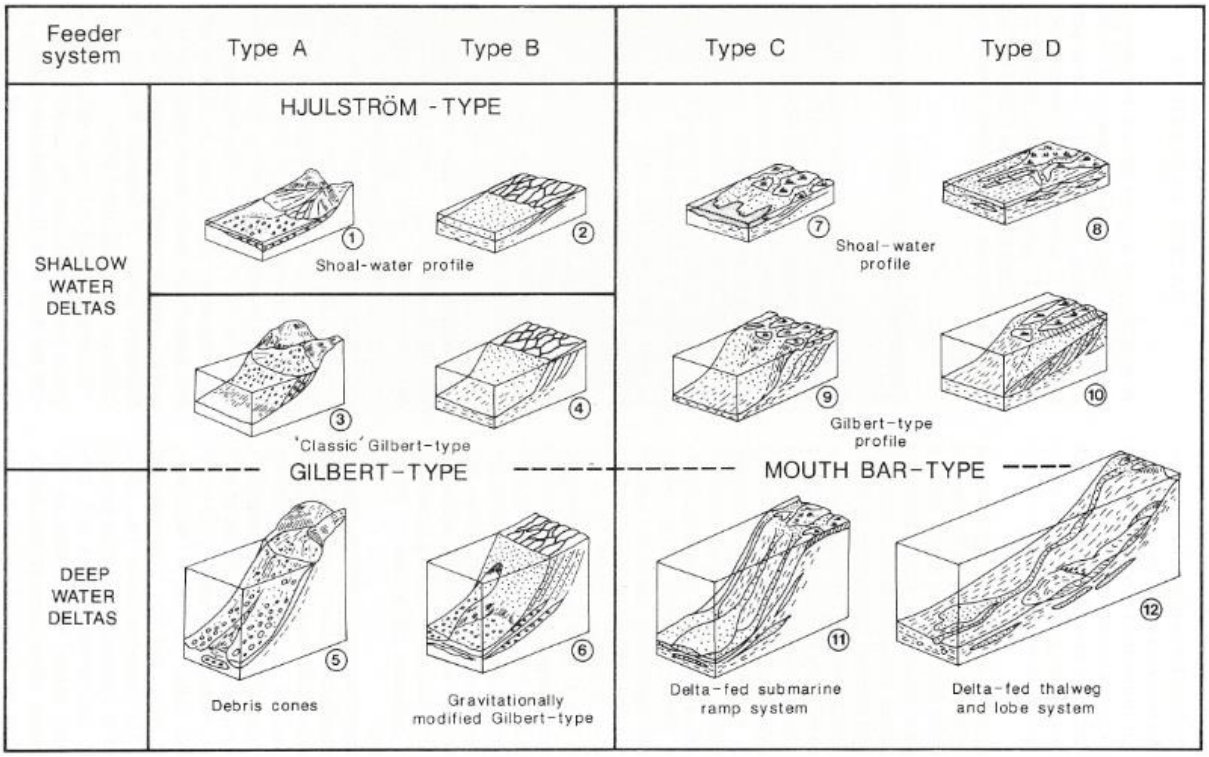

Figure 11:. Twelve prototype deltas, pictured as being dominated by fluvial processes. Type A feeder system= steep foreset angles, mass flows, unconfined streams/ Type B feeder system=steep gradient, unstable channels, bedload rivers / Type C feeder system=moderate gradient, stable channels, bedload rivers/Type D feeder system= low foreset angles, highly stable channels, suspension – load rivers. From Postma (1990)

3.3 Deltaic Processes

The morphology and stratigraphy of a delta are the result of the rate of sediment input relative to the ability of energy sources within the basin to rework and remove sediment (Galloway 1975). To understand the full range of variability in a deltaic system many parameters have to be considered (see Fig. 1 in Galloway 1975). Wave and tidal energy are the primary long-term processes, reworking bed-load sediments (sand), while current energy is responsible for the transportation of suspended load sediment (clay, silt, very fine sand). Gravitational processes pull both, bed-load sediments and suspended load sediments to the slope and into basinal environments. In respect to the sediment input, three main factors have to be considered: The annual sediment discharge, the ratio of bed-load (sand and gravel) to suspended load (clay and silt) and seasonal variations in sediment input. Furthermore, the total stratigraphy of a delta is influenced by two additional factors: First is the preservation of deltaic facies which is in part controlled by the rate of basin subsidence and second the climate, which determines the type of delta plain facies (Galloway 1975).

3.4 Delta features

Fluvial systems collect and transport sediments into lacustrine or marine basins and their river patterns provide information on the rivers behavior and characteristics (Schumm 1985). Their depositional patterns are mostly aggradational. Channels are considered the most important features of fluvial systems because that is where most of the sediments are deposited. Fluvial channels can take a broad spectrum of forms, ranging from very low (straight channels) to high sinuosity (meandering channel) geometries (Galloway & Hobday 1996) Two channel patterns have been recognized in fluvial systems: anastomosing and distributary. Anastomosing patterns occur when contemporaneous branches of a single river flow around permanent islands or a disconnected segment of a floodplain. Distributary patterns are characteristic for certain types of rapidly aggrading alluvial surfaces, such as deltaic plains and alluvial fans (Galloway &Hobday 1996). A fluvial system nearly always has three main components: a drainage basin, representing the source area for fresh water and sediments, a river or stream, forming a canal or valley which transports the material away from the drainage basin to a site of deposition, mostly located at the coast. The drainage basin is of great importance, as the nature and quantity of sediment produced directly controls the morphologic character of the river, and in further consequence also the morphologic character of the depositional realm. Rivers can be classified into five distinct patterns, 1) straight; and 2) sinuous patterns where little sediment is transported and the bed-load to total load-ratio as well as stream power is very low; 3) meandering patterns reflecting relatively low to moderate values in sediment transport, bed-load/total-load ratio and stream power; 4) meandering braided transitional pattern; and 5) braided pattern reflecting relatively high values in the abovementioned categories. For detailed description see Schumm (1985, Figs. 2, 3 and 4).

Deltaic distributary channel networks

The morphology of a distributary channel network sets the fundament on which nutrients, sediment and water are transported across the river delta and into its receiving basin (Ke et al. 2019). Those networks are very similar to alluvial channels in many categories, but are influenced by periodic fluctuations, mainly tides or other

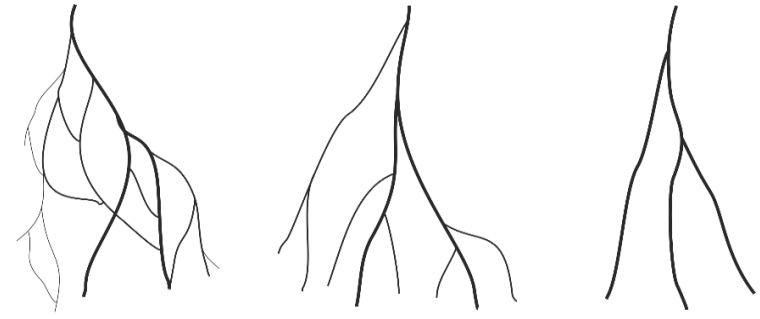

Figure 12: End-member distributary channel patterns (modified from Hart 1995).

sea level changes (Hart 1995). Three main types of distributary channel networks can be recognized on deltaic plains: 1) rejoining channel systems (Fig. 12a) show complicated patterns of bifurcation and rejoining channel segments with fewer active river mouths (Hart 1995); 2.) bifurcating channel systems (Fig. 12b), where the river starts to bifurcate upon entering the delta plain, leading to the development of many river mouths with different discharge values; and 3) straight channel systems (Fig. 12c) with few distributary channels, originating from a single point where the river enters the delta plain (Hart 1995).

Delta front estuaries

Estuaries can be defined as tidally influenced transition zones between marine and riverine environments (Schuchardt et al. 1999). Deposition in an estuarine setting is strongly affected by a complex combination of tidal processes, oceanic waves, river discharge, temperature, precipitation and local flora and fauna (Cliffton 1982). Estuary sedimentation is mostly dominated by tidal effects, shaping the estuary into tidal flats and channels. Two types of channels exist: 1) tidal channels extending below the lowest tides, and 2) runoff channels, which are graded to the lowest low tide (Cliffton 1982). Sediments in an estuarine environment consist of well-sorted fine sand and mud. The sand is mostly contributed by the ocean whereas the mud derives from the supplying river. Sediments show a tendency to become finer in proximal direction (Cliffton 1982). For detailed description of estuaries see Cliffton (1982) and Hart (1995).

Deltaic constructional processes

Deltas are the product of interplay between deposition by constructional processes and sediment reworking and redistribution by reservoir processes (Galloway & Hobday 1996). Deltaic facies reflect many depositional processes like overbank flooding and consequent levee and floodplain aggradation, channel migration, incision and filling as well as channel avulsion and crevassing.

River mouth deposition

River mouths mark a point where river-derived sediments disperse and contribute to the delta formation. They are the most fundamental element to deltaic systems and involve a variety of

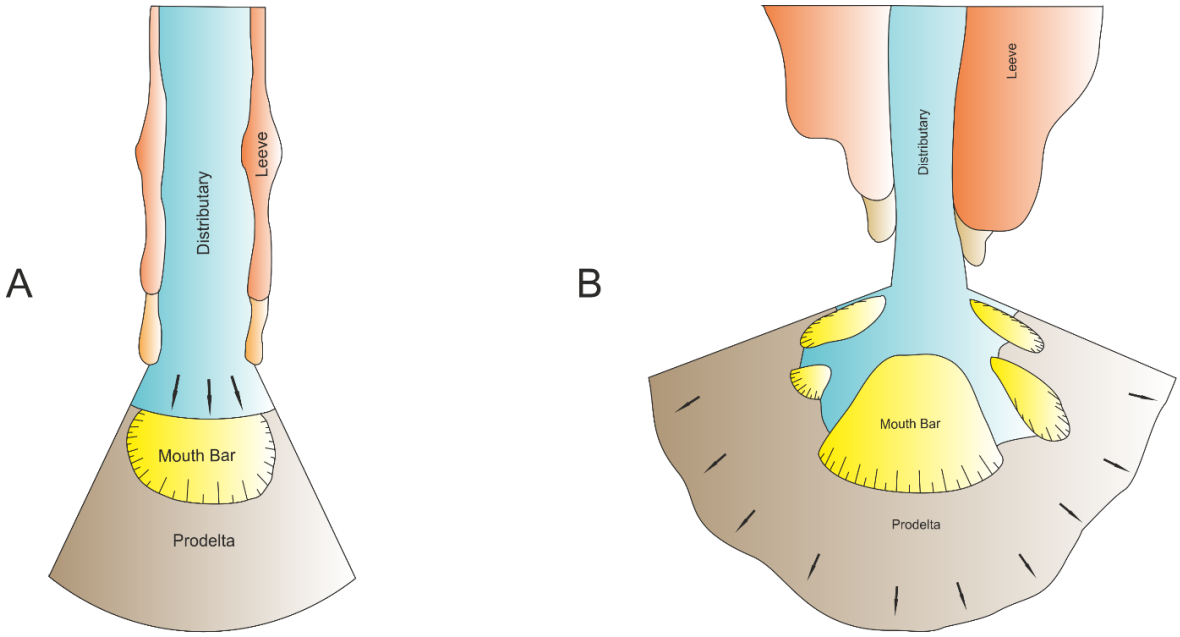

A: single lunate mouth bars, occuring where mud-rich distributaries enter deep water. Flow seperation concentrates

B: Complex radial mouth bars, occuring where sandy channels empty into shallow water. Friction dominated deceleration results in

Figure 13: Types of channel mouth-bars (after Galloway & Hobday 1996).

interactions between marine and riverine waters (Wright 1977). When a stream discharges from a confined channel into a reservoir, it spreads and mixes with the waters of the receiving basin (Galloway & Hobday 1996) marking the location where the degree of interaction between basinal and fluvial processes is the greatest. As the river leaves its confinement of the distributary channel, sediment transport and deposition are reduced (Hart 1995) and sediments distribute in a much wider array. The rate and geometry of the spreading and mixing flow depend on three basic criteria: 1) the momentum (function of velocity and density) of the discharged waters, 2) the density contrast between the mixing waters; and 3) bed friction, which is a function of reservoir depth at the channel mouth (Wright 1977). The discharge process sorts the sediments delivered by the river. Sand is concentrated at the channel mouth, fine sand and coarse silt are swept to the upper prodelta where they settle out of suspension. The finest suspended material (clay and silt) is moved basinward, forming the prodelta slope. Two types of channel mouth bars can be recognized: single lunate mouth bars occurring where mud-rich distributaries open into deep-water and complex radial mouth bars forming where sandy channels open into shallow water (Fig. 13) (Galloway and Hobday 1996, Fig 5.2 A&B).

Channel avulsion and lobe formation

Avulsions are primarily features of aggrading floodplains. It develops when a channel progrades basinward and the effective hydraulic head is continually reduced, decreasing stability with continued channel extension across a base level depositional surface (Galloway & Hobday 2006). Newly formed channels will always follow topography, occupying alternate courses with steeper gradients. Avulsions are not necessarily restricted to any particular river channel, and exist in any fluvial system as long as aggradation continues. Therefore, avulsion does not occur in floodplains where aggradation rates are zero or negative (Slingerland & Smith 2004). A distinction between two ranges of avulsion can be made, full and partial avulsion. Full avulsion implies that the parental channel was completely abandoned, whereas partial avulsion lead to new channels coexisting with the parental channel. Partial avulsion leads to anastomosing channels if the divided channels rejoin, and distributary channels if they do not rejoin. (Slingerland & Smith 2004). Fluvial deltaic systems develop over timescales of decades to millennia and are characterized by repeated lobe switching: a process where a channel progrades basinward and builds a lobe. Avulsion causes the channel to shift and produce a new lobe (Moodie et al. 2019). Deltas grow by repeated cycles of lobe development, which amalgamate to produce a composite landform (Moodie et al. 2019). The delta lobe, comprises facies of a river and its distributary deposits, marking the fundamental building block of highly constructional deltaic systems (Galloway & Hobday 2006).

3.5 Deltaic Environments

A delta, generally, is comprised of three main geomorphic environments of deposition. The subaerial delta plain, dominated by river processes, the delta front which is the area of interaction between river and basinal processes and the prodelta which marks the most seaward section of a delta, lying below low tide and receiving fluvial sediment. Those environments roughly represent the topset, foreset and bottomset strata of a delta (Fig 16) (Bhattacharya 2006).

3.5.1 Subaerial Portion of the Delta plain

The delta plain can be subdivided into an upper and a lower portion. The lower delta plain is marked by tidal incursion of seawater and the more landward upper delta plain is marked by the occurrences of major distributary channels and no influence of marine waters (Coleman & Prior 1982). It is defined by distributary channels and includes many nonmarine to brackish subenvironments like swamps, marshes, tidal flats, lagoons and interdistributary bays. The margin between upper and lower delta plain is referred as “bay line” (Posamentier et al. 1988) whereas the limit of the lower subaerial delta plain is either defined as high-tide shoreline or low-tide shoreline, including the foreshore (Coleman &

Prior 1982). Referring to lacustrine delta deposits, it is clear that lakes lack tides and therefore such a distinction between upper and lower delta plain cannot be made (Olariu & Bhattacharya 2006). Distributary channel fills reflect the condition of the supplying fluvial system and the classification applies to delta plain distributaries not modified by marine processes (Galloway & Hobday 2006).

The upper delta plain (Fig. 16) is unaffected by marine processes and most of the sedimentary deposits originate from migratory tendencies of distributary channels, overbank flooding, annual highwater periods and periodic breaks in riverbanks. The major depositional realms of the upper delta plain include (Coleman & Prior 1982): braided channel deposits, often characterized by dominant bedload transport of sediment, high downstream gradients, a large width-depth ratio and high variations in water discharge delta; meandering channel deposits most commonly associated with rivers displaying non-erratic flooding characteristics, high suspended-sediment load and low downslope gradient delta and lacustrine delta fill deposits where climate mostly defines the internal strata of the delta

The lower delta plain (Fig. 16) is defined by river-marine interaction and is located landward from the shoreline to the limit of tidal influence (bay line). Major deposits of this realm include: Bay-fill deposits are one of the major facies associated with many deltas. Crevasses or bay fills break off main distributaries and fill many interdistributary bays in the lower delta plain. Abandoned distributary deposits occur in deltas where channel migration can take place and the abandoned channels are filled by upstream and downstream sediments producing similar channel deposits as found in the upper delta plain (Coleman & Prior 1982).

3.5.2 Subaqueous Portion of the delta plain

The subaqueous part of the delta plain lies below the low-tide water level and is populated by relative open marine fauna (Coleman & Prior 1982). Water depths range from 50 to 300 m and sediments may extend from a few kilometers to tens of kilometers. It is often characterized by seaward fining of sediments, where sands and coarse clastics are deposited close to the river mouths and finer sediments settle offshore out of suspension. The most seaward section is mostly referred as prodelta and is composed of the finest material deposited. When sediments deposited seaward of the river mouth accumulate faster than subsidence takes place, progradation occurs with the effect that the subaerial deposits overlie the upper parts of the subaqueous delta forming a complete deltaic sequence. The subaqueous portion consists of three depositional realms: 1) distributary mouth bar deposits, where seaward flowing water leaves the channel and spreads into the ambient waters of the receiving basin; 2.) River-mouth tidal-ridge deposits where tidal processes disperse and redistribute fluvial clastic; and 3) subaqueous slump deposits where gravity induced mass movements are an integral part of the normal deltaic processes (Coleman & Prior 1982).

The Delta front (Fig. 16) is defined as the shoreline and adjacent dipping sea bed (Elliot 1986). It represents an area where coarser sediment (sand or gravel) is dominant and includes the subaqueous topset and foreset beds (Olariu & Bhattacharya 2006). The delta front is the proximal part of deposition where the sediment supplied to the delta from rivers accumulates most actively (Saito et al. 2001). Delta front environments include channel-mouth bars, wave reworked beach ridges, tidal inlets, estuaries and tidal flats. The delta front is affected far more by waves and tides then the other deltaic environments, thus reflecting most clearly the basin process setting and resulting delta type (Galloway & Hobday 1996).

Prodelta sediments (Fig. 16) represent the most seaward section of the subaqueous delta where mud and silt settle slowly out of suspension (Bhattacharya 2006). Prodelta silts and clays grade landward and upward vertically into the coarser silts and sands of the distal bar and form the foundation upon which the delta is constructed (Galloway and Hobday 1996). The coarsest deposits lie directly at the mouths of active distributary channels commonly referred as “distributary-mouth-bar deposits”. Those

deposits represent one of the major sand bodies within the deltaic realm. For detailed description see Coleman & Prior (1982).

3.6 Process classification of delta systems

Galloway (1975) identified three parameters determining delta geometry and sediment distribution (Fig. 14): 1) Sediment input, 2) Wave energy flux, and 3) Tidal energy flux. The geometry and features of the progradational framework are largely derived from the interplay between fluvial sediment input and wave and tidal components of reservoir energy flux (Galloway & Hobday 1996). Marine deltas can therefore be characterized in terms of three end-members: 1) fluvial dominated deltas, 2) wave-dominated deltas and 3) tide-dominated deltas. Each process determines the distribution of environments and facies geometry of a delta (Galloway 1975) leading to basic similarities retained in a broad range of basin settings (Galloway & Hobday1996). Fluvial dominated deltas often show elongate to irregular lobate areal geometries, wave dominated deltas show cuspate to lobate outlines and tide dominated deltas have irregular lobate and pseudoestuarine outlines (Galloway & Hobday 1996).

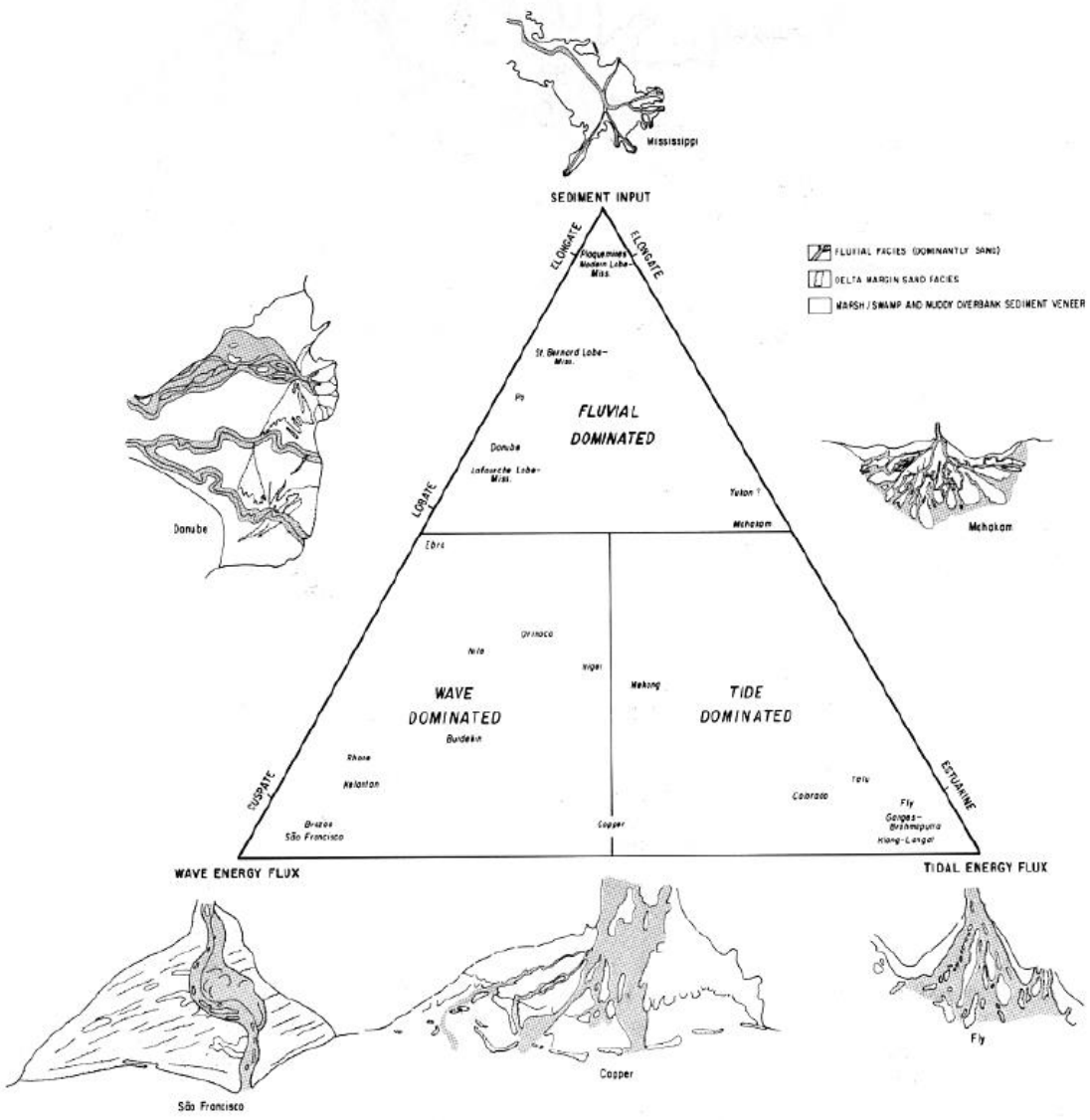

Figure 14: Morphologic division of delta systems based on relative influence of wave, riverine and tidal processes (after Galloway 1975).

3.6.1 Fluvial-dominated deltas

Commonly characterized by a sheet-like sediment body, deltas which are strongly fluvial dominated, result from high sediment input and low-energy shelf processes. This produces coalesced mouth bars. Those mouth bars are likely to be sandy. With increasing distance from the channel-axis deposits are increasingly likely to be mudprone. This leads to finger like sandstone isopach in the lower delta plain and the shallow delta front. The delta plain of fluvially dominated deltas adapts the character of the fluvial system. Three main types have been recognized: rivers, braidplains and alluvial fans, forming the corresponding delta type (Emery & Myers 1996). The facies architecture of fluvial dominated deltas is characterized by several aspects: 1) The major portion of vertical sequences through the delta-plain is dominantly progradational, as shown by characteristic upward-coarsening textural sequences; 2) The upper portion, or sometimes all of the progradational section is locally cut out and replaced by distributary channel network fills; 3) Progradational mouth bar and distributary channel sands form a highly divergent, in most cases dip-oriented permeable sand framework of the component lobes of the delta system; 4) Sediment accumulation is autocyclic; and 5) lateral continuity of the sand and encasing mud facies is limited (Galloway & Hobday 1996).

3.6.2 Wave–dominated deltas

In this type of delta, most bed-load initially deposited at the distributary mouths is reworked by waves and redistributed at the delta front by longshore drift (Galloway & Hobday 1996). This type of delta is characterized by straight coastlines and shore parallel sand isopaches. Fairweather waves move sediments onshore and provide a barrier to its offshore transport. The sand is redistributed to the inner shelf to increase the shore-perpendicular width of coastal sands (Emery & Myers 1996). Facies architecture is pretty similar to fluvial dominated systems, although wave dominated deltas are under greater influence by marine processes. Shelf and prodelta muds grade into an upward coarsening sequence of delta front beach-ridge sands. In actively subsiding basins, cyclic lobe progradation and abandonment can produce stacked sequences of beach-ridge sands (Galloway & Hobday 1996).

3.6.3 Tide-dominated deltas

Tidal currents produce multiple coeval channels at the delta front and result in finger-like irregular sand isopach. Depending on tidal influence, the signature may penetrate deep into the delta plain and enable the formation of tidally influenced lagoons, tidal flats and creeks. The strongest tidal influence is located at the upper portion of the delta front and in the lowermost delta plain (Emery & Myers 1996). With increasing tidal range, tidal currents increasingly redistribute bed-load sediment and modify distributary mouth geometry. Sediment transport is mostly in dip-direction, where it moves out of the channel mouth and then is deposited onto an extensive shoal-water prodelta platform which is characteristic for tide-dominated deltas. Channel-mouth bars are reworked into elongate bars, extending from the channel mouth onto the upper delta-front platform. Delta plain geometry is irregular or estuarine (Galloway & Hobday 1996).

3.7 Sandwaves

Submarine dunes and sand waves are situated in the deep seafloor and shallow-water continental shelves and many other depositional systems like e.g. lacustrine environments. The formation and evolution of sandwaves is controlled by the predominant hydrodynamic conditions in the area. Their migration can be caused by many factors, such as residual currents, tidal asymmetry, wind-induced currents and storms. Two distinct spatial scales can be recognized: giant sand waves with a height of ~15 m and a length of 750 m and small sand waves with a height of ~1.5 m and a length of 30 – 100 m (Bao et al. 2020)

4. Sequence stratigraphic concepts

Sequence stratigraphy is a methodology that provides a framework for the elements of any depositional setting, facilitating paleogeographic reconstructions and the prediction of facies and lithologies away from control points (Catuneanu 2011). The main tool used in sequence stratigraphy is the stacking of pattern of strata and the key surfaces which they terminate against, defined by different stratal stacking patterns. Trends in geometric character, defining stratal stacking patterns, include upstepping, forestepping, backstepping and downstepping. A sequence stratigraphic framework may consist of three different types of sequence stratigraphic units: sequences, systems tracts and parasequences. A sequence is defined as a relative conformable succession of genetically related strata bounded by unconformities of their correlative conformities (Mitchum et al. 1977). In general, a sequence corresponds to a full stratigraphic cycle. This specification is important to separate a sequence from component system tracts. Systems tracts and Parasequences are briefly explained in the following. For detailed information see Catuneanu (2006), Catuneanu et al. (2011).

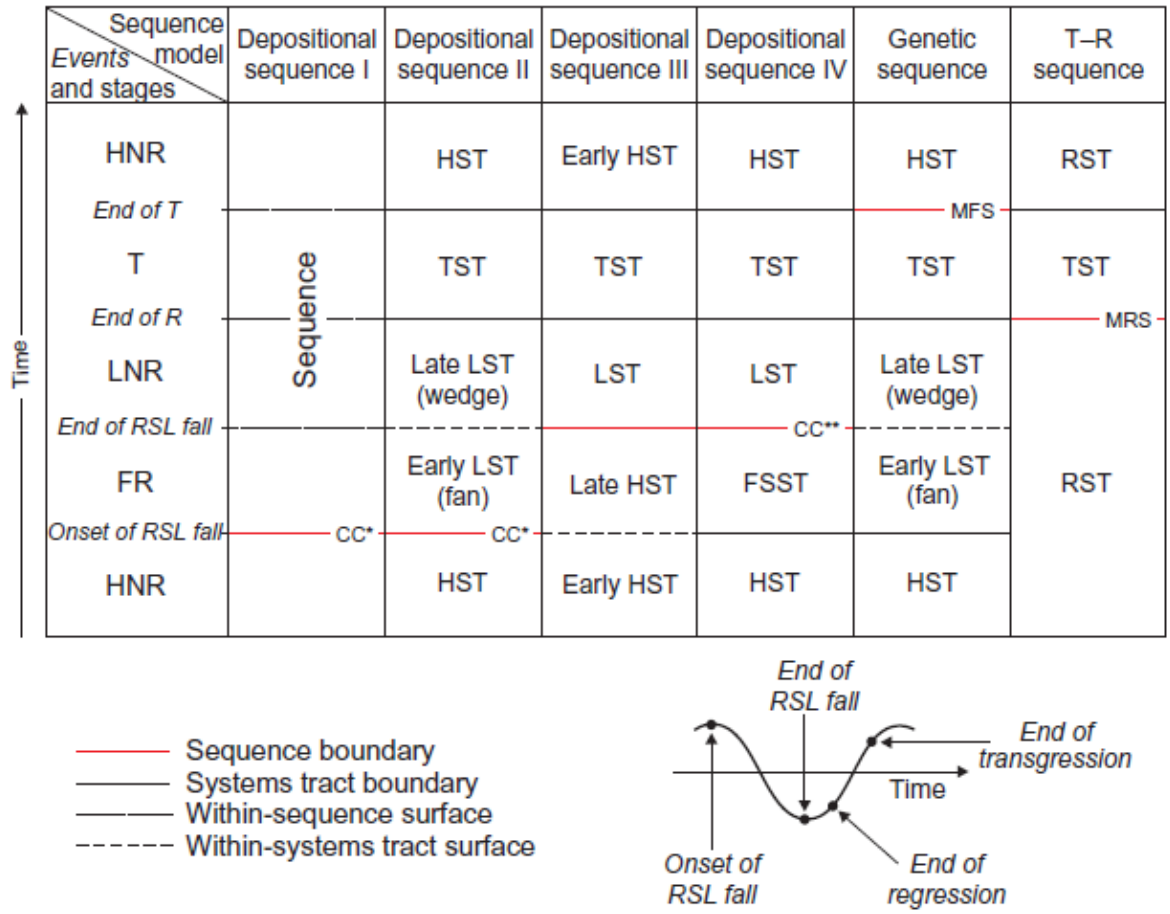

Figure 15: Nomenclature of system tracts, and timing of sequence boundaries for the various sequence stratigraphic approaches. Abbreviations: RSL = relative sea-level, T = transgression, R = regression, FR = forced regression, LNR = lowstand normal regression, HNR = highstand normal regression, LST = lowstand systems tract, TST = transgressive systems tract, HST = highstand systems tract, FSST = falling stage system tract, RST = regressive system tract, T -R transgressive regressive, MFS = maximum flooding surface, MRS = maximum regressive surface. (Catuneanu 2011)

4.1 Accommodation:

Accommodation defines the space available for sediments to fill. It may be modified by the interplay between various independent controls which may operate over a wide range of temporal scales. Marine accommodation is primarily controlled by basin tectonism and global eustasy. Changes in marine accommodation are referred to as relative sea-level changes. Fluvial accommodations respond

to changes in marine accommodations within the downstream portion of the fluvial system, and to changes in discharge, gradient and sediment supply that may be controlled and/or source area tectonism within the upstream portion of the fluvial system. Depositional trends of aggradation, erosion, progradation and retrogradation can be explained by changes in accommodation or by the interplay between accommodation and sediment supply. Positive accommodation indicates sediment aggradation and negative accommodation results in downcutting. During stages of positive accommodation, excessive sediment supply results in progradation, whereas underfilled accommodation results in retrogradation.

4.2 Systems tracts

A systems tract is "a linkage of contemporaneous depositional systems, forming the subdivision of a sequence" (Brown & Fisher 1977). This definition is completely independent of spatial and temporal scales. They consist of a relatively conformable succession of genetically related strata bounded by conformable or unconformable sequence stratigraphic surfaces and are interpreted on a basis of types of bounding surfaces, position within the sequence and stratal stacking patterns. Typically, there are two distinct types of systems tracts, depending on a possible genetic link to coeval shorelines. Here only shoreline-related system tracts are discussed.

Shoreline related systems tracts can be linked to particular types of shoreline trajectory (forced regression, normal regression, transgression) and may be observed at different scales. They are normally linked to specific phases of the relative sea-level cycle. The most important systems tracts are discussed below (after Catuneanu 2006)

- **The falling stage systems tract (FSST)** is comprised of all regressive deposits, which accumulate after the relative sea-level fall and before the start of the next seal-level rise. It occurs during forced regression and is capped by the overlying lowstand systems tract (LST). Many different parasequence stacking patterns might be produced during the FSST. Posamentier et al. (1988) defined this systems tract as "lowstand fan" (Fig. 16)
- **The lowstand systems tract (LST)** include all deposits that accumulate after the beginning of relative sea-level rise and overlie the FSST deposits during normal regression. Characteristic stacking patterns include forestepping, aggrading clinoforms and a topset of fluvial-, coastal- or deltaplain deposits. Often LST sediments infill incised valleys that were cut into the highstand systems tract (HST) and other early deposits during forced regression. Accomodation space is created by the rising base level and a lowstand wedge, which can be compromised of basically all depositional systems (shallow-marine, deep-marine, fluvial to coastal (Fig. 16).
- **The transgressive systems tract (TST)** includes the deposits which were accumulated from the onset of transgression until maximum regression of the coast. It lies directly on the maximum regressive surface (end of regression) and is overlain by the maximum flooding surface (MFS), which forms when sediments reach their most landward position. Typical stacking patterns display retrogradational clinoforms thickening landwards, backstapping patterns and onlaps (Fig. 16).
- **The highstand systems tract (HST)** is deposited in the late stages of sea-level fall, progradational deposits develop when sediment accumulation rates exceed the rate of increase in accommodation. The HST lies directly on the MFS and stacking patterns illustrate prograding and aggrading clinoforms, which are typically capped by a topset of fluvial-, coastal-, or deltaplain deposits. (Fig. 16)

4.3 Parasequences

Compared to sequences and systems tracts, which normally can be mapped across an entire sediment basin, parasequences are geographically restricted to the coastal and shallow-water areas where marine flooding surfaces may form (Posamentier & Allen 1999), e.g. prograding coarsening upward lobes. Parasequences usually modulate the higher order building blocks of coastal pro- and retrogradation and can often be placed in larger scale systems tracts. They are commonly separated from other parasequences by flooding surfaces, and are represented in well-logs by fining- or coarsening upward sediment cycles. The flooding surfaces mark an abrupt change in grain size, which is associated with marine and/or lacustrine processes, such as waves and currents. These abrupt changes in grain size make it easy to recognize parasequences in well-logs (Catuneanu 2006)

4.4 Delta stratigraphy:

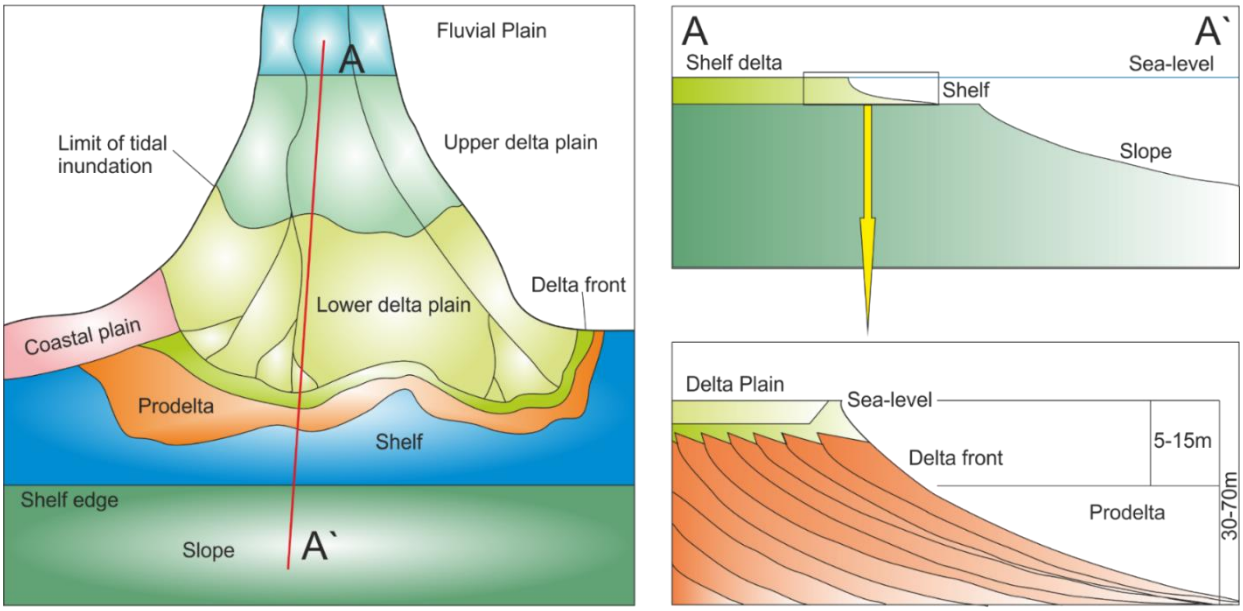

Delta terminology after Coleman and Prior 1982

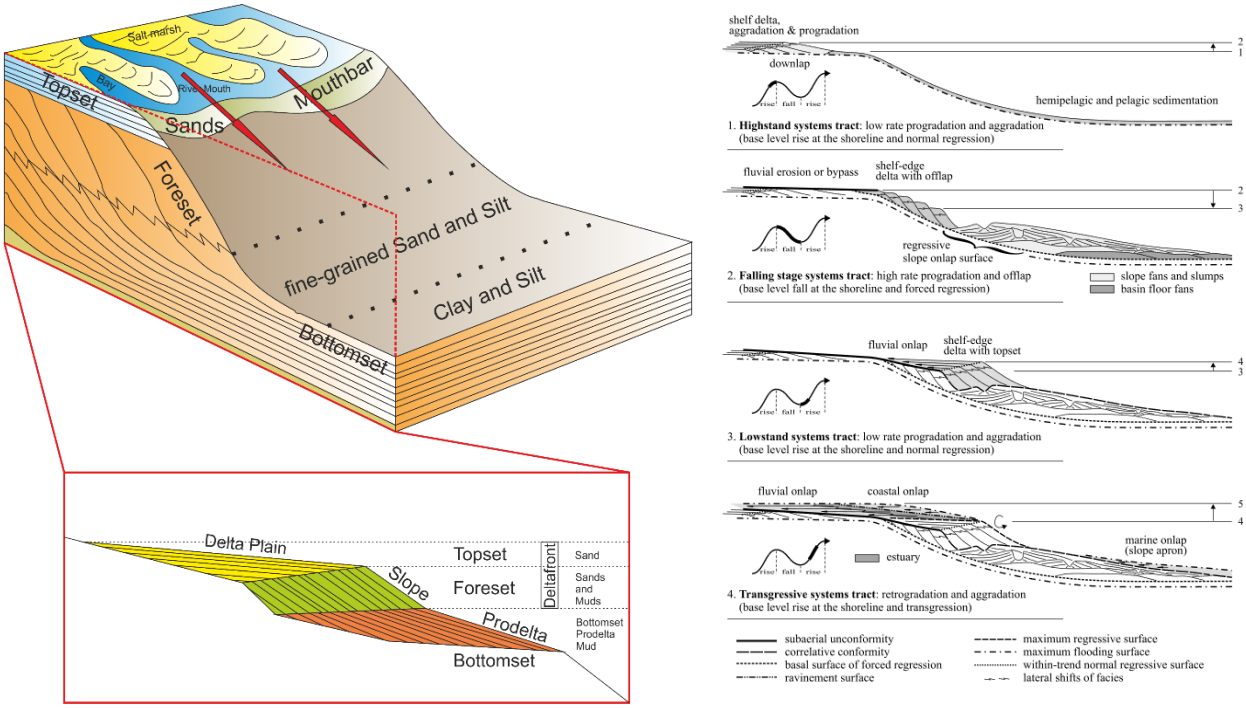

Figure 16: Terminology (A) and stratigraphic model (B) for deltaic environments modified after Coleman & Prior (1982) (See chapter 3.5 for details). (C) Terms needed to describe a deltaic environment. (D) System tracts model after Catuneanu (2006) (see chapter 4.2 for details)

5. Methodology

5.1 Data

All processed digital data were provided by OMV Exploration and Production GmbH and handled according to their privacy policy. In total one seismic volume, 10 wells and an already mapped horizon were used in the seismic interpretation with the software Petrel. For detailed information about reflection seismic see Brown et al. (2004)

5.1.1 Seismic volume

The investigated area is bound by a 3D seismic volume (Cropped_3D_VBSM_PSDM_Pannon) provided by OMV (fig 17), depicting the Neogene basin fill in the central Vienna Basin. The block is 45 km long and 25 km wide, amounting to an area of 1125 km^2 and represents a small part of the Vienna Basin Supermerge (VBSM), where seismic data of several seismic vintages (1994-2013) was merged to an approximately 1800 km^2 seismic survey (Siedl et al. 2020). Z – coordinates are expressed is TVD (true vertical depth) and show approximate true values, making them serviceable for in-seismic measurements. cross-lines represent SW-NE oriented sections and Inlines are oriented NW-SE.

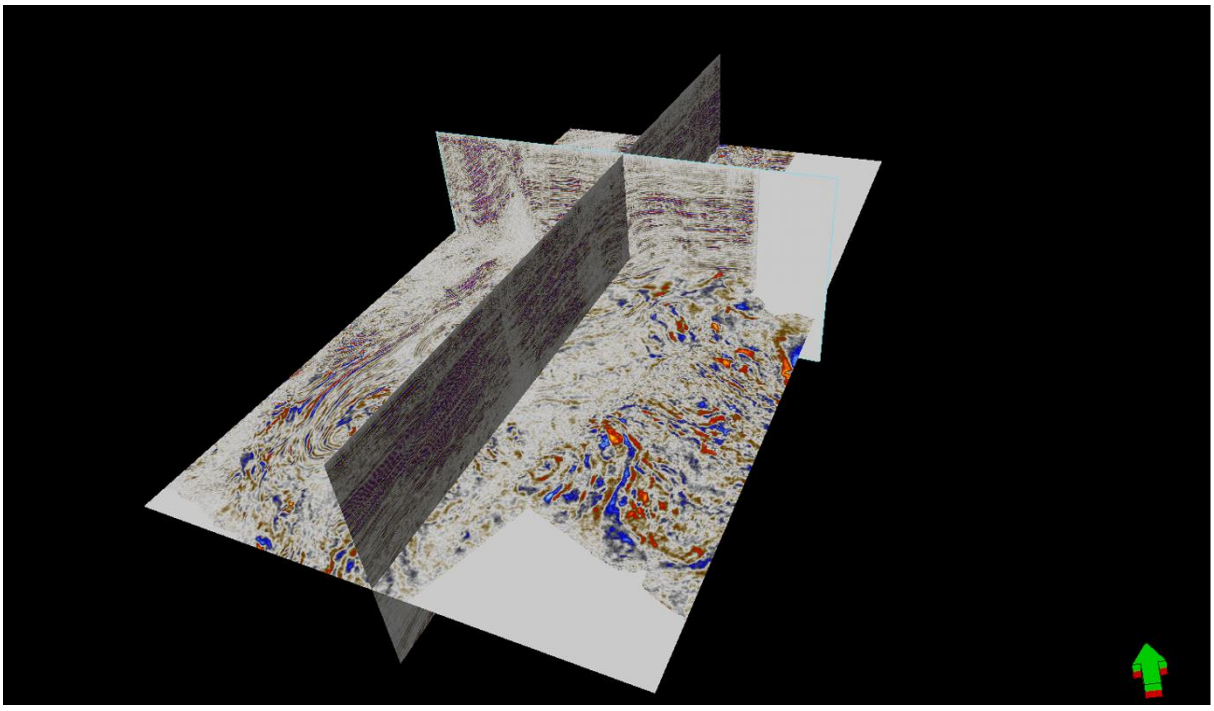

Figure 17: The investigated seismic block

5.1.2 Wells

Ten boreholes and their well-log patterns of the central Vienna Basin were investigated; Matzen 201, Matzen 101, Prottes 008, Spannberg 002, Spannberg 006, Zwerndorf 004, Matzen 128, Tallesbrunn 016, Matzen 190 and Bockfließ 013 (Fig. 1) were identified, interpreted and correlated to recognize transgressive and regressive patterns as well as different electro-facies trends throughout the well-log data. Well-log data was provided by OMV and mainly include petrophysical data (Spontaneous Potential [SP] and conventional resistivity [Ω]). These observations were correlated to the existing age model of Harzhauser et al. (2004) (Fig. 5) to implement a sequence stratigraphic model.

5.1.3. Reference Horizon

An already mapped seismic horizon named 5UP_IG was provided in the form of a calculated surface (Fig. 18). This surface defines a stratigraphic horizon interpreted as the Sarmatian/Pannonian boundary. This boundary was the lowermost part of the investigated areas

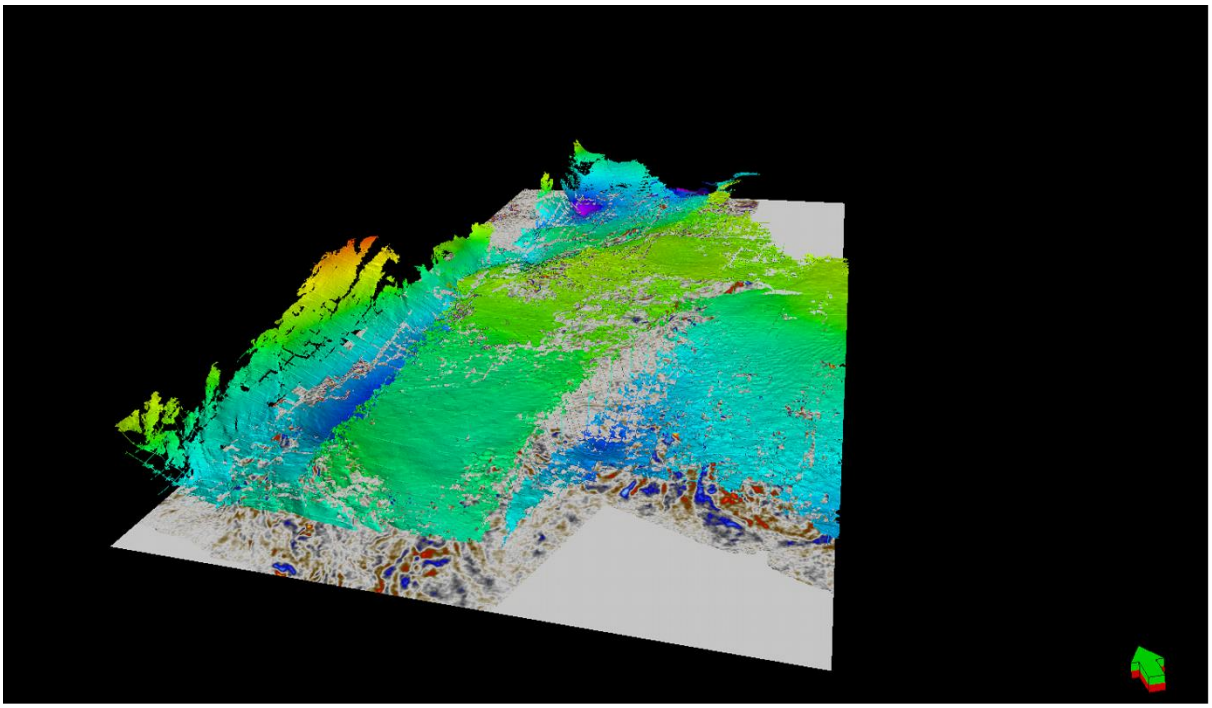

Figure 18: Reference Horizon 5UP_IG, provided by OMV

5.2 Use of the software Petrel

5.2.1 Analysis of the 3D block

The first step upon receiving the seismic survey was an initial scrolling through the data (side to side, front to back, top to bottom) in order to assess the overall structural and stratigraphic style and to determine what working hypotheses are geologically reasonable for the data set. Following this first step, areas of interest, where characteristic seismic bodies are located, were highlighted and restrained in space by inserting a box probe, which is a tool to limit the block to a desired size to decrease the time the program needs to calculate properties (Fig. 19). Theses boxes were further investigated and deltaic deposits were highlighted, if possible on cross -lines, inlines and in the Z-plane. To define the seismic bodies as of deltaic nature, seismic stratal patterns and general deltaic depositional features like foreset, topset and bottomset accommodations were identified and highlighted (Fig. 16). After identification of the deltaic structures seismic horizons were drawn on a reflector, which corresponds to the maximum flooding surface, marking the onset of the Pannonian deltas after Harzhauser et al. (2004) (C1 in Fig. 6). The next step was to create a surface, which is necessary to (a) flatten the horizon and (b) to determine the margin of a horizon. The mapped surfaces were flattened and structures of interest were highlighted. These flattened horizons correspond to a horizon slice, which then can be used as a tool for interpretation.

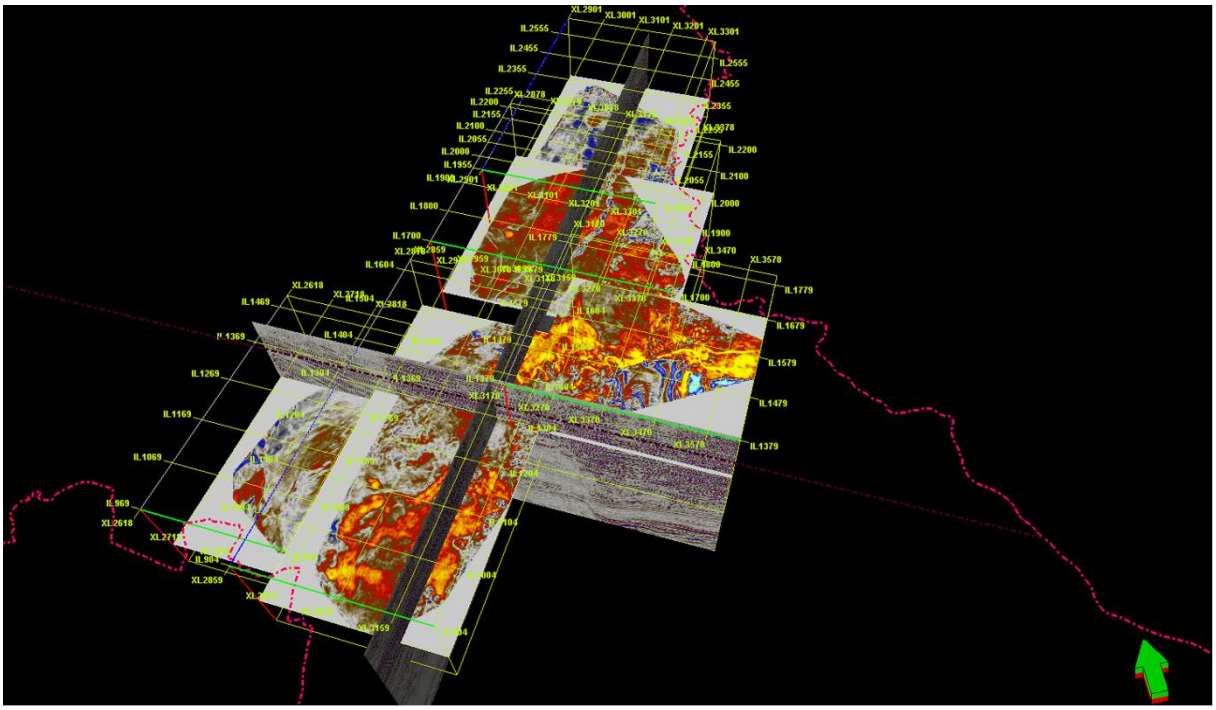

Figure 19: Box probes within the seismic block. Each probe corresponsds to one of the investigated areas (from south to north: Gr. Engersdorf, Aderklaa, Zwerndorf, Matzen, Zistersdorf)

5.2.2 Horizon picking:

The first- and most-time-consuming step is to locate a horizon of interest. The lower boundary of interpretation is marked by the 5UP_IG horizon provided by OMV. Above this horizon a characteristic continuous reflector was found, which corresponds to the onset of the Pannonian deltas, and shows a high positive amplitude. High amplitudes are indicated by a red colour and low amplitudes by a blue color respectively. These values are obtained by displaying the seismic through the property template *Seismic (default) 1*. This reflector was highlighted and followed in order to establish an appropriate horizon interpretation grid (Fig. 20). In general Petrel provides different features for horizon interpretation like manual tracking, seeded 3D autotracking and guided autotracking. Manual tracking was usually applied for this work because the other options can yield very unsatisfying results, especially in the further steps because often those tools jump between reflectors. For a successful manual tracking the interpreter has to follow the chosen horizon and redraw it manually. For guided autotracking the interpreter chooses two points on a reflector and the interpretation automatically follows the event between these points. For 3D seeded autotracking the interpreter has only to click the reflector and the program will trace the reflector in 3D as far as possible, basically creating a surface. The result of the abovementioned process is a 3D grid indicating the TVD (true vertical depth) of the interpreted horizon at a certain position. (Fig. 20)

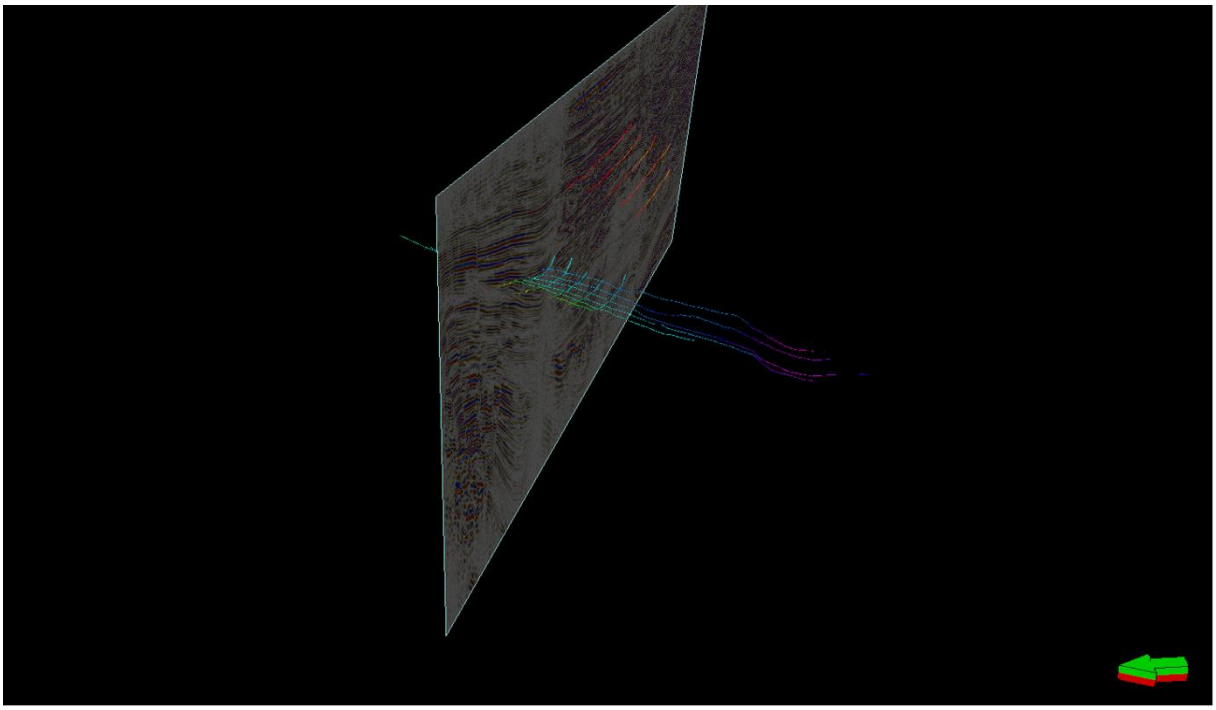

Figure 20: Example of the mapping process, 3D – grid drawn on the base reflector.

5.2.3 Make surface

To establish a surface, the recently created horizon grid, has to be displayed in a 2D window, so that the Paintbrush tool can be used. This tool tries to connect all points of the horizon grid and clearly shows if the surface is continuous or major gaps arise. If the surface is continuous the surface will be illustrated as a smooth plane without gaps (Fig. 21), whereas areas that cannot be traced by the Paintbrush tool (the reflector is not recognized laterally anymore) are just left out black. In a subsequent process using the make/edit surface utility in Petrel, the created grid can be used to calculate a comprehensive result surface (Fig. 22). This surface can now be displayed in 2D and 3D and be used to create a horizon slice.

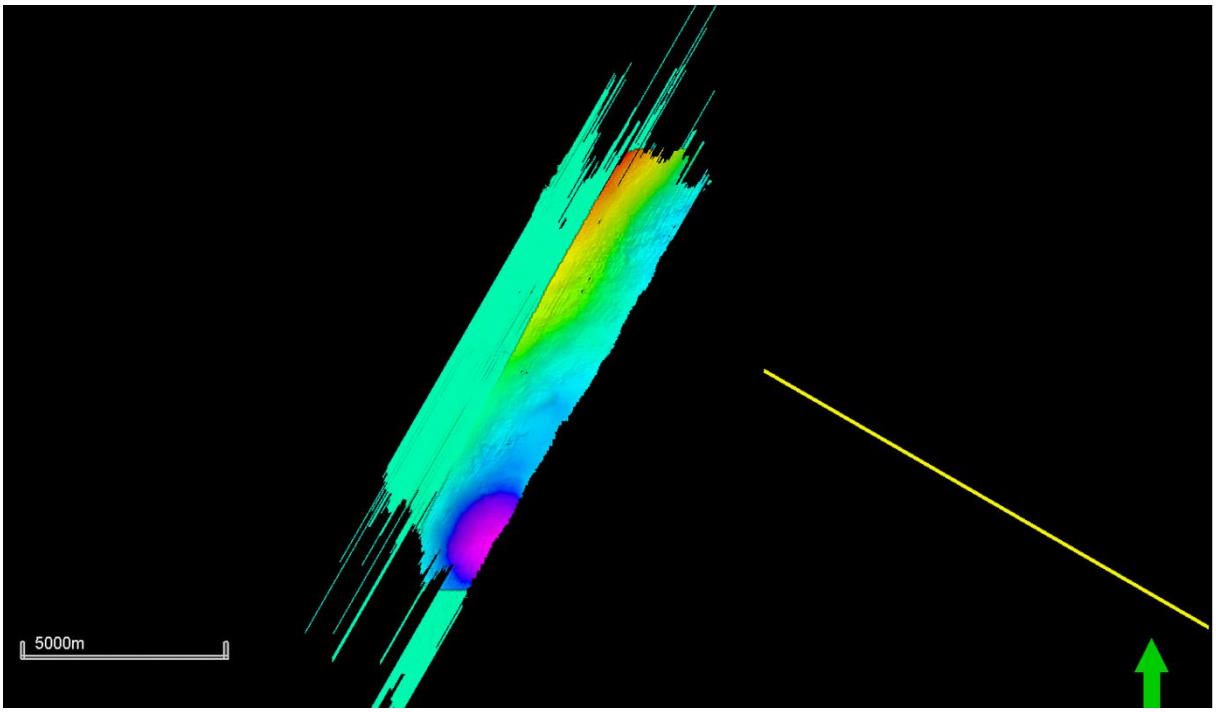

Figure 21: Creating a surface with the Paintbrush tool.

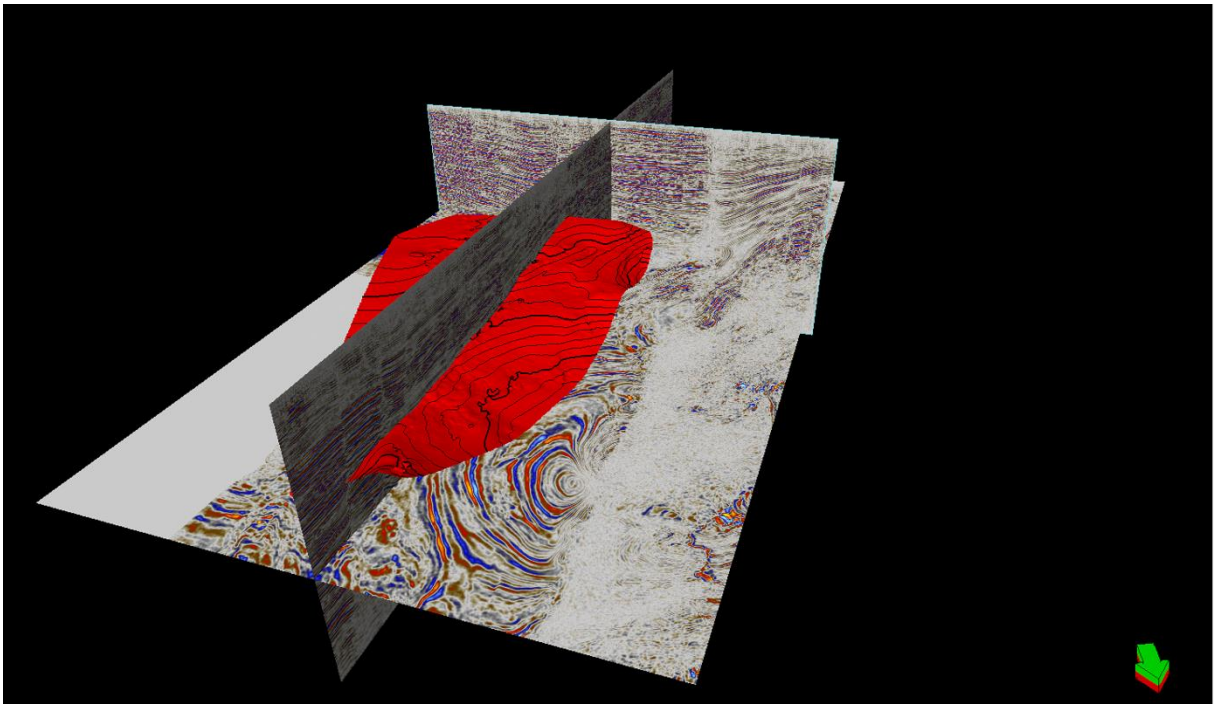

Figure 22: Calculated result surface in the Matzen region

5.2.4 Horizon Slices

Horizon slices enhance the visualization of geomorphologic and depositional elements of specific paleodepositional surfaces, by picking the geological horizon of interest as described above. If the interpretation of seismic reflections is correct, the slices should be very close to time lines, providing a snapshot of past depositional environments. To create a horizon-slice the reference surface has to be flattened before attributes can be extracted. This work uses solely amplitude extraction to depict the deltaic bodies as well as paleochannels that might occur, where blue marks negative amplitudes and red positive amplitudes (Fig. 23).

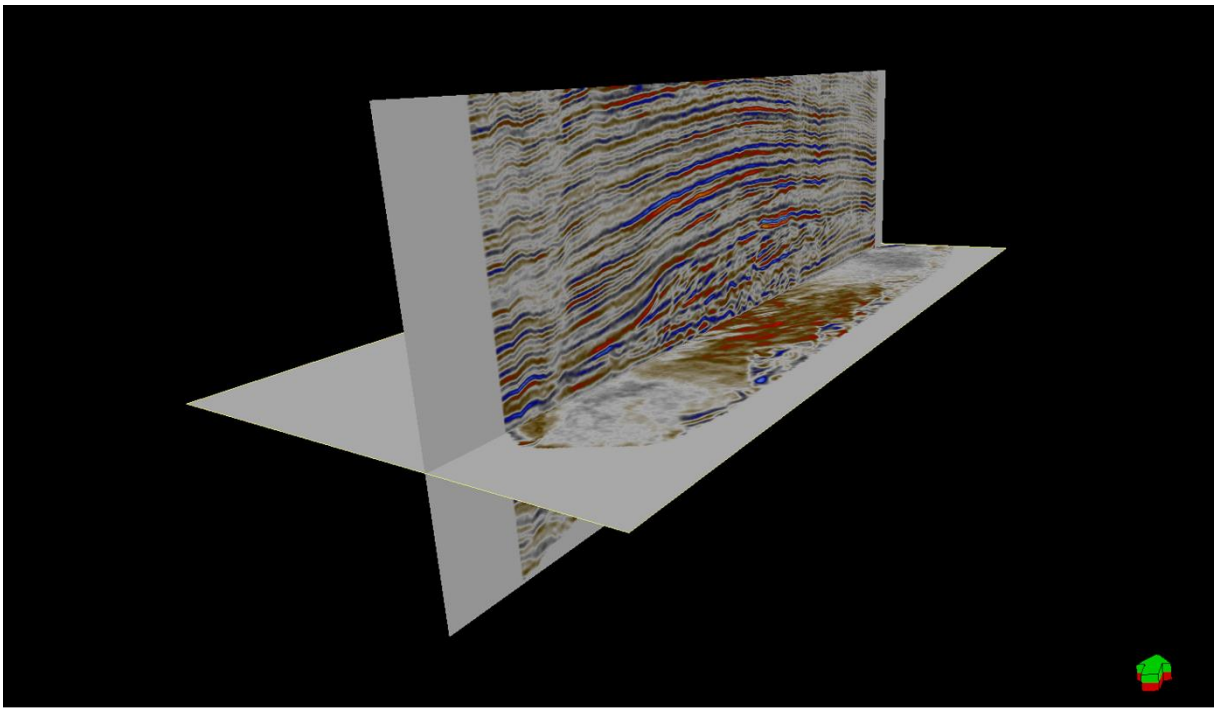

Figure 23: Horizon slice flattened on a reference horizon (MFS) in the Gr. Engersdorf area

5.2.5 Reflection patterns

Seismic facies can be mapped as a 3D seismic unit composed of groups of reflections whose parameters differ from those of adjacent units (Mitchum et al. (1977). Such facies can be analyzed by interpreting seismic reflection parameters like configuration (reflection geometry), continuity, amplitude, frequency or interval velocity in a depositional sequence. Three main groups of reflection configuration patterns are recognized: parallel reflection patterns (including sub-parallel and divergent) and discontinuous and prograding reflector patterns. Parallel, subparallel, as well as wavy reflections indicate uniform deposition rates expected on a uniformly subsiding surface like a shelf or a basin plain, while divergent patterns imply lateral variations of depositon rates or tiliting of a deposition surface. Hummocky patterns might indicate point bars or crevasse splays while chaotic configuration patterns indicate coarse-grained fluvial or turbidite channel fills. (Fig. 24) These patterns were mainly used in the early stages of the workflow, when the general stratigraphic style was assessed.

5.2.6 Reflection termination patterns:

Reflection terminations are characterized on a 2D seismic section by the geometric relationship between the reflection and the seismic surface they terminate against (Mitchum et al. 1977). To describe those reflection terminations the following terms are used: truncation, toplap, onlap and downlap (Fig. 25). Lapout is the lateral termination of a reflector at its depositional limit. Conversely, truncation implies that the reflector originally extended further but has either been eroded or truncated. Baselap is the lapout of reflections against an underlying seismic surface and can consist of an onlap (when the dip of the surface is greater than the dip of the overlying strata) or a downlap (when the dip of the surface is less than the dip of the overlying strata). Downlaps are commonly seen at the base of a prograding clinoforms and usually represent progradation of a basin-margin slope system into a deep-water or lacustrine system. Onlaps are defined as the termination of low-angle reflections against a steeper seismic surface. Toplap is the termination of inclined clinoforms against an overlying lower angle surface, possibly representing the proximal deposition limit. Reflection

termination patterns were used to understand the relation between the distinct deltaic deposits and to argue their geographic development through time.

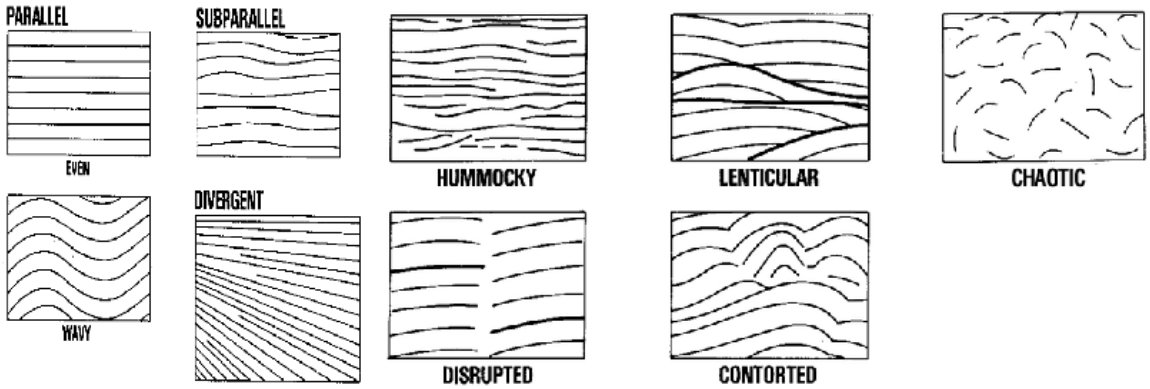

Figure 24: Types of parallel (parallel, subparallel, divergent) and discontinuous (hummocky, disrupted, lenticular, contorted, chaotic) reflection patterns, modified after Mitchum et al. (1977).

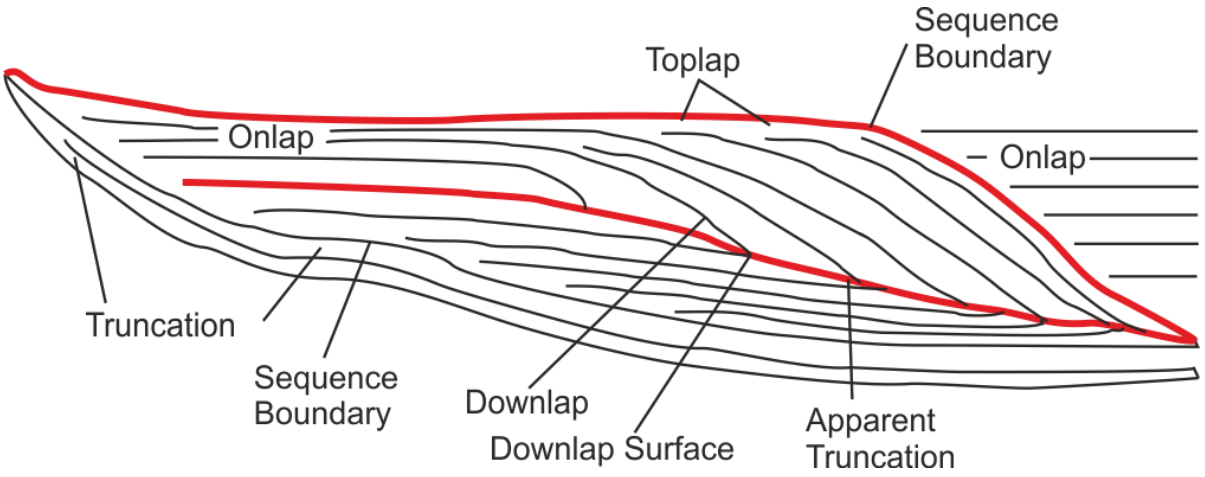

Figure 25: Stratal termination patterns, modified after Emery & Myers (1996).

5.3 Well-log analysis

Well-logs represent geophysical recordings of various rock properties in boreholes and can be used for geological interpretation. The log types which were used for this study are spontaneous potential and conventional resistivity. Spontaneous potential (SP) is measured in millivolts and measures the natural electric potential relative to the drilling mud. It allows interpretation of lithology, correlation, curve shape and porosity analysis. For interpreting SP-logs, first a shale base line has to be defined, which marks the typical SP level for shales and can be obtained by comparing the SP log with the Gamma Ray (GR) log response. From this line formations will express various intensity to the left or right of this line. Conventional resistivity is measured in Ohm (Ω) and measures the resistance to electric current flow. We analyzed well-log trends and compared them to the age model of Harzhauser et al. (2004). In general, five distinct idealized log trends are defined (cleaning-up- or funnel-trend, dirtying-up-, or bell-trend, boxcar- or cylindrical trend, bow- or symmetrical trend and irregular trend; fig. 24). Funnel trends indicate an upward decrease in spontaneous potential (SP-log), representing either a change in lithology or a gradual change in the proportions of thinly interbedded units below the resolution of the logging tool. The bell trend illustrates an upward increase of spontaneous potential, related to a gradual upward change in the clay-mineral component, implying a decrease in depositional energy. Boxcar trends have an internally relatively constant SP-log reading and their boundaries to the over- and underlying unit are very abrupt. They are typical of some types of fluvial channel sand, turbidites

and deltaic deposits. A bow trend consists of a funnel trend and a bell trend with a clear separation between those two. Bow trends are often the result of a decrease in sedimentation rate in a basinal setting, where the sediments are unconstrained by base level, which leads to thicker progradational and thinner transgressive units. Irregular trends show no clear trend away from the base-line and represent aggradation of shaly or silty lithology, typical for shelf or deep-water settings, lacustrine successions or muddy alluvial overbank facies (Emery & Myers 1996).

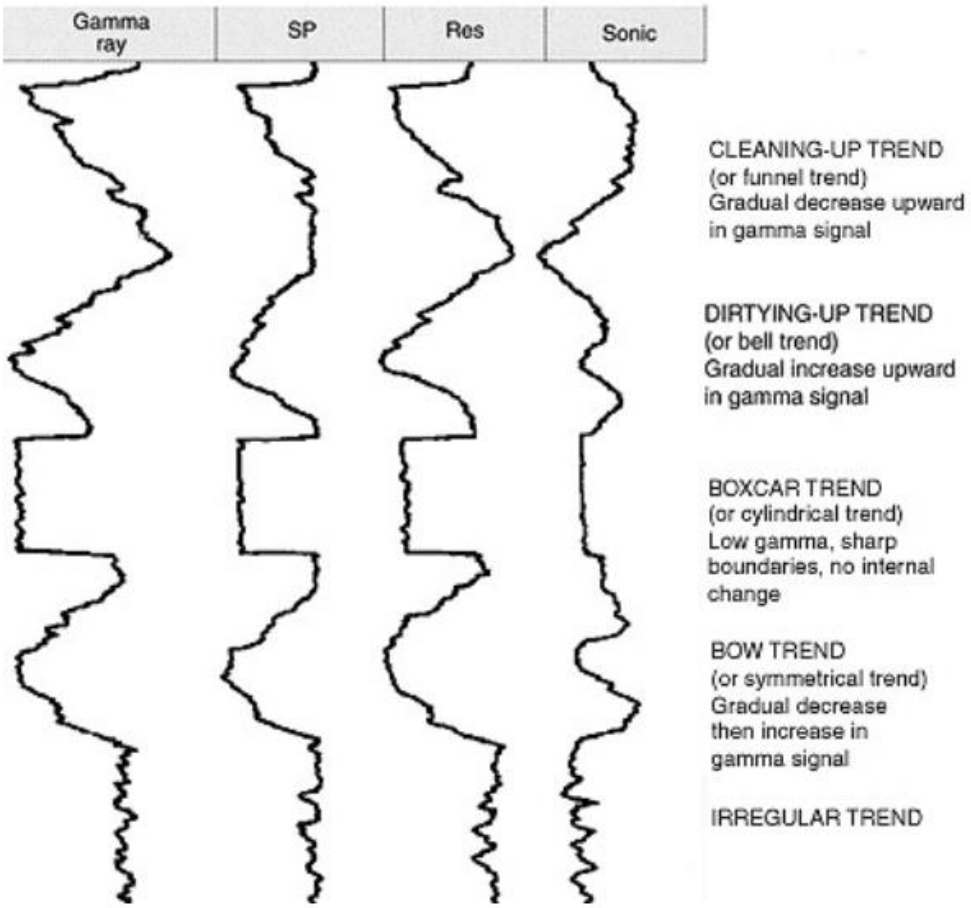

Figure 26: Idealized log trend after Emery & Myers (2000), assuming saltwater porosity.

6. Results

6.1 Well-Log Analysis

Ten well-logs of the central Vienna Basin were investigated: Matzen 201, Matzen 101, Prottes 008, Spannberg 006, Spannberg 002, Zwerndorf 004, Matzen 128, Tallesbrunn 016, Matzen 190 and Bockfließ 013 (Fig.1). All SP well-logs show a clear subdivision in a lower serrated part followed by a general funnel pattern which reflects a general progradation trend. This major change in well-log-patterns is generally interpreted as the Sarmatian/Pannonian boundary and the onset of the Pannonian paleo-Danube delta and serves as an interpretational base for this study. The upper limit is marked by a general change in well-log-patterns, where a transition to ultra-serrated irregular trends displays a change from a generally prograding system to a generally aggrading system. These observations serve as a base and argumentation tool, for a correlation with the existing age model of Harzhauser et al. (2004).

6.1.1 Well-Log description

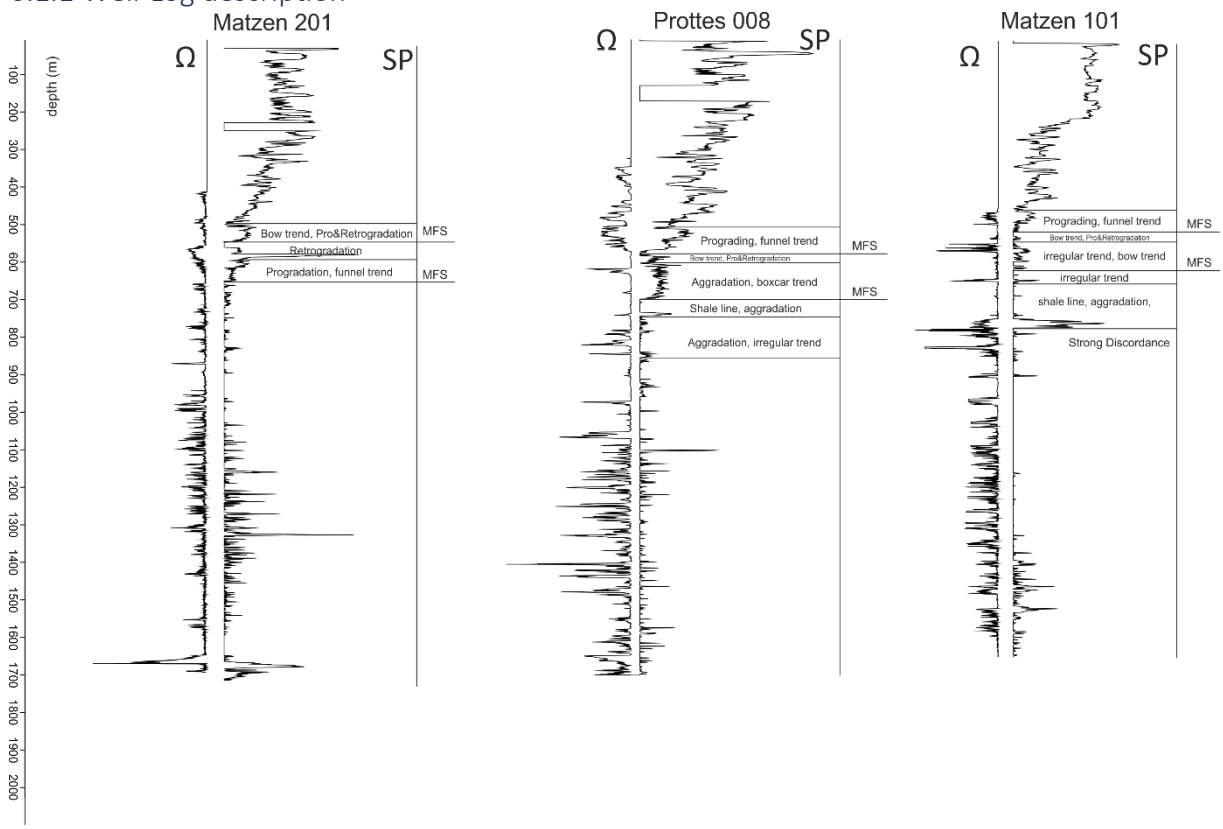

Figure 27:Well-log-trend interpretation for the wells Matzen 201, Prottes 008 and Matzen 101. MFS = maximum flooding surface

The well Matzen 201 shows a serrated trend up to 650 m depth which is interpreted as aggradational, before a funnel trend, indicating progradation, can be obtained. This progradational trend is continuous up to 590 m depth, and is followed by a bell trend which portrays retrogradation. In this interval, which ranges from 690 m to 670 m depth, an uncharacteristic strong peak is recognizable at 580 m depth. After the retrogradation, a clear bow trend can be observed hinting to a pro- and retrogradation occurring in this succession. Between those two uppermost intervals, the change from this bell trend unit (retrograding) and the bow trend unit (pro- and retrograding) indicates a flooding surface.

The irregular serrated trend, depicting aggradation, which ranges up to 650 m depth in the well Matzen 201 is also detected in the wells Prottes 008 (up to 850 m depth) and Matzen 101 up to 730 m depth.

The signal from well Prottes 008 continues this irregular trend from 850 to 740 m depth, before a strong peak at 730 m depth occurs. This peak is followed by a shale-line illustrating retrogradation, ranging from 730 to 700 m depth. Above the shale-line an easily recognizable flooding surface occurs between the retrograding unit (shale-line) and an overlying prograding unit (boxcar trend). The flooding surface is followed by a heavily serrated blocky succession of around 90 m where a clear boxcar-trend can be observed depicting progradation, before a transition to a bow trend takes place in a thin interval between 580 m and 560 m depth. On top of this succession, a flooding surface is marked by a strong increase in the SP-log signal at 550 m depth. Following the flooding surface, an interval between 550 m depth and 490 m depth illustrates a funnel trend that hints to a progradational system.

Compared to the other two wells, which either continue the irregular trend depicting aggradation described above (Prottes 008) or show progradational patterns (Matzen 201), the well Matzen 101 shows a strong, thin peak in spontaneous potential ranging from 760 m depth to 730 m. This peak shows an opposing trend on the resistivity curve and is therefore interpreted as an erosional discordance. This is followed by a shale-line pattern indicating aggradation, ranging from 720 m to 640 m depth before a small peak, which marks the beginning of a bell trend. This bell trend interval, ranging from 620 m to 600 m depth, illustrates a progradational system, culminating in a flooding surface at 620 m depth. The next interval shows an irregular bow trend which is continuous up to 510 m depth, before another progradation occurs as indicated by the funnel trend.

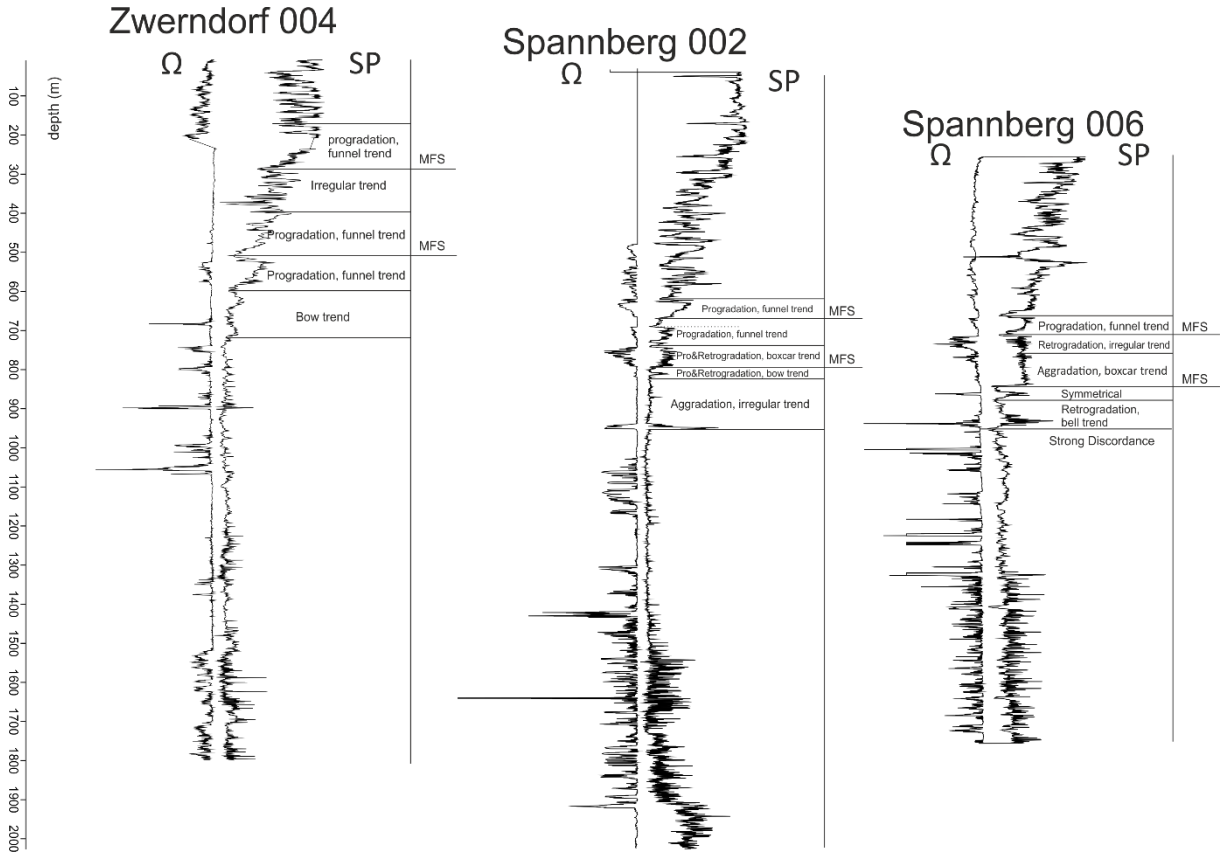

Figure 28: Well-log-trend interpretation for the wells Zwerndorf 004 (left), Spannberg 002 (middle) and Spannberg 006 (right). MFS = maximum flooding surface.

Similar to the abovementioned well-logs, the well-logs Zwerndorf 004, Spannberg 002 and Spannberg 006 (fig. 43) show an irregular serrated pattern indicating aggradation before other trends are recognizable. At Zwerndorf 004 this lower succession ranges up to 720 m depth before a bow-trend becomes observable hinting to pro- and retrogradation. This interval is around 120 m thick and

followed by an interval, ranging from 600 m depth to 532 m depth, depicting a funnel trend which indicates progradation. The next interval presents a very similar pattern but is separated from the abovementioned succession by a flooding surface, situated between the retrogradational and progradational unit at 520 m depth. On top of this interval, a 100 m thick succession shows a heavy irregular trend, that can be interpreted as prograding. This irregular trend culminates in a flooding surface as indicated by the decrease in spontaneous potential, before another funnel trend can be recognized, again hinting to a progradational system.

The wells Spannberg 006 and 002 both show a strong peak at similar depths, also depicting opposing trends on the resistivity curve (950 m depth, Spannberg 002 and 930 m depth, Spannberg 006) hinting to the same discordance as found in the well Matzen 101 (Fig 2). Spannberg 002 displays a serrated irregular trend from 920 m depth to 810 m depth, suggesting an aggradational system. After this 90 m thick interval, a short interval of 20 m shows a bow trend depicting pro- and retrogradational patterns, before a flooding surface can be observed between those two successions. This is followed by a heavily serrated blocky succession of around 60 m thickness illustrating a boxcar trend between 790 m and 740 m depth and is interpreted as aggradational before a funnel trend is recognized, again hinting to progradation. After another flooding surface at 650 m depth another progradation is visible as displayed by the funnel trend.

Spannberg 006 shows a clear bell trend above the discordance indicating retrogradation before a symmetrical peak can be observed at 850 m depth, hinting to another pro- and retrogradational system during this interval. On top of this symmetrical pattern and after retrogradation (decrease in spontaneous potential right after the top of the peak at 850 m depth), a flooding surface can be identified, which then is followed by a moderately serrated blocky succession ranging from 810 m to 710 m depth interpreted as aggradatatonal system. Above this interval a heavily serrated mostly irregular trend occurs which is generally retrograding, before another flooding surface separates the retrogradational patterns from the next interval at 700 m depth where a clear funnel trend can be observed, hinting to a progradational system.

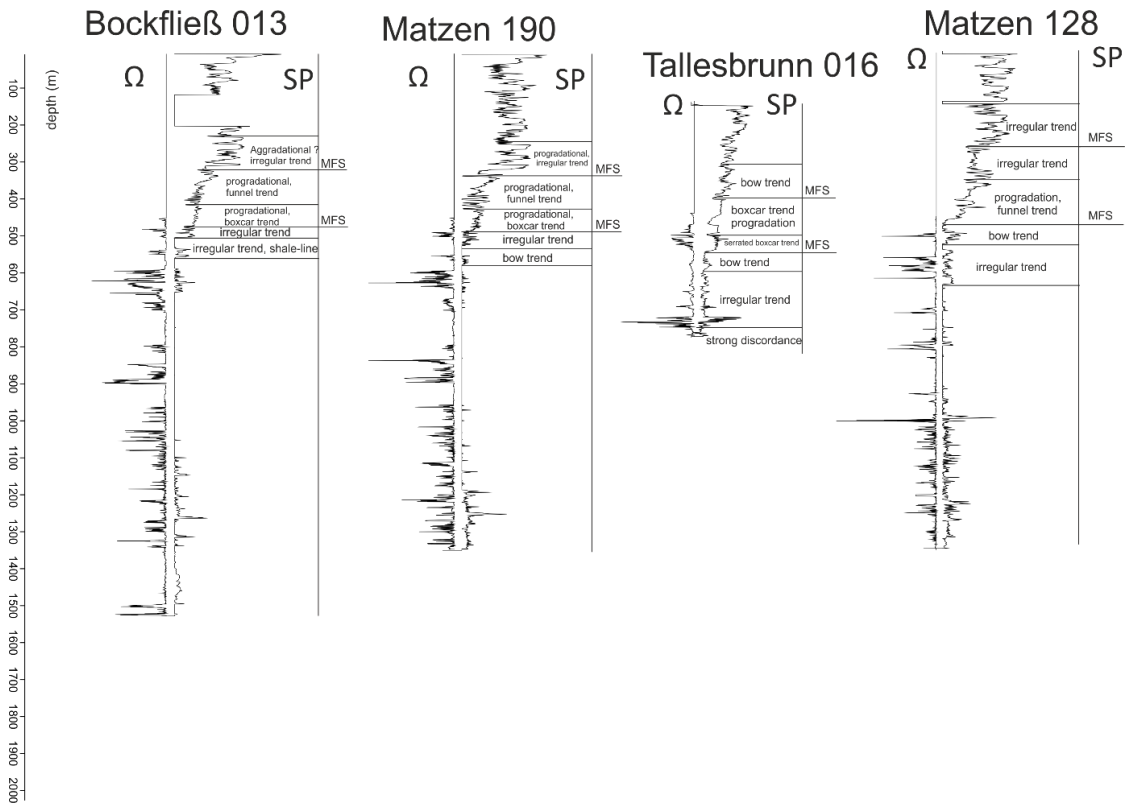

Figure 29: Well-log-trend interpretation for the wells Bockfließ 013, Matzen 190, Tallesbrunn 016 and Matzen 128. MFS = maximum flooding surface.

Except for the well Tallesbrunn 016, which only reaches a depth of 750 m, the wells depicted in Fig. 29 also show an irregular serrated trend for the lower part. Bockfliess 013 continues this trend, before a small succession shows a shale-line pattern between 540 m and 520 m depth. A flooding surface separates this shale-line pattern from the above positioned moderately serrated blocky succession, where a boxcar trend can be observed indicating a progradational system. This system, in general, continued as depicted by the funnel trend and culminates in a flooding surface at 310 m depth which is marked by a strong decrease in spontaneous potential. Above the flooding surface an irregular trend can be observed, which is mostly aggrading.

Compared to the Bockfließ 013 signature, the Matzen 190 well shows a bow trend hinting to a pro-and retrogradational system on top of the irregular pattern which depicts an aggradational system, before another bow trend is observable. This trend ranges from 580 m to 540 m depth and indicates pro- and retrogradation and culminates in a flooding surface before a progradational moderately serrated boxcar trend can be observed, with a thickness of approximately 70 m. A funnel trend ranging from 420 m to 350 m depth indicates a continuing progradation before the next flooding surface is recorded at a depth of 320 m. Above the flooding surface a heavily serrated irregular trend can be observed, which generally indicates progradation.

The well Tallesbrunn 016 also shows a strong characteristic peak in spontaneous potential and also depicts the opposing trend in the resistivity curve, similar to the wells Spannberg 002, 006 and Matzen 101. Above the discordance, an irregular serrated pattern can be recognized ranging from 760 m to 580 m depth, which indicates aggradation. Above this irregular trend a bow trend (590 m– 540 m depth) is displayed and illustrates a pro- and retrograding system, culminating in a flooding surface at 540 m depth. This surface is followed by a serrated blocky interval of 60 m which is generally prograding. This boxcar-trend is further recognizable to a depth of 390 m, indicating a progradation

culminating in a flooding surface. Above this surface a bow trend is displayed, hinting to pro- and retrogradation.

Finally, the well Matzen 128 displays an irregular trend, ranging from 610 m to 500 m depth, which is similar to the well Tallesbrunn 016 depicting aggradation. Above this interval, a bow trend is observable showing pro- and retrogradational patterns. On top of the bow trend interval, a funnel trend is observable, hinting to a progradational system, ranging from 570 m to 330 m depth. This is followed by a long interval of serrated irregular patterns, which firstly retrograde (350 m to 260 m depth) before it starts to prograde after a flooding event.

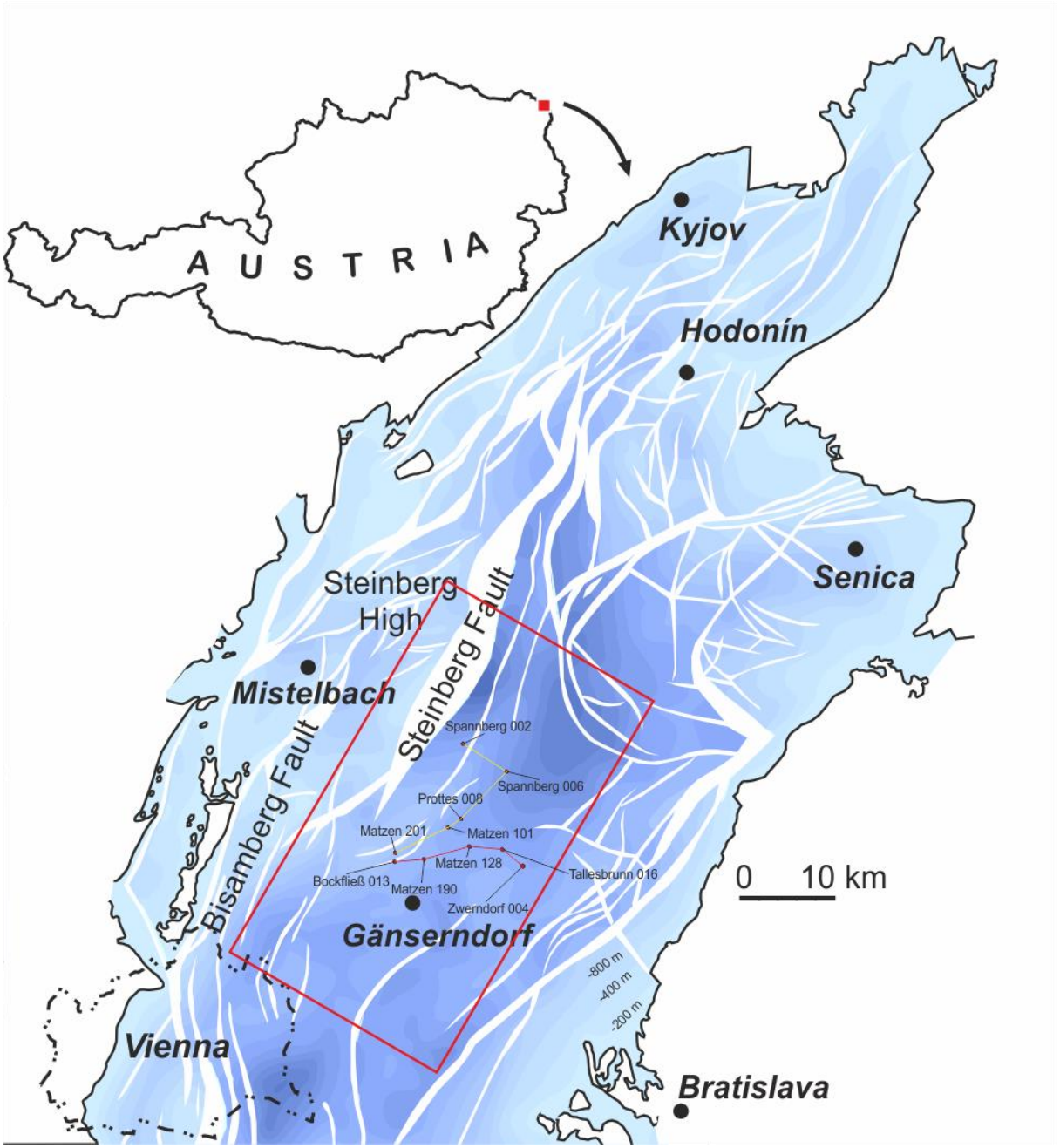

Figure 30: Chosen lines for well-log interpretation. The yellow line includes the wells Matzen 201, Matzen 101, Prottes 008, Spannberg 006 and Spannberg 002 (fig 46). The red line includes the wells Zwerndorf 004, Tallesbrunn 016, Matzen 128 Matzen 190 and Bockfließ 013 (fig. 47)

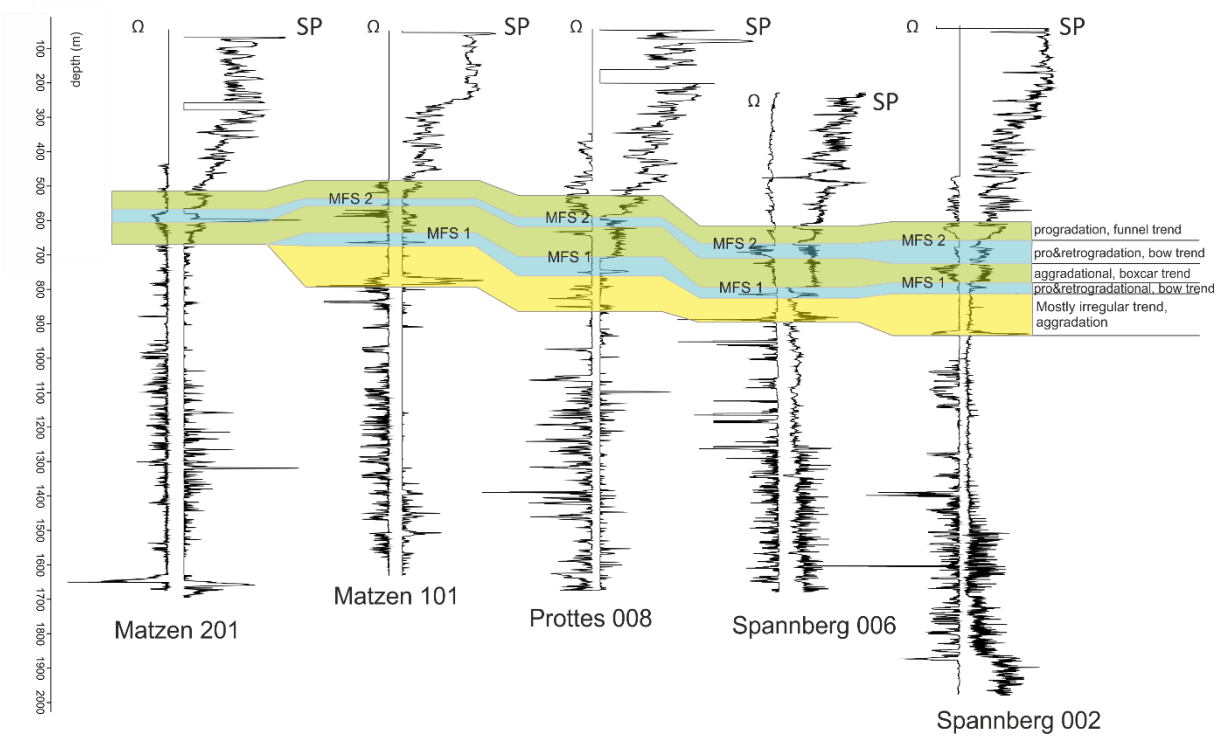

Figure 31: Correlation of the observed well-log-trends for the wells Matzen 201, Matzen 101, Prottes 008, Spannberg 006 and Spannberg 002.

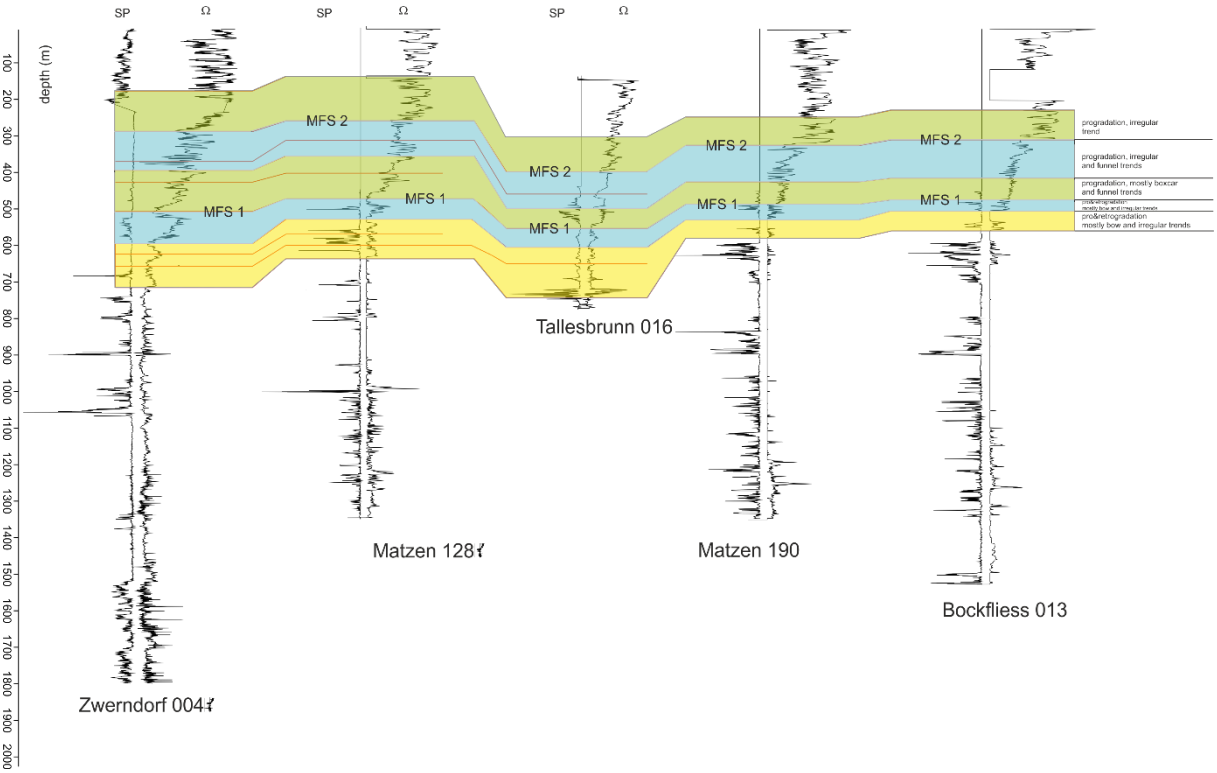

Figure 32: Correlation of the observed well-log-trends for the wells Zwerndorf 004, Matzen 128, Tallesbrunn 016, Matzen 190 and Bockfließ 013.

6.1.2 Correlation of well-log trends

The wells have been chosen to be arranged along lines which are approximately oriented SW-NE (yellow line in Fig. 30) and E-W (red line in Fig. 30). Striking similarities in well-log-patterns and flooding

surfaces were correlated in order to establish distinct intervals, displaying prominent trends throughout the well-log-data.

The SE-NW oriented well-logs (Fig. 31) are interpreted above the discordance, marked by a remarkable peak which also displays an opposing trend in the resistivity curves. This pattern is especially prominent in the wells Matzen 101, Spannberg 002 and Spannberg 006, and is also to a lesser extent visible in the well Prottes 008. Those discordances mark the base of the interpreted part of as described above. The first recognizable interval (yellow), displays a mostly irregular trend which is interpreted as generally aggrading. This trend is not displayed in the well Zwerndorf 004, which is the most distal well. This section is followed by a moderately serrated, blocky interval illustrating a boxcar trend, which is interpreted as mostly aggrading (green). Two exceptions were recorded in the wells Matzen 201 and Matzen 101. Matzen 201 represents a funnel trend indicating a progradation in this area, whereas Matzen 101 shows a heavily serrated irregular trend interpreted as aggradational. On top, another trans-regressive event is recorded in the well-log-patterns, again indicated by a bow trend, which is recognizable throughout all recorded wells (blue), before a very prominent funnel trend is recognized, indicating a progradational system (green).

The E-W oriented well-logs (Fig. 32) use the same base of correlation as the abovementioned well-logs. Here, the discordance is less prominent and only well reflected in the well Tallesbrunn 016 and to a lesser extent in the well Bockfließ 013. The first interval (yellow) composed of many different trends, which becomes obvious in the wells Zwerndorf 004 and Matzen 128, where multiple bow trends are stacked on each other, and a subdivision in transgressive and regressive events is plausible. The other well-logs do not show this exact pattern and hint to an irregular bow trend, indicating a pro- and retrograding setting at this interval. The other well-logs do not show this exact pattern and hint at an irregular bow trend, indicating a pro- and retrograding setting at this interval. The following section (blue) clearly shows a bow trend, with only one well hinting at a progradation (Zwerndorf 004) as indicated by the funnel trend. Above this interval, the green marked interval shows a moderately to heavily serrated boxcar trend, whereas the wells Zwerndorf 004 and Matzen 128 show two funnel trends stacked on each other. In general, this interval shows a strongly prograding pattern. The next interval (blue) is also marked by progradation, as indicated by the heavily serrated irregular funnel trends. Again, an exception occurs at the well Tallesbrunn 016, where two weakly serrated boxcar trends are stacked on each other, which generally also indicate progradation. The uppermost interpreted interval (green) shows an ultra-serrated irregular pattern throughout all wells except the well Zwerndorf 004, which depicts a funnel trend. This interval is also clearly prograding.

6.2 Time slice and cross-section analysis

Three time slices were created and analyzed to show location, size, and depositional direction of possible seismic structures in the work area Figs. 34-37, 38, 39. Time slices were flattened on three distinct seismic horizons: the lower one is situated in the Zwerndorf area at the boundary between the lower yellow interval and the lower green interval as illustrated in Fig. 31 & 32. The following time slice spans across the whole investigated area and depicts the first, in the well-logs recorded maximum flooding surface 1 (Fig. 34-37) between the lower blue interval and the lower green interval (Fig. 31 & 32). This corresponds to the onset of the Pannonian deltas described as Pannonian C_1 by Harzhauser et al. (2004) and serves as an interpretational base of seismic bodies expressing deltaic deposition. The upper time slice marks the boundary between the upper limit of the lower green interval and the base of the upper blue interval (Figs 31 & 32) and is recorded in the Zistersdorf - Matzen area. General characteristic architectural and geometric features such as topset and foreset accommodations, clinoforms and stratal patterns were investigated to proof that the investigated sedimentary structures are of deltaic nature. In-seismic measurements were carried out in true vertical-depth, and should be regarded as rough estimates and not accurate values. Seismic cross-sections (Figs. 34 - 37) were not flattened to show deposits without any distortions, however, water depth and slope angles were calculated on flattened seismic horizons (Fig. 40)

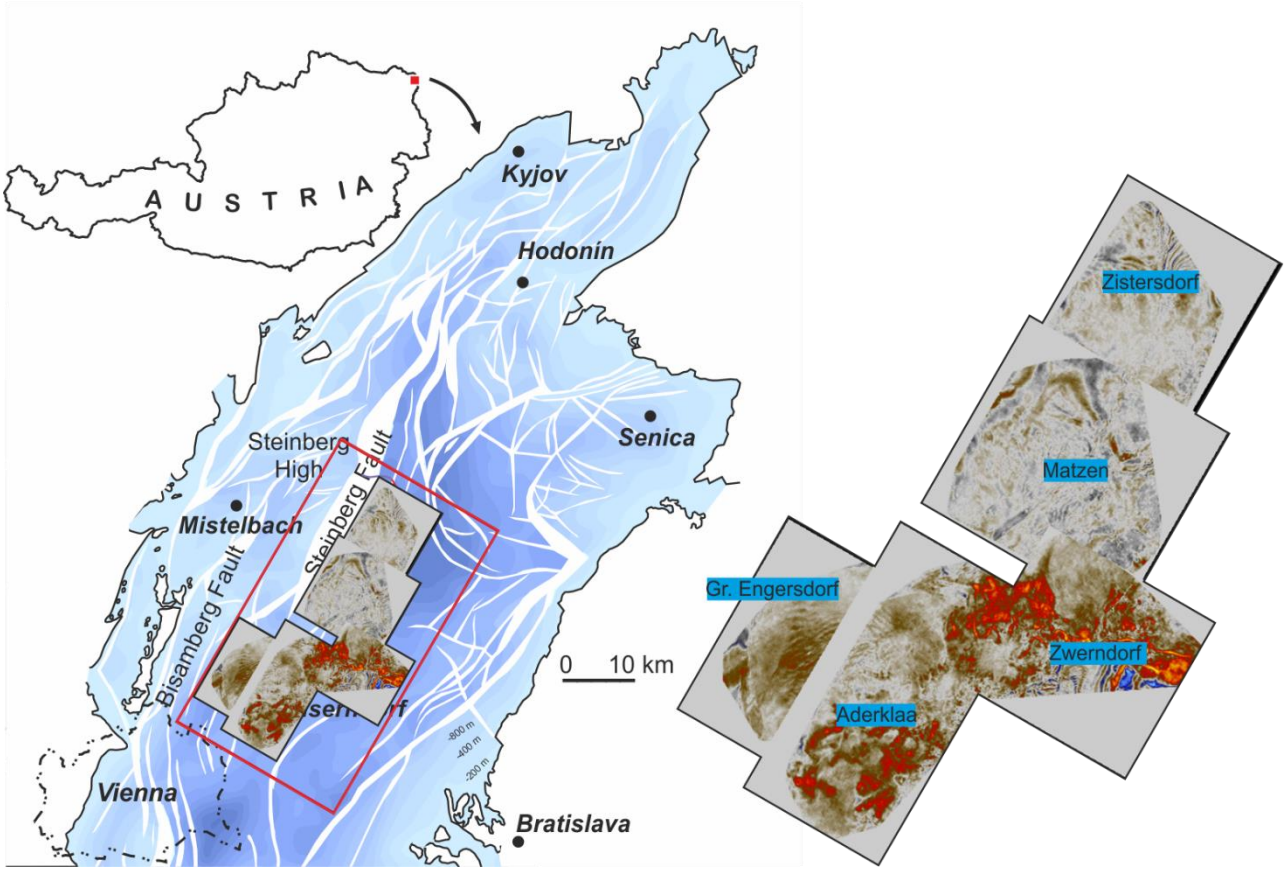

Figure 33: Overview of the mapped areas. The red rectangle indicates the work area. Brown/red colored areas show the time slice for five areas: Gr. Engersdorf, Aderklaa, Zwerndorf, Matzen and Zistersdorf. Except for the Zwerndorf area which is flattened at the boundary between the lower yellow interval and the lower green interval (Figs. 31 & 32), the time slices are flattened on the maximum flooding surface (MFS 1) corresponding to the onset of the lower Pannonian deltas (Pannonian C_1 after Harzhauser et al., 2004).

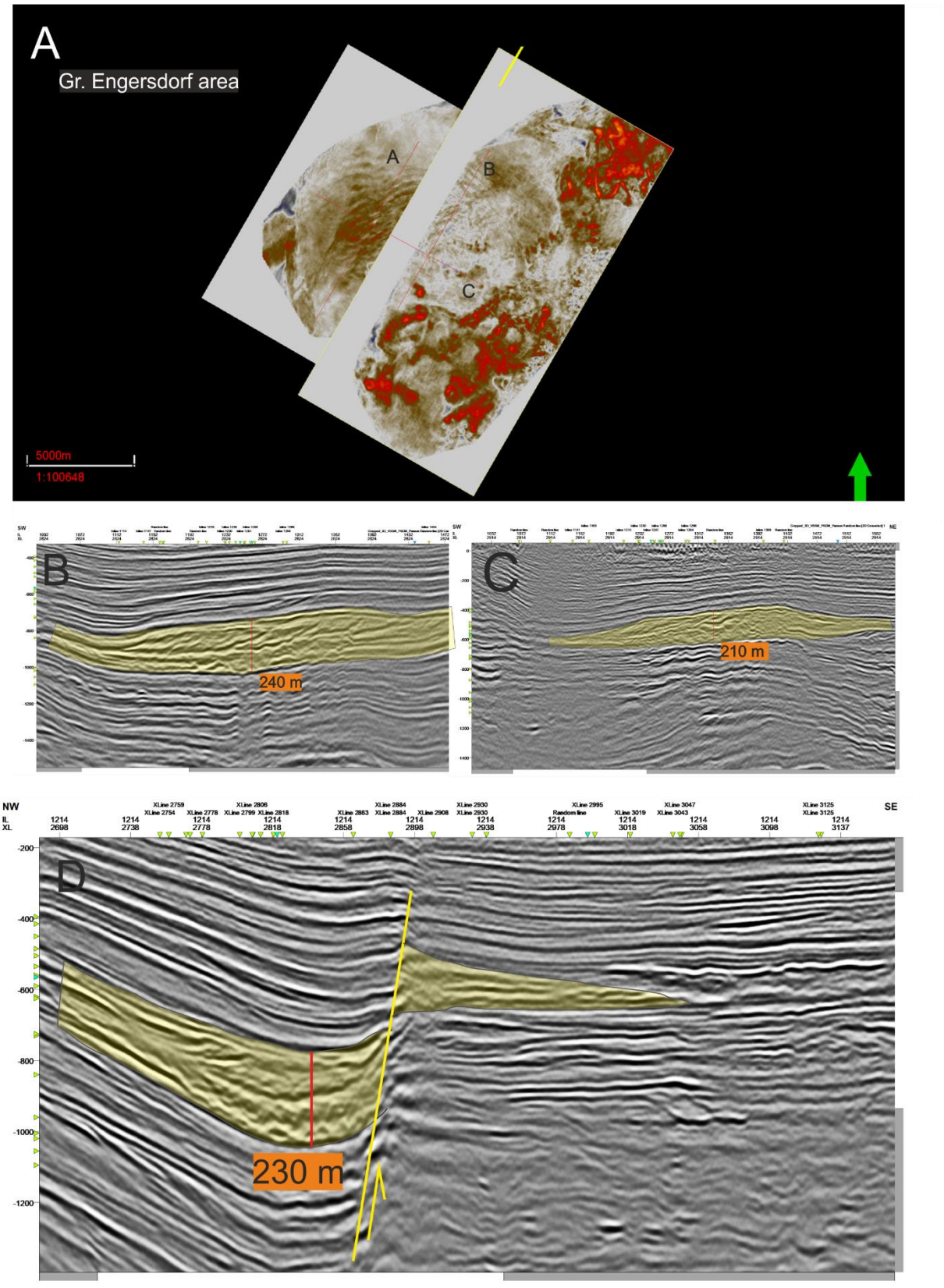

Figure 34: Investigated seismic body in the Gr. Engersdorf area and in the Aderklaa area. Yellow marked areas show the orientation of interpreted seismic structure, numbers (orange box) express in-seismic measurements of thickness in meters. Characteristic foreset deposits can be recognized (A & B) and a fault cuts through the system with a vertical offset of 400 m (C).

The southernmost deposits were found in the Gr. Engersdorf area (Fig. 34 A) where a seismic body of around 35 km^2 and a thickness of approximately 230 m is situated. The base-reflector of this structure is situated at around 1000 m depth. The northwestern part of the structure is situated on the downthrown block of a fault, cutting through the seismic body with a vertical offset of around 400 m (Fig. 34 D). Characteristic foreset deposits are easily recognizable (Fig. 34 B&C) and mostly dip into southern direction indicating progradation in this direction. Visibility of this structure is strongly limited in the Z–plane, therefore no outline of this lobe is illustrated.

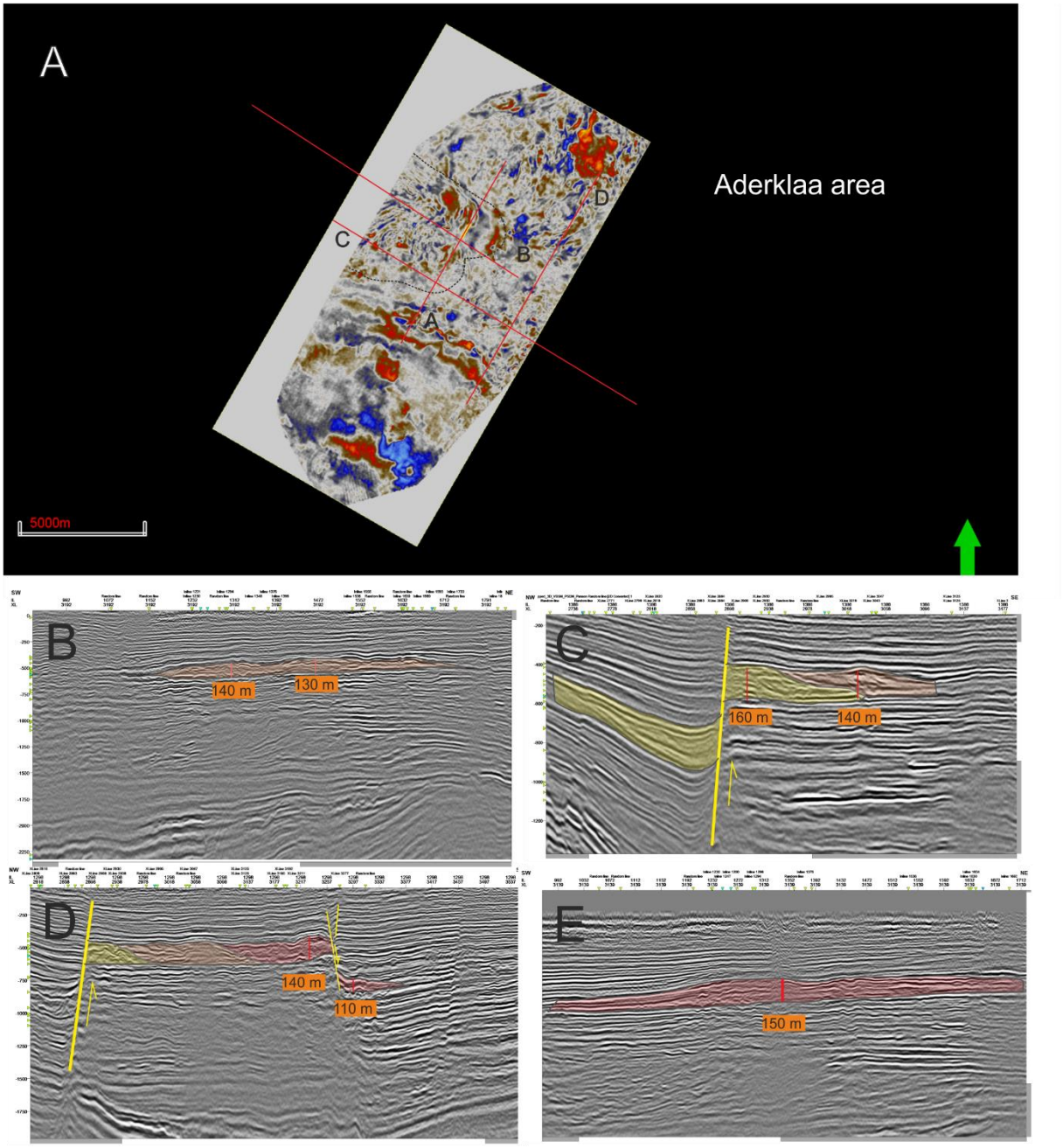

Figure 35: Investigated seismic body in the Aderklaa area. Yellow marked areas show the Gr. Engersdorf structure, orange marked areas indicate the first deposition in the Aderklaa area and red marked structures show the continuation of the Aderklaa delta. Numbers (orange box) express in-seismic measurements of thickness in meters. (A) shows the Aderklaa structure from a front view. (B) illustrates the relation between the Gr. Engersdorf structure and the Aderklaa structure. (C) depicts the continuation of the Aderklaa delta, which is cut by a fault. (D) front view of the Aderklaa continuation structure.

The next structures were found south-east of the Gr. Engersdorf structure close to Aderklaa (fig. 35 A). This structure can be subdivided into two distinct bodies which here are termed Aderklaa structure for the north-western part and Aderklaa – continuation for the south-eastern part of the structure. The Aderklaa structure is found at a depth of around 600 m. It has a size of roughly 35 km^2 and a thickness of 140 m. This structure is oriented into southeastern direction as indicated by the foreset deposits visible in Fig. 35 C and marks a change in the general depositional direction compared to the Gr. Engersdorf structure which progrades into southern direction. Fig 35 B illustrates this structure from a front-view, displaying two thicker successions of 130 m and 140 m which are separated by a thinner succession. This seismic structure is easily recognizable from the map view and is marked as a black dashed line in the time slice (Fig. 35 A). This subdivision of the structure into two thicker successions is also represented in the Z-plane where the structure clearly shows, that the most distal depositions coincide with the thicker parts, whereas the most proximal part coincides with the thinner succession in the middle.

The Aderklaa structure continues into south eastern direction into another structure, with a size of about 75 km^2. This Aderklaa continuation is displayed in Figs 35 D & E as a red marked area. Fig 35 D shows the relation between those two structures (Aderklaa = orange, Aderklaa continuation = red). This seismic body is also cut by a fault, producing a very offset of approximately 380 m (Fig 35 D)., similar to the offset recorded in the Gr. Engersdorf area. It has a thickness of 140 m and is also situated at a depth of ca. 600 m. Similar to the Gr. Engersdorf structure, no outline can be traced. As indicated in Fig. 50 C, this seismic body is terminated to south eastern direction, indicating that this structure did not prograde further in that direction.

The biggest sedimentary structure was found in the Matzen area (Fig. 36 A) with around 170 km^2 and a thickness of 120 m. The base of this body is situated at around 750 m. This lobe marks a major switch in deposition as indicated by the foreset deposits, changing the sediment direction from south – east to north – east (Fig 36 B). The Matzen structure is very well recognizable in the Z–plane, and the outline has been marked with a black-dashed line. Unfortunately, this structure becomes difficult to observe in proximity to the nearby fault, and is heavily distorted (Fig. 36 C).

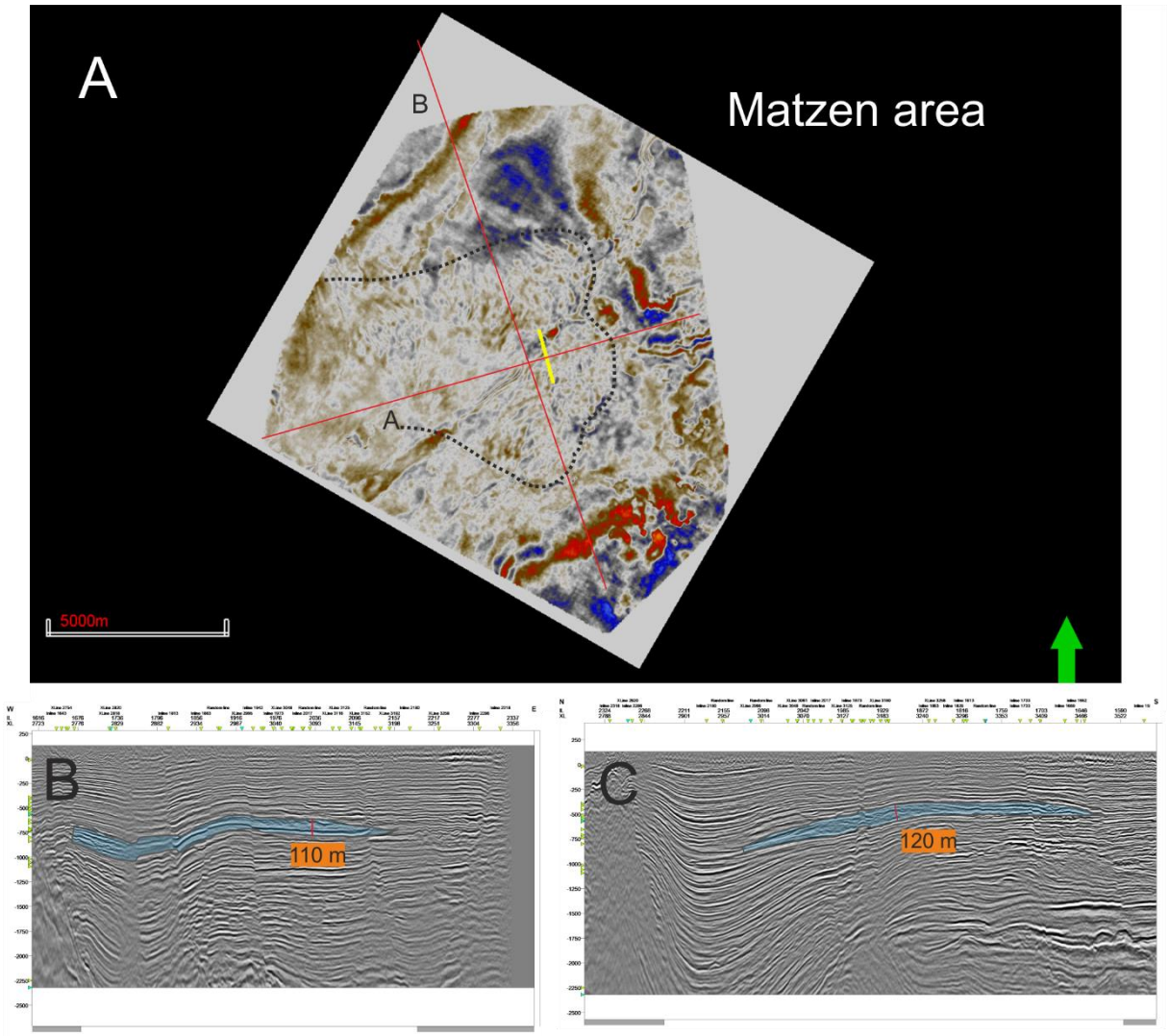

Figure 36: Investigated seismic body in the Matzen area. Blue marked successions show the interpreted seismic structure, numbers (orange box) express in-seismic measurements of thickness in meters. Characteristic foreset deposits can be recognized (A), indicating progradation into north eastern direction. Faults heavily distort this structure (B)

The most northern situated observable seismic body was recognized in the Zistersdorf area. Between the abovementioned Matzen lobe and the Zistersdorf lobe a considerable gap can be recognized. However, the structures still overlap in a small area (Fig. 37 B). This lobe covers an area of roughly 70 km^2 and has a thickness of around 115 m. Progradation is again oriented towards the south-east, which is easily recognizable by investigating the foreset deposits. The base of this seismic body is situated at 730 m depth and is recognizable from a maps eye-view. To summarize: five seismic structures were identified. Characteristic sedimentary structures like foreset-deposits indicate that those are of deltaic nature. A generalized map (Fig. 41) shows the distribution of these deltaic lobes throughout the workarea.

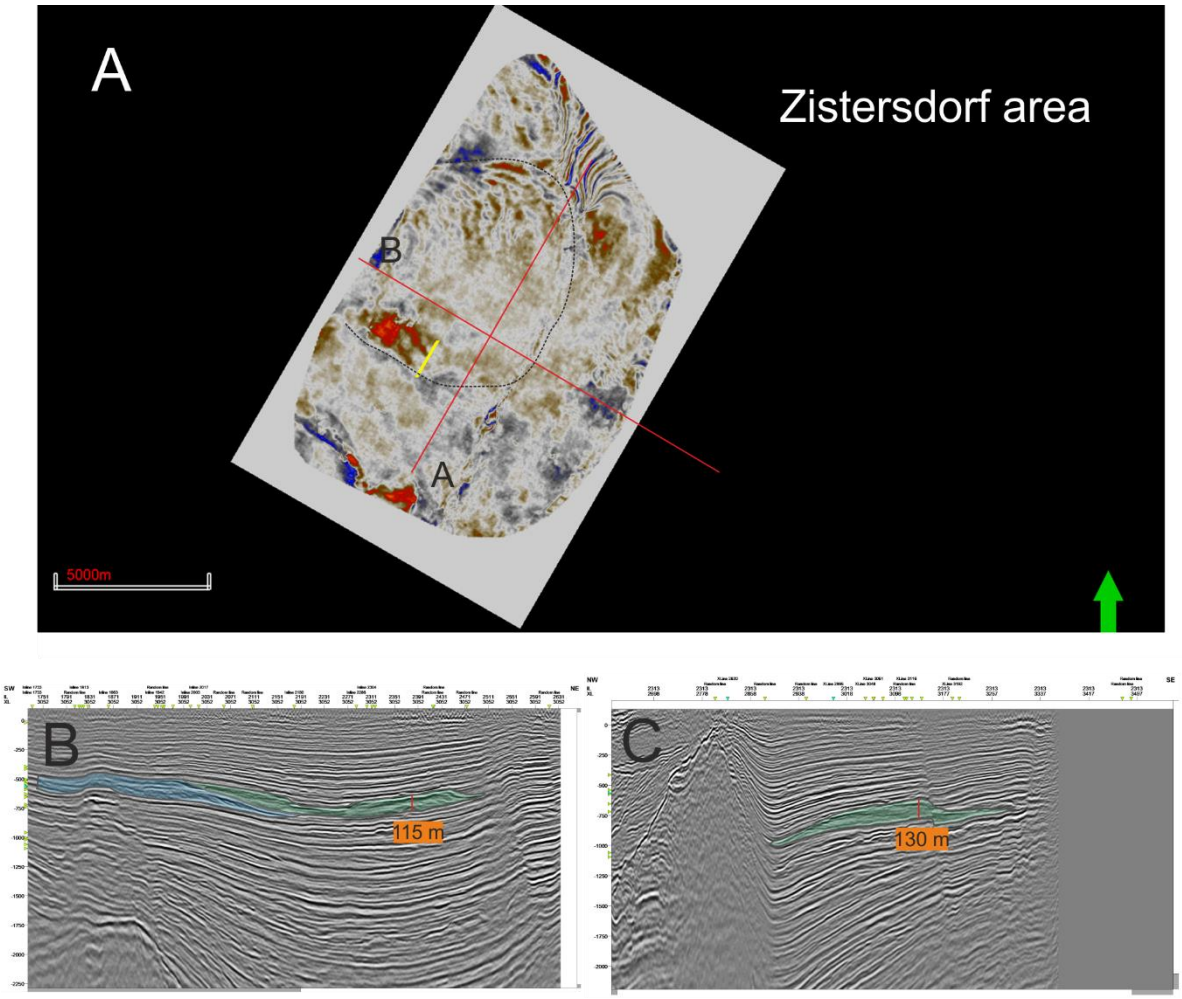

Figure 37: Investigated seismic body in the Zistersdorf area. Green marked areas show the interpreted seismic structure, numbers (orange box) express in-seismic measurements of thickness in meters. This structure overlaps with the Matzen structure (A). Characteristic foreset deposits can be recognized (B), indicating progradation into south eastern direction. Faults heavily distort this structure (B)

6.3 Channel deposits

Two structures were interpreted as channels (blue marked areas in Figs. 38 and 39). One is recorded in the Zwerndorf area (Fig. 38) at the boundary between the lower yellow interval and the lower green interval as illustrated in Figs. 31 and 32 and resembles the maximum flooding surface, serving as interpretational base. The observable part of the channel is approximately 12 km long and 200 m wide. The channel is oriented into southeastern direction and can be subdivided into three segments: the westernmost part shows a sinuous pattern with two crevasse splays (white circle), the middle part is mostly straight (yellow circle) and the easternmost part is laterally spreading out (green circle).

The second channel was recorded at the boundary between the lower green interval and the upper blue interval (Figs. 31 and 32) in the Zistersdorf – Matzen area. The measurable part of the channel is 22 km long when drawing a straight line between the northernmost section and the southernmost section, 240 m in average wide and can be subdivided in three segments: The northernmost segment (white circle Fig 39) shows a multiple channel system, which can be interpreted as braidplain. The middle segment shows a clear meandering pattern (yellow circle) and the southernmost part depicts a highly sinuous meandering part, that splits in two branches (green circle), where the northern branch can either indicate a braidplain (if the northern branch is continued), or a crevasse splay.

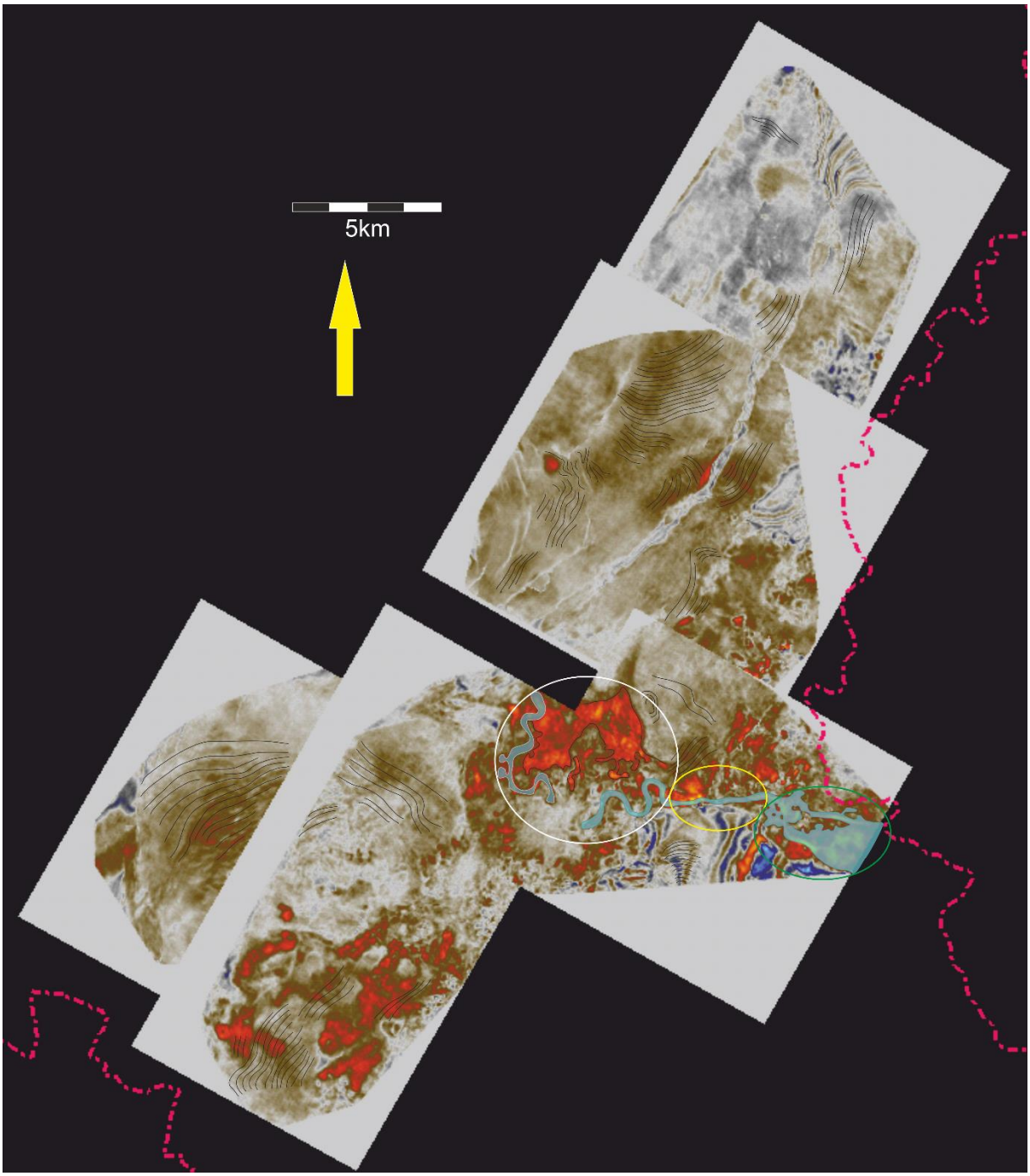

Figure 38: Detected channel in the Zwerndorf and Aderklaa area. Blue marked area illustrates the mapped channel which shows a subdivision into three sections: Sinuous part and crevasse splays (white circle), straight part (yellow circle) and a laterally spreading out section (green circle). Black lines indicate sandwaves. The observable length of the channel is 12 km and the width 200 m.

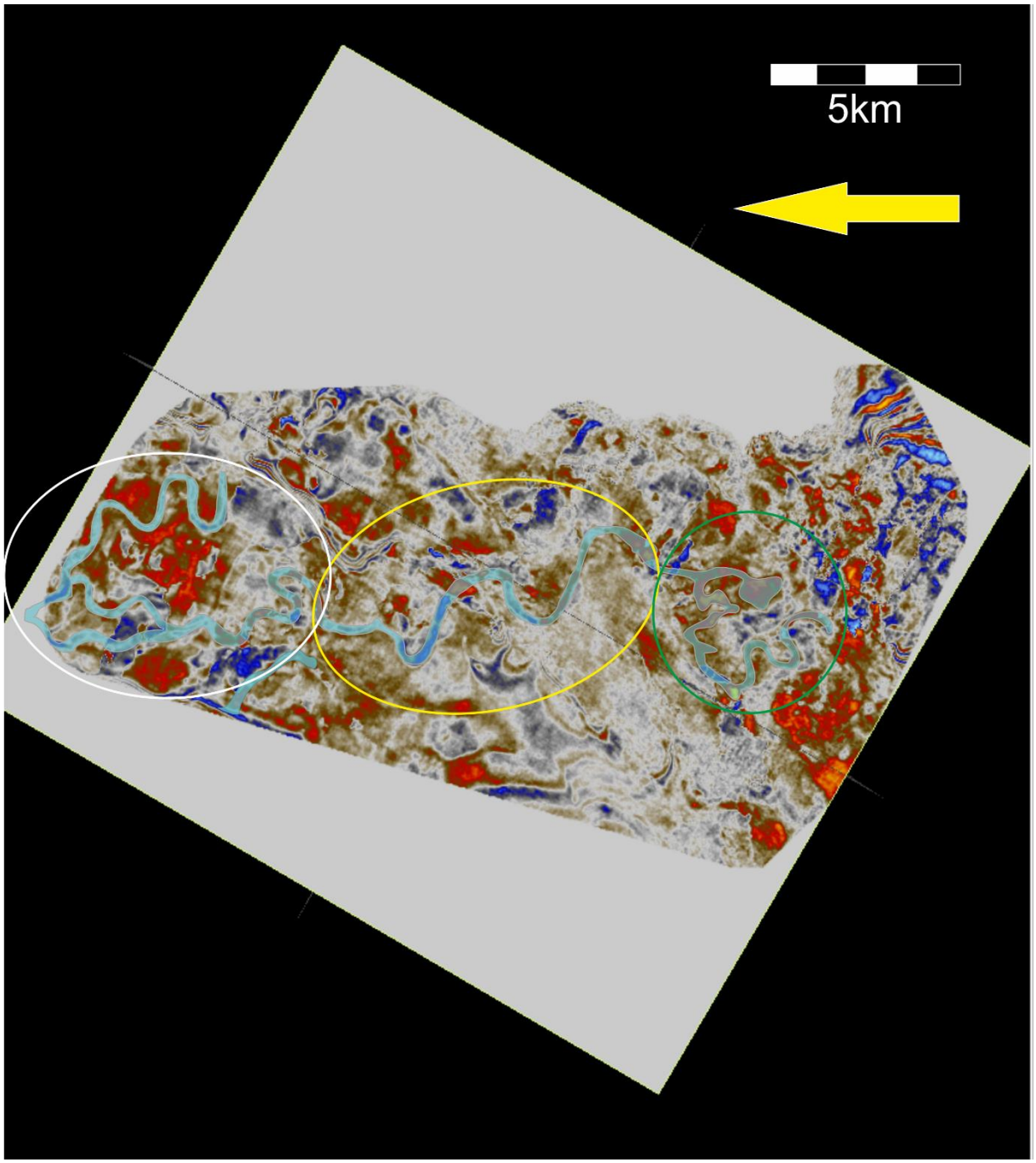

Figure 39: Investigated channel in the Matzen area. The blue marked area illustrates the mapped channel, which can be roughly subdivided into three sections: multiple sinuous channel system (white circle), meandering part (yellow circle), highly sinuous meandering part and crevasse splay (green circle). The observable and measurable part of the channel is 22 km long and 240 m wide.

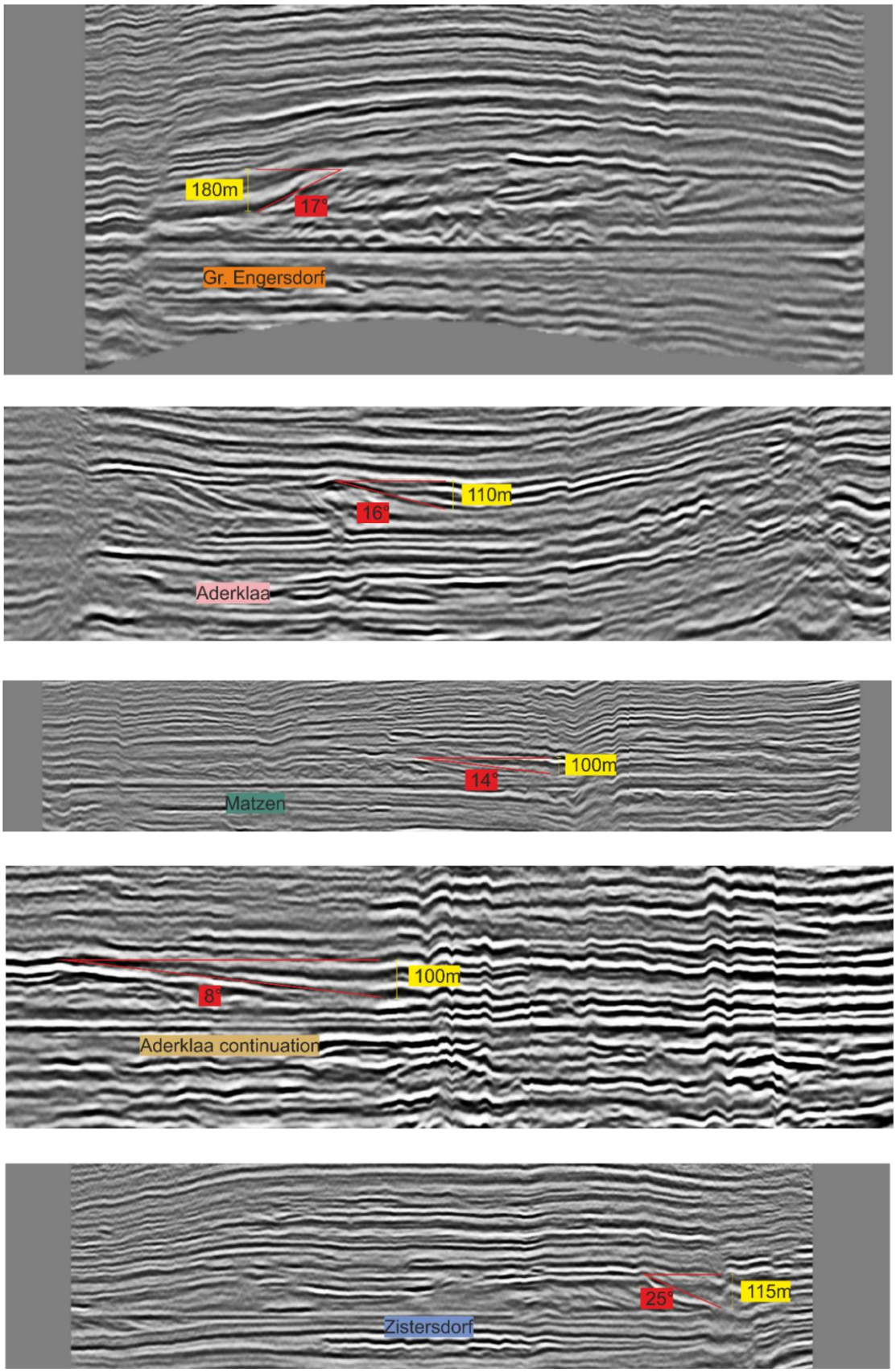

Figure 40: Water depths estimates and slope angles for the five observed deltaic structures. The reference surface (MFS) was flattened in a 3D – window in Petrel to illustrate the seismic bodies without distortions, before in- seismic measurements were carried out. Yellow numbers indicate water depth, red boxes indicate slope angles and red lines resemble the space between a downlap and the shoreline break

6.4 Water depth estimates, slope angles and stratal patterns

In–seismic measurements were carried out in true vertical depth (see chapter 5). The reference horizon (MFS 1 in Figs. 31 and 32) was flattened to display the seismic structures without distortions. Water depth is calculated between topset deposits of the deltaic structure and the base of the bottomset deposits. Angle measurements were calculated by drawing two lines, which resemble the space between the position of a downlap and the shoreline break, measuring the angle between them. The seismic cross-sections were chosen in a way that they represent the delta in the direction of deposition. Results show a water depth of around 180 m for the Gr. Engersdorf area, 100 - 110 m for the Aderklaa area, 100 m for the Matzen area and 115 m for the Zistersdorf area. This indicates that water depth decreases significantly between the deposition of the first and second structure, before showing consistent values of ~100 m water depth across the rest of the seismic bodies. Angle measurements reveal an inclination of 17° for the Gr. Engersdorf structure, 16° for the Aderklaa body, 8° for the Aderklaa continuation, 14° for the Matzen structure and 25° for the Zistersdorf seismic body (Fig. 40).

Downlaps were used to indicate the base of the seismic structures at its depositional limit and onlaps mark the lateral termination of the seismic structures at its depositional limit (Fig. 25). The blue line represents the abovementioned base reflector (MFS 1 in Figs. 31 and 32), which serves as the interpretational base. These seismic stratal patterns were used to depict the relations between the distinct seismic structures and therefore to indicate a depositional evolution of the seismic bodies. The implementation of stratal termination patterns, revealed that the Aderklaa delta continuation onlaps on the Aderklaa delta, the Matzen delta onlaps onto the Aderklaa continuation delta and the Zistersdorf delta onlaps onto the Matzen delta.

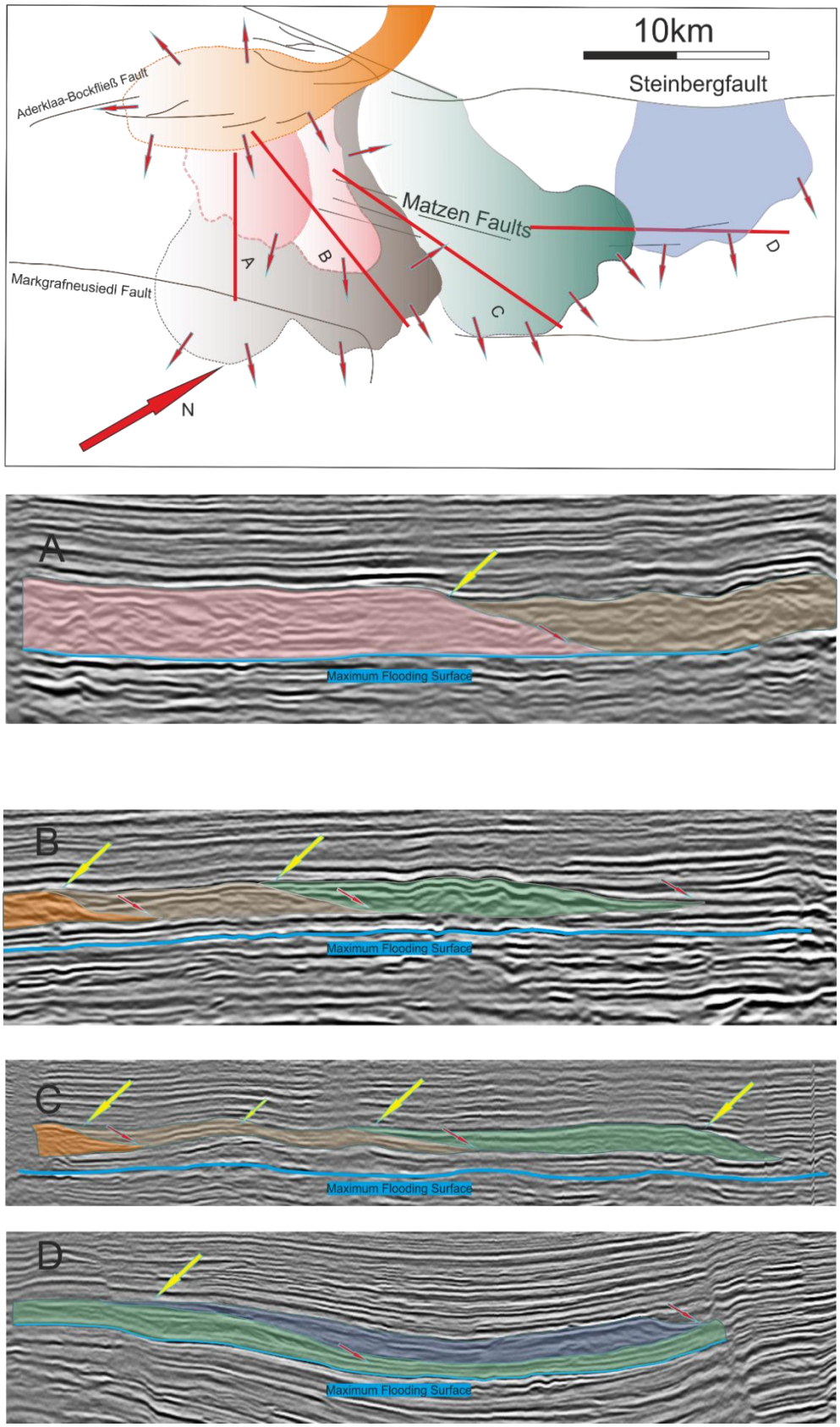

Figure 41: Generalized map of the studied seismic structures. Downlaps (red arrows) indicate the base of the seismic structures at its depositional limit, onlaps (yellow arrows) mark the lateral termination of the seismic structures at its depositional limit. Blue lines indicate the maximum flooding surface, serving as reference horizon and base of interpretation (MFS 1 in fig 46 and 47). A shows the relation between the Aderklaa structure and the Aderklaa–continuation structure, B illustrates the relation between the Gr. Engersdorf and both Aderklaa structures, C depicts the relation between the Matzen structure and the Aderklaa structures, D shows the overlap between the Matzen structure and the Zistersdorf seismic body.

7. Discussion

7.1. Sequence Stratigraphy

Third-order cycles of relative sea-level changes in the sedimentary record of the central Vienna Basin

The Sarmatian-Pannonian Boundary is characterized by deep valley incisions and erosion in the Vienna Basin, corresponding to the glacio-eustatic sea-level lowstand of cycle TB 3.1 at 11.6 Ma (Kovac 2004, Kosi et al. 2003). The lower Pannonian strata corresponds to a 3rd order lowstand systems tract (LST) (Pa1-LST – Pa1-HST in Figs. 43 & 44) labeled as Pa1 and the base of this sequence is represented in the well-logs by jagged log motifs, representing coarsening upward channel fills. This sequence is also modulated by two higher order cycles, a TST and a HST. The beginning of the 3rd order transgressive systems tract (TST) (Pa2-TST), labeled as Pa2, is marked by the transgression of Lake Pannon during the *Mytilopsis hoernesi* Zone (Harzhauser et al. 2004, C_3 in Fig. 6) and is well reflected in the well-logs as the maximum flooding surface (MFS 2) between Pa2-TST and Pa2-HST (Pannonian C_3). This sequence is modulated by at least four higher order cycles and culminates in a MFS in the upper middle Pannonian. These sequences were not further investigated in this study.

Fourth-order cycles of relative sea-level changes in the sedimentary record of the lower Pannonian in the central Vienna Basin

Within the Pa1-LST at least one higher order sequence can be recognized. First transgressive pulses of this higher order sequence are expressed in the well-logs as shale-line intervals representing marly prodelta facies typically named “schiefrige Tonmergel” with a thickness of ~100 m (Pa1-TST in Figs. 43 & 44). This cycle is followed by the deltaic facies of the “large lower Pannonian Sands” (Harzhauser et al. 2004) of Pa1-HST represented in the well-logs as a typical moderately serrated, cylinder-shaped blocky succession. The “large lower Pannonian Sand” (C_1 in Fig. 6) is linked to the prograding delta of the Paleo-Danube in the northwestern part of the Vienna Basin, with a thickness of around 100–120 m. This high order HST culminates in a MFS at around 11.1 Ma (Pannonian C_3), before the sedimentary record grades to the 3rd order TST. Hence, the total lower Pannonian succession (Pa1-LST, Pa1-TST, Pa1-HST) is represented by a ~400m thick basin fill in the central Vienna Basin.

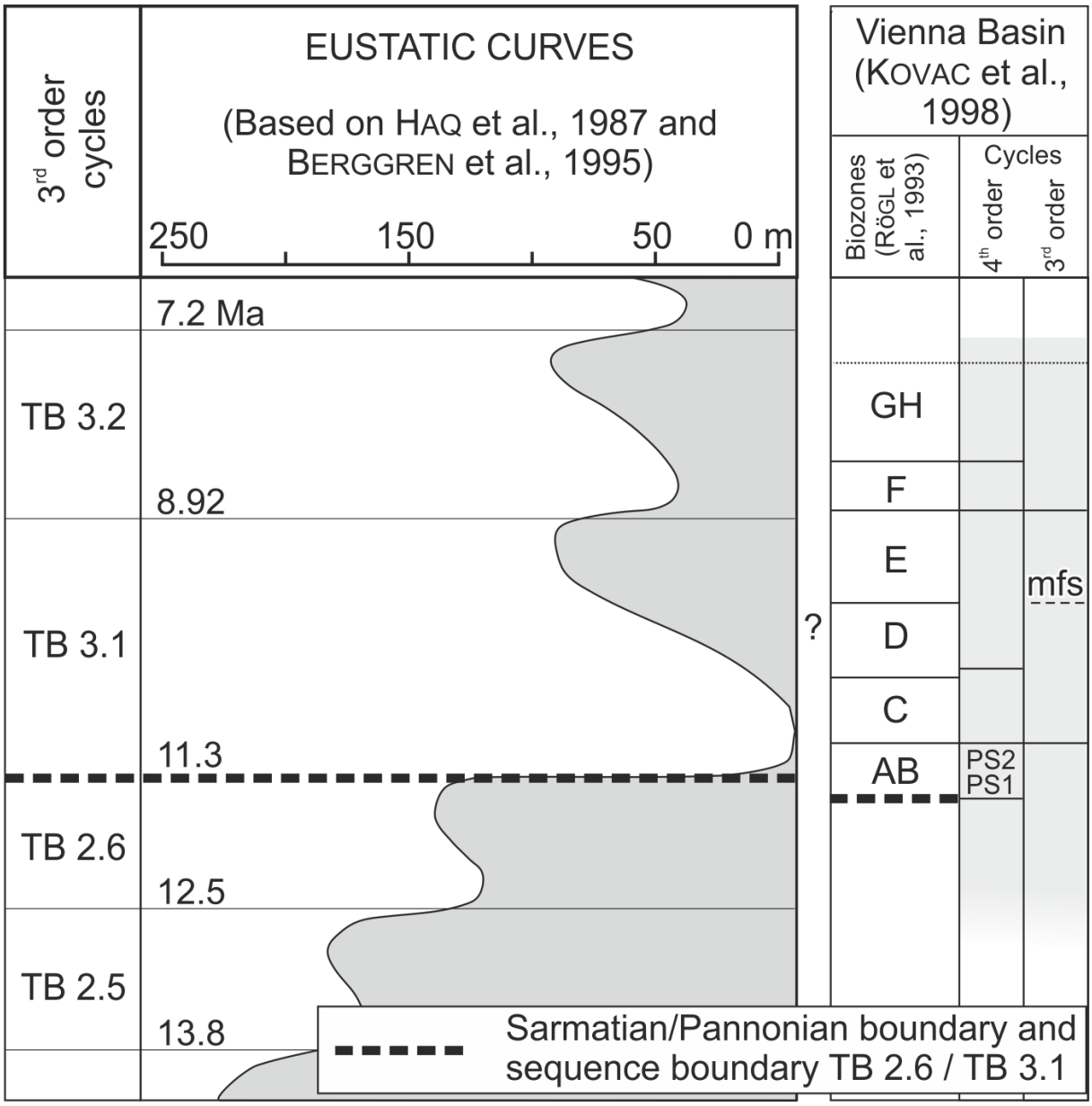

Figure 42: 3rd order cycles based on Haq et al. (1988) and the Sarmatian/Pannonian boundary (dashed line). 3rd order cycles are correlated to Pannonian biozones (A-H after Papp 1951). A, B and C correspond to a 3rd order lowstand systems tract (LST), D corresponds to a 3rd order transgressive Systems tract (TST) and E corresponds to a 3rd order highstand systems tract (HST).

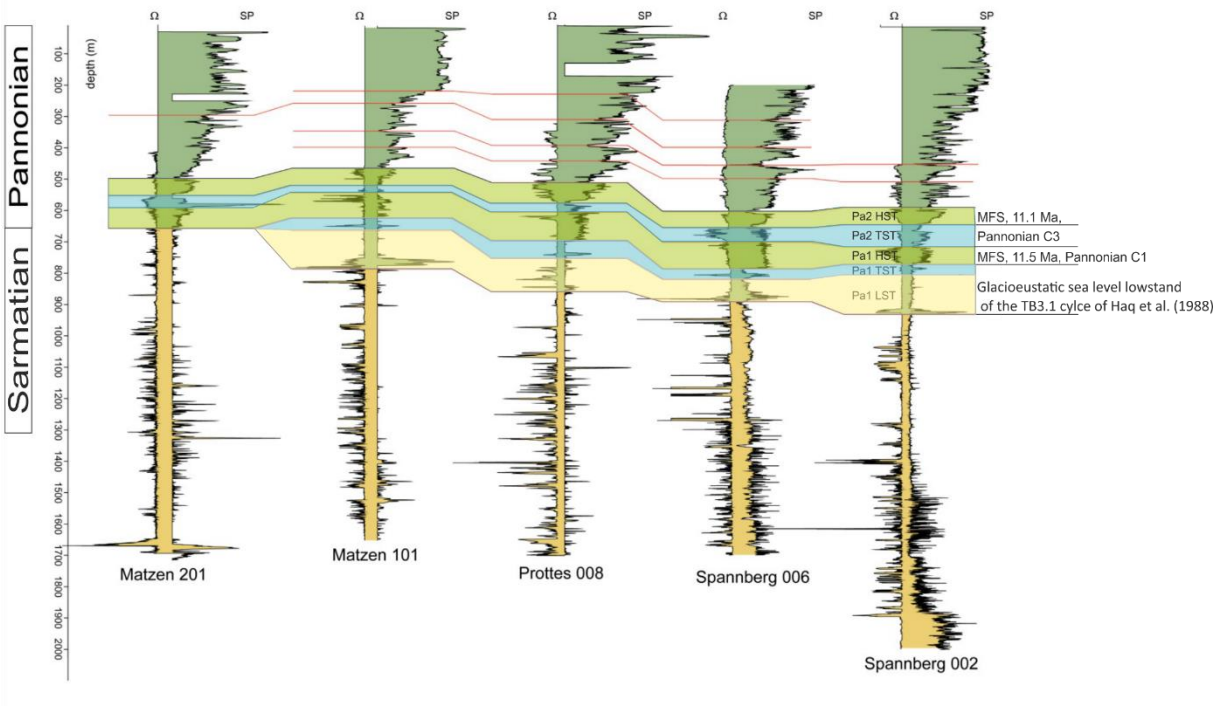

Figure 43: Well -logs of the central Vienna Basin. Sarmatian deposits are in yellow, Pannonian deposits in green. Similar well-log patterns are correlated between wells to show depositional patterns. Exact positions of the wells are shown in Fig. 1.

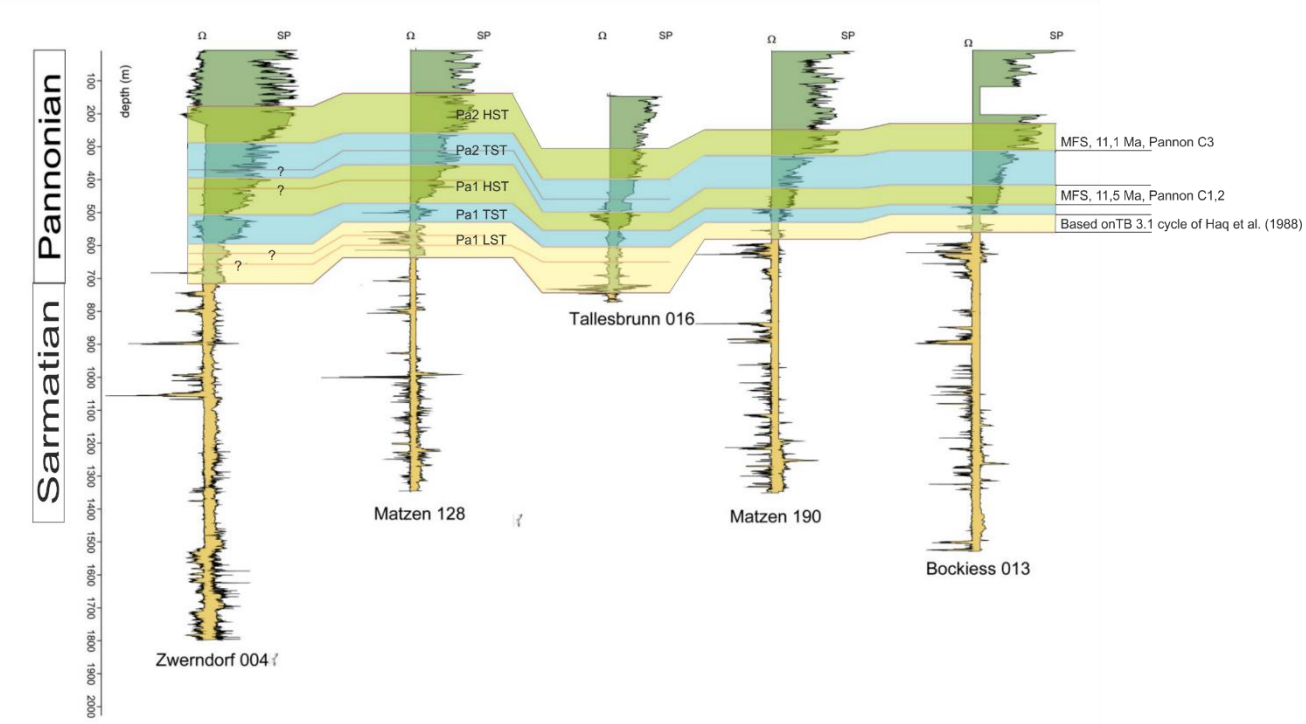

Figure 44: Well -logs of the central Vienna Basin. Sarmatian deposits are in yellow, Pannonian deposits in green. Similar well-log patterns are correlated between wells to show depositional patterns. Exact positions of the wells are shown in Fig. 1.

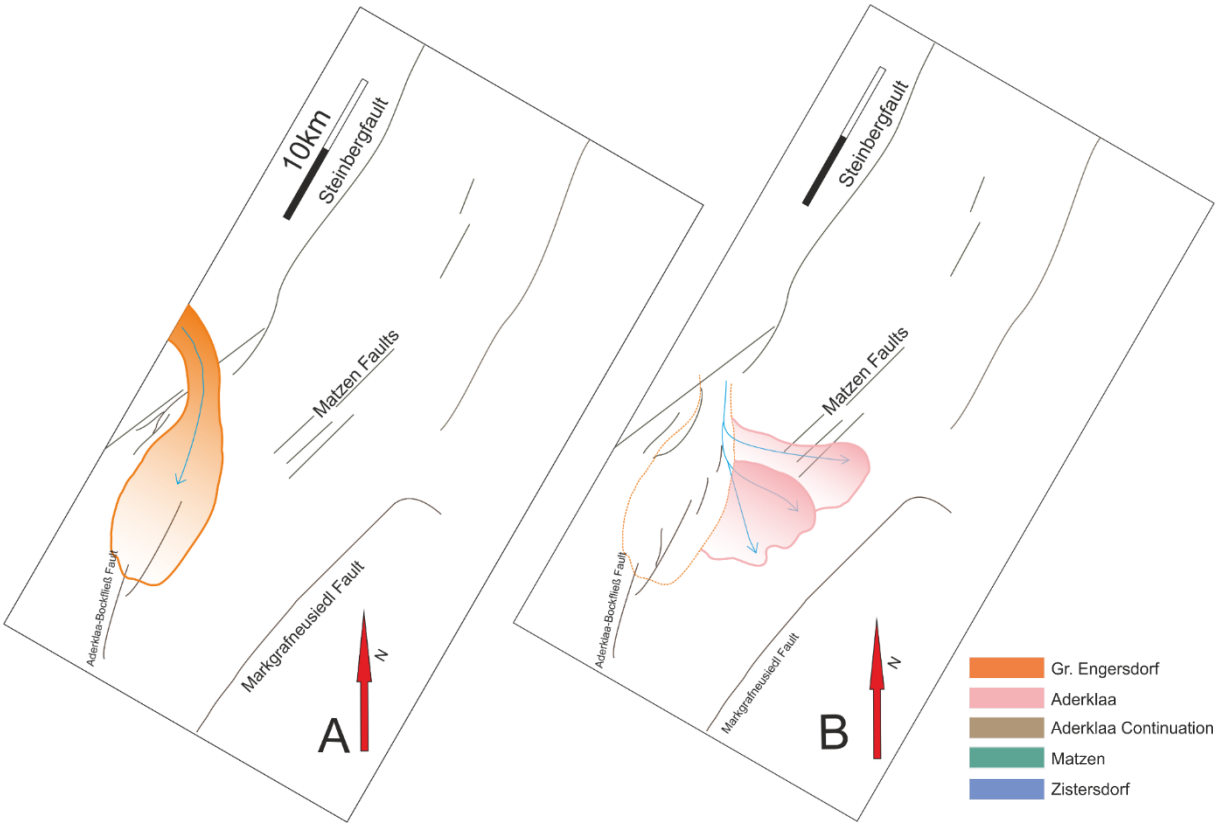

Figure 45: Beginning of the deltaic evolution. Gr. Engersdorf lobe (A) and Aderklaa lobe (B).

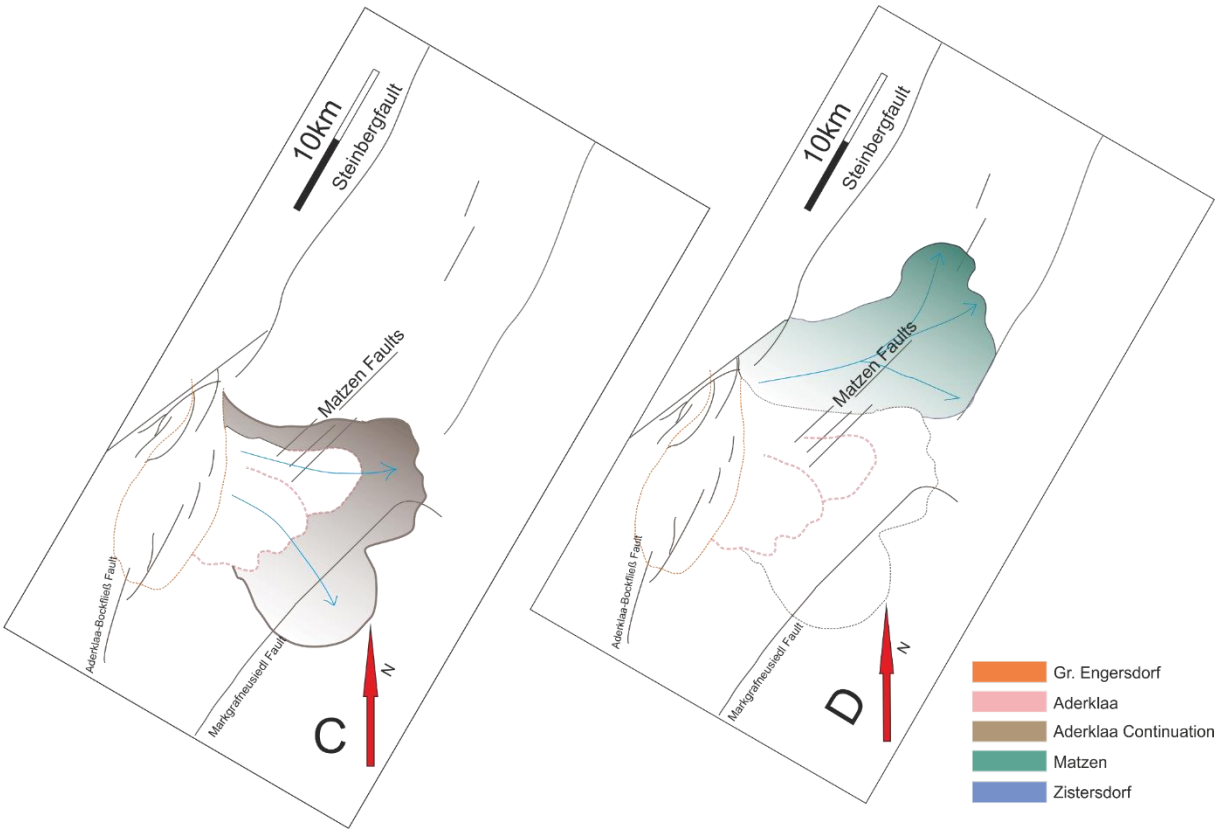

Figure 46: Continuation of the Aderklaa delta (C), before the Matzen delta (D) progrades to northeast.

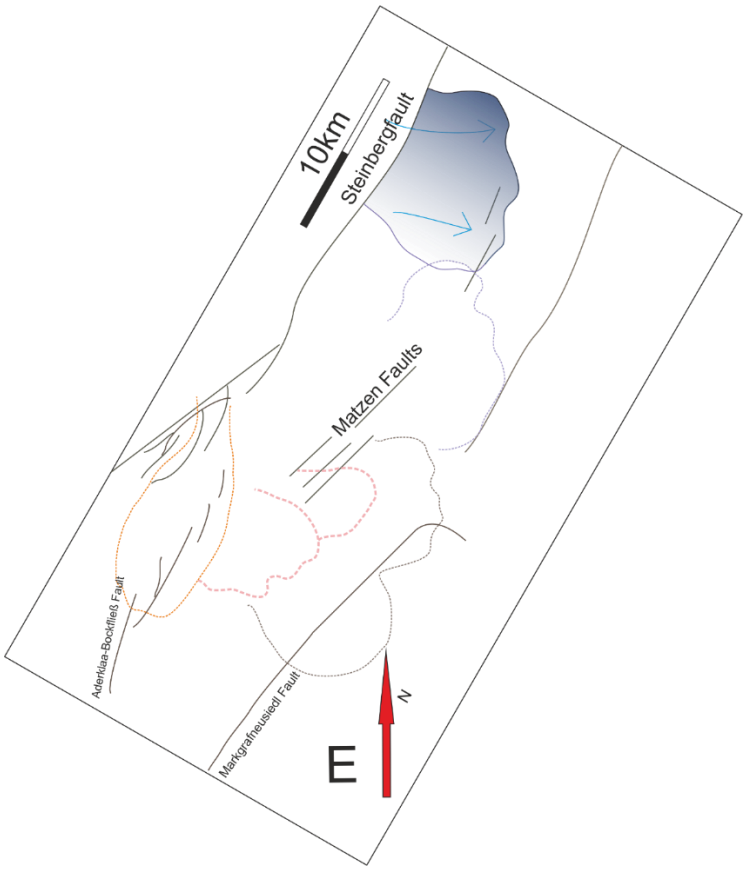

Figure 47: Uppermost observable deposition of the Zistersdorf delta (E).

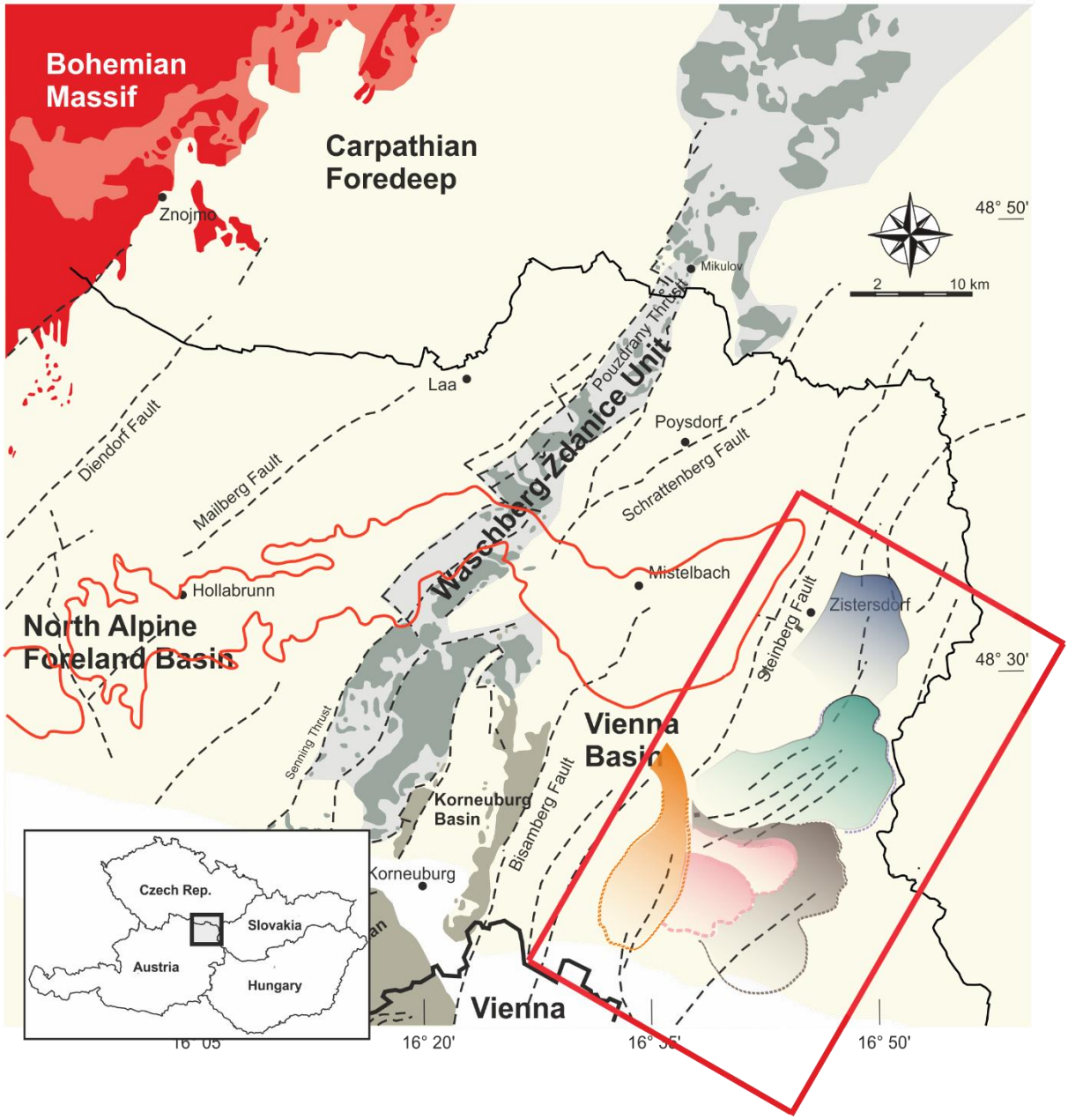

Figure 48: The Hollabrunn-Mistelbach Formation, red line (after Nehyba & Roetzel 2004) and the mapped delta within the study area (inside the red rectangle).

7.2 Delta evolution

Beginning with the base of Pa1-LST, seven paleogeographic maps were created. The lowermost map (Fig. 38) shows the transition from Pa1-LST to Pa1-TST. Here, a major channel was investigated. The visible part of the channel is around 10 km long, 200 m wide and incises into Sarmatian deposits before it was filled with lowstand sediments at Pa1-LST. During the transition to the Pa1-TST, the system was transgressed leading to the formation of sandwaves, with a thickness of at least 24 m (minimum resolvable size in the seismic survey). Sandwaves can also be found in the modern Danube Delta, for details see Duţu et al. (2020) and Vespremeanu-Stroe & Preoteasa (2006)

After the transgression (Pa1-TST), deposition of the "large lower Pannonian Sands" (Pa1-HST, Pannonian C_1, C_2) commences with the deposition of an elongated lobe located in the Gr. Engersdorf depression (Fig. 45 A). This lobe has an area of roughly 35 km^2 and marks the thickest succession of the investigated lower Pannonian deltas with around 230 m. It progrades into southern direction

before the single main distributary channel changes its orientation. A lobe switch took place and the system started to prograde into southeastern sediment direction into the Aderklaa region (Fig. 45 B). This first succession of the Aderklaa-delta is approximately 35 km^2 in size and marks the continuation of the Gr. Engersdorf lobe. It has a thickness less than the Gr. Engersdorf lobe of around 200 m. Here, at least two channels are responsible for deposition as indicated in the map. (Fig. 45 B). The Aderklaa-delta continues into southeastern direction, crossing the Markgrafneusiedl-Fault, and laterally spreading out reaching a size of 75 km^2 (Fig. 45 C).

Thickness is considerably decreasing during further progradation reaching only 140 m at the Aderklaa-delta continuation. The lobes in the Aderklaa region (Fig. 46 C) are completely abandoned therefore no further signs of progradation to the southeast could be found. Deposition continues across the Matzen region (Fig. 46 D), where the biggest investigated lobe was found. This lobe marks a point of a major change in sedimentation, where the system shifts from southeastern progradation to northeastern progradation, forming a delta with a size of 170 km^2 and a thickness of around 120 m.

The final investigated step in the delta evolution is displayed with the deposition of the delta in the Zistersdorf region (Fig. 47). The Matzen delta deposition and progradation to northeast ceases completely. A major gap between the Matzen delta and the Zistersdorf delta reveals a major shift of the distributary system to northern direction, where a delta with a size of 70 km^2 and a thickness of 130 m was mapped. This delta again progrades into southeastern direction before the fluvial system is pushed back with the transgression of Lake Pannon at 11.1 Ma. The time between the final delta deposition and the transgression of Lake Pannon is marked by rivers incising on the deltaplain and moving to southern direction. This is reflected in Fig. 39 which shows a river, with a length of 22 km and a width of ca. 240 m. This river marks the end of the fluvial system before it is pushed back during Pannonian C_3 (Harzhauser et al. 2004).

To summarize: four lobe switches were recognized and one major shift in progradation direction was identified. The deltaic system as a whole progrades into southeastern direction and fully develops in ca. 400.000 years. The gap between the Matzen delta and the Zistersdorf delta suggests a major northward shift of the distributing river.

7.3 Seismic Stratal Patterns

In total, five lobes were mapped, which together form the lower Pannonian Danube delta. Stratal terminations provide critical information regarding type and direction of synsedimentary shoreline shifts and refer to the geometric relations between strata and the stratigraphic surfaces they terminate against (Catuneanu 2006). This tool is used here to clearly show that deltaic evolution starts with the Aderklaa delta and the Gr. Engersdorf delta. The Aderklaa delta continued in southeastern direction, onlapping on the first succession of the Aderklaa delta (Fig. 41 A) and terminated before the Matzen delta is deposited (Fig. 41 B) which onlaps on the Aderklaa-continuation delta. Onlaps show that the Matzen delta deposition (green) clearly was deposited after the Aderklaa delta (Fig. 41 C). The Zistersdorf delta (blue) onlaps onto the Matzen delta (Fig. 41 D) revealing the fact that it was the last delta deposited or that it is the last recognizable delta in the seismic survey. Here it becomes evident that deposition occurred in two steps: the first is marked by the deposition of the Gr. Engersdorf, Aderklaa and Matzen lobes more to the south and the second is marked by a big gap between the Matzen-lobe and the Zistersdorf lobe, indicating that the main distributary channel, responsible for deltaic deposition, migrated northwards. This could be caused by a multitude of factors but the most prominent are the tectonic influence of the Steinberg or other faults, the change in the meandering fluvial system or a relation to astronomical forcing (100 ky eccentricity).

7.4 Water depth

Water-depth estimates are carried out with in-seismic measurements of the true vertical depth between the topset deposits of the delta and the base of the bottomset deposits (Fig. 40). Results show a water depth of around 180 m for the Gr. Engersdorf lobe, 110 m for the Aderklaa delta, 100 m for the Aderklaa delta continuation, 100 m for the Matzen delta and 115 m for the Zistersdorf delta. This indicates that water depth decreased significantly between the deposition of the first and second lobe, before showing consistent values of ~100 m water depth across the rest of the lobes. Magyar et al. (2012) studied the progradation of the paleo-Danube across the Pannonian basin, reporting a paleo-water depth of 200 - 600 m after the shallow water Vienna Basin was filled with sediments. This Indicates that water depth did not exceed 200 m before the Paleo-Danube reached the Kisalföld/Danube sub-basin at around 10 Ma ago (Magyar et al. 2013), which corresponds well to the here presented water depth.

7.5 Slope angles

The lower Pannonian deltalobes show rather steep inclination angles (Fig. 40), which are typically found in strongly river-dominated settings (Postma 1990). The Gr. Engersdorf delta reveals an inclination of circa 17°, the Aderklaa delta shows 16°inclination, the continuation of the Aderklaa delta shows a value of 8°, the Matzen-delta 14°and the Zistersdorf delta has an inclination of 25°. In total the lobes show relative typical slope angles, as would be expected in river-dominated settings. Modern examples of lacustrine, river dominated deltas such as the Lake Uri delta (14°) and Lake Brienz (17°) in Switzerland show similar slope angles (Adams et al. 2001).

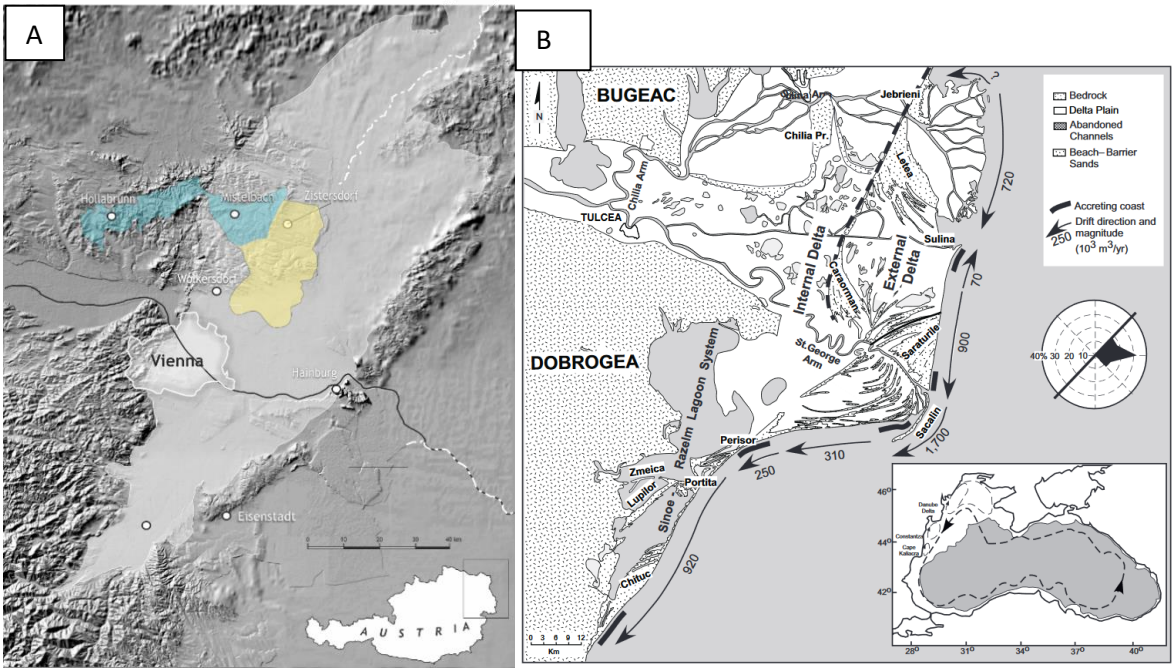

Figure 49: (A): Sketch connecting the Hollabrunn-Mistelbach-Formation (blue) and the mapped delta (yellow) [left],. (B) Danube delta basemap and oceanographic processes after Giosan 2004, Note the smooth shoreline and that lobes clearly build several kilometers out in the basin (right)

7.6 Delta classification

A rough attempt on delta classification was carried out solely based on geometry and shape and then compared to the recent Danube-delta (Fig. 49), which was classified as mostly river-dominated delta with influences of wave reworking processes (Postma 1990). Fig. 49 A shows the mapped Paleo-Danube deposits of the Hollabrunn-Mistelbach Formation after Nehyba &Roetzel (2004) (blue) and its

subsurface continuation into the delta as mapped herein (yellow). This was compared to the modern Danube delta (Fig.49 B), revealing two major similarities: first, the lobes reach far out into the basin (especially the Gr. Engersdorf lobe) and second, the smooth shoreline, indicating the power of wave reworking processes, being present in the Pannonian and modern Danube delta. The lower Pannonian Danube delta is approximately 1/10 of the size of the recent Danube delta, where the deltaplain covers an area of 5800 km^2 (Panin 2016) The conclusion is that the lower Pannonian delta is a river-dominated delta with influence of wave reworking processes. No elongated sediment structures were observed at the channel mouths excluding a strong tidal influence.

7.7 Calculation of sedimentation rates

Orton & Reading (1993) proposed the idea to calculate sedimentation rates of the supply feeding a delta. In general, the supply of a delta is characterized by the nature of the catchment area, its size (in particular the length of the main stream), its shape, relief, ruggedness, climate bedrock character and tectonic setting. These factors determine the volume of the sediment in supply, the proportion of the bedload, suspended load and dissolved load, hence the grain-size of the sediment, the total sediment load, the river discharge and the regularity of supply to the delta (Orton & Reading 1993). It is evident, that through the means of seismic interpretation such factors cannot be defined. What can be defined is volume, size and a time interval. Through this it should be theoretically possible to roughly calculate the mean sedimentation rates of a delta over a certain timespan. So, if the exact volume of the deltaic deposits is known as well as the timespan of their deposition, it should be possible to get an approximate annual sedimentation rate by dividing the volume by the time,

so $\frac{V}{t} = \frac{Volume}{time} = volume\ of\ sediment\ per\ year.$

A rough attempt was carried out, to find an approximate annual sedimentation rate for the lower Pannonian deltas. The volume is estimated by calculating the approximate length of the delta (35 km) with the width (16 km) and an average thickness of 121m, revealing an estimated volume of 67,760 km^3. This is divided by 400.000 (estimated time of deltaic evolution) to reveal an annual sedimentation rate of 0,1694 km^3. This does not include regional subsidence, diagenesis and other factors distorting the structures.

7.8 Tectonics

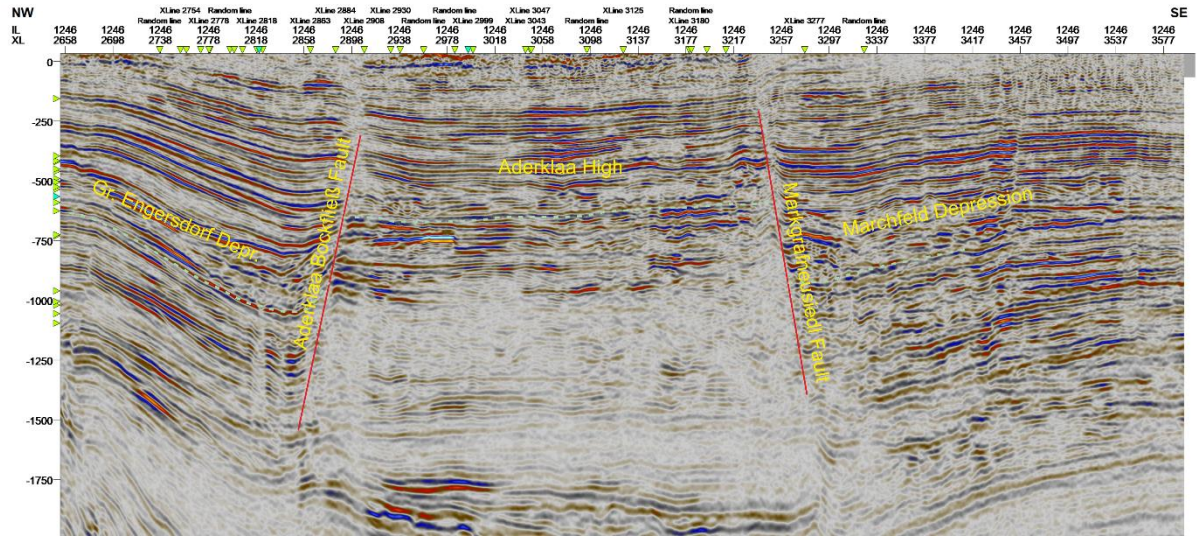

Figure 50: Aderklaa-Bockfließ fault and Markgrafneusiedl fault cutting through the delta.

Three faults were investigated to show how tectonics influenced deposition as well as how deltas can be used as stratigraphic tool, by examining if a fault was active during deposition or not. In Fig. 50 two faults are recognizable, the Aderklaa-Bockfließ fault and the Markgrafneusiedl fault. The Aderklaa-Bockfließ fault separates the Gr. Engersdorf delta and the Aderklaa delta, clearly revealing that this fault could not have been active during the Pannonian, because characteristic synsedimentary structures are missing. It is also possible to calculate the offset, by measuring the distance between two characteristic reflectors, which shows a value of around 400 m. The same applies for the Markgrafneusiedl fault, which cuts through the continuation of the Aderklaa delta. The second example is the Steinbergfault, which was active during the Pannonian (Decker et al. 2005). Here a major problem arises because the upthrown block of the Steinbergfault (Fig. 51) consists of ultra-condensed sediments, making it nearly impossible to correlate the lower Pannonian deltas to the Hollabrunn-Mistelbach Formation with the tools of seismic interpretation.

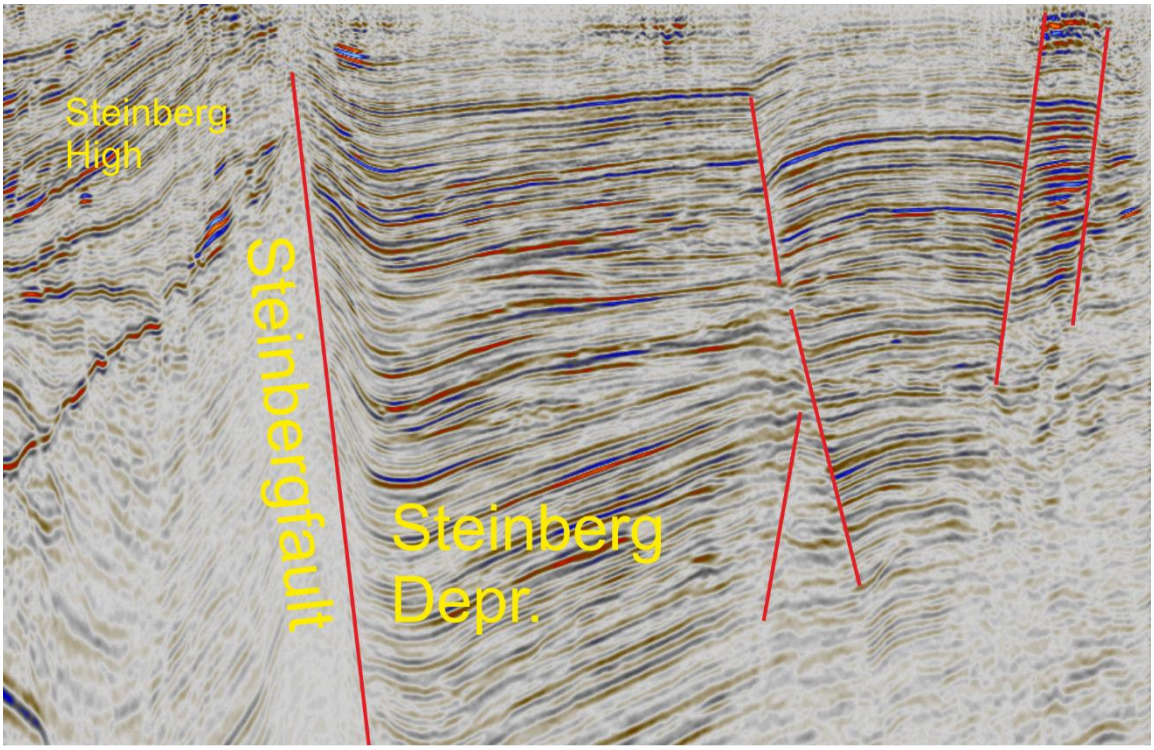

Figure 51: Sesimic expression of the Steinbergfault. Note how condensed the upthrown block (Steinberghigh) is compared to the downthrown block (Steinberg depression)

8. Conclusions

The lower Pannonian deposits can be subdivided into four system tracts: Pa1-LST, Pa1-TSt, Pa1-HST and Pa2 TST where the Pa1 cycle corresponds to a 3rd order lowstand systems tract (LST) and the Pa2 cycle corresponds to the beginning of a 3rd order transgressive systems tract (TST). Deltaic deposition commenced with the Pa1-HST at around 11.5 Ma, or Pannonian C $_{1,2}$ after the age model of Harzhauser et al. (2004) with the deposition of the Gr. Engersdorf lobe and ceases with the Pa2-TST at around 11.1 Ma with the deposition of the Zistersdorf lobe. Therefore, the delta fully developed in 400.000 years and the majority of lobes prograded mostly into south-eastern direction, with the only exception, of the Matzen delta which prograded into north-eastern direction. After the deposition of the delta, rivers incised into the abandoned deltaplain (Fig. 39), flowing into southern direction before the riverine system was transgressed and pushed back by Lake Pannon at around 11.1 Ma. A depositional gap between the Matzen delta (Fig. 46 D) and the Zistersdorf delta (Fig. 47) indicates a major change in the system and a northward movement of the distributing channel. This is also indicated by the stratal

patterns, especially through the connection of those two lobes. Reasons for this channel migration active during the Pannonian are changes in the meandering fluvial system. The delta was classified as river-dominated with strong influence of wave-reworking processes, solely based on geometry and shape, however, also the slope angles indicate that it is most likely river-dominated because such steep slopes (Fig. 40) are typically associated with river-dominated settings (e.g., Postma 1990). Water depth is shallow for the major part of deltaic deposition with only 100 m, which corresponds well to the work of Magyar (1999), who reported that there were no deep-water environments at that time. Finally, we proof that the mapped distribution of the Hollabrunn-Mistelbach Formation fits to the herein mapped subsurface delta deposits, which for the first time clearly links the observed delta lobes to the late Miocene (early Pannonian) Paleo-Danube (Fig. 48). The link cannot be established seismically, but concluded, based on the same stratigraphic age between Pannonian deltas in the Vienna Basin, the stratigraphic age of the Hollabrunn-Mistelbach Formation, facies correlation and implications of the reconstruction of the paleo-environment.

References

Adams, E. W., Schlager, W., & Anselmetti, F. S. (2001). Morphology and curvature of delta slopes in Swiss lakes: lessons for the interpretation of clinoforms in seismic data. *Sedimentology, 48*, pp. 661-679.

Arzmüller, G. B. (1988). The Vienna Basin. In Golonka, J., & Picha, F. *The Carpathians and their Foreland: Geology and Hydrocarbon Resources* (AAPG Memoir 84). Tulsa, Oklahoma, U.S.A.: The American Association of Petroleum Geologists, pp. 191-204.

Bao, J., Cai, F., Shi, F., Wu, C., Zheng, Y., Lu, H., & Sun, L. (2020). Morphodynamic response of sand waves in the Taiwan Shoal to a passing tropical storm. *Marine Geology, 426*.

Bakrač, K., Koch, G., & Sremac, J. (2012). Middle and Late Miocene palynological biozonation of the south-western part of Central Paratethys (Croatia). *Geologia Croatica*, *65*(2), 207-222.

Bhattacharya, J. P. (2006). Deltas. In Posamentier, H. W., & Walker, R. G., *Facies Models Revisited*. Tulsa, Oklahoma: SEPM (Society for Sedimentary Geology), pp. 237-292.

Brix, F., & Schultz, O. (1993). *Erdöl und Erdgas in Österreich* (Vol. 19). Wien: Veröffentlichungen aus dem Naturhistorischen Museum in Wien.

Brown, L. F., & Fisher, W. L. (1977). Seismic stratigraphic interpretation of depositionals systems: examples from brazilian rift and pull-apart basins: section 2. Application of Seismic Reflection Configuration to Stratigraphic Interpretation. *AAPG Special Volumes*, pp. 213-248.

Brown (2004). *Railsback`s Petroleum Geoscience and Subsurface Geology. (Online)*

Catuneanu, O. (2006). *Principles of Sequence Stratigraphy.* Amsterdam, Oxford: Elsevier BV.

Catuneanu, O., Galloway, W. E., Kendall, C. G., Posamentier, H. W., Strasser, Á., & Tucker, M. E. (2011). Sequence Stratigraphy: Methodology and Nomenclature. *Newsletter on Stratigraphy, 44/3*, pp. 173-245.

Clifton, H. E. (1982). Estuarine Deposits. In Scholle, P. A., & Spearing, D., *Sandstone Depositional Environments*. Tulsa, Oklahoma, U.S.A: The American Association of Petroleum Geologists pp. 179-190.

Coleman, J. M., & Wright, L. D. (1975). Modern River Deltas: Variability of Processes and Sand Bodies. In Broussard, M. L., *Deltas: Models for Exploration* (pp. 99-149). Houston, Texas: Houston Geological Society, pp. 99-149.

Ctyroky, P. (2000). Nové litostratigafické jednotky pannonu vídenské pánve na Morave. *Vestnik Ceskeho geologického ústavu, 75*, pp. 159-170.

Decker, K. (1996). Miocene Tectonics at the Alpine-Carpathians Junction and the Evolution of the Vienna Basin. *Mitt. Ges. Geol. Bergbaustud. Österr.* , pp. 33-44.

Decker, K., Peresson, H., & Hinsch, R. (2005). Active Tectonics and Quaternary basin formation along the Vienna Basin Transform fault. *Quaternary Science Reviews, 24*, pp. 307-322.

Duţu, F., Panin, N., Gabriel, I., & Duţu, L. T. (2018). Multibeam Bathymetric Investigations of the Morphology and Associated Bedforms, Sulina Channel, Danube Delta. *Geosciences, 8*.

Elliott, T. (1986). Deltas. In H. G. Reading, *Sedimentary Environment and Facies* (pp. 113-154). Oxford, England: Blackwell Scientific Publications.

Emery, D., & Myers, K. J. (1996). *Sequence Stratigraphy.* Oxford, England: Blackwell Science Ltd.

Ethridge, F. G., & Wescott, W. A. (1984). Tectonic Setting, Recognition and Hydrocarbon Reservoir Potential of Fan-Delta Deposits. *Sedimentology of Gravels and Conglomerates, Memoir 10*, pp. 217-235.

Galloway, W. E. (1975). Process Framework for Describing the Morphologic and Stratigraphic Evolution of Deltaic Depositional Systems. *Deltas: Models for Exploration*, pp. 87-98.

Galloway, W. E., & Hobday, D. K. (1996). Fluvial Systems. In Galloway, W. E., & Hobday, D. K., *Terrigenous Clastic Depositional Systems.* Springer, Berlin, Heidelberg, pp. 60-90.

Haq, B. U., Hardenbol, J., & R., V. P. (1988). Mesozoic and Cenozoic Chronostratigraphy and Cycles of Sea-Level Change . *SEPM Special Publications, 42*, pp. 71-108.

Hart, B. S. (1995). Delta Front Estuaries. *Developments in Sedimentology, 53*, pp. 207-226.

Harzhauser, M., & Piller, W. E. (2004). Integrated Stratigraphy of the Sarmatian (Upper Middle Miocene) in the Western Central Paratethys. *Stratigraphy, 1*, pp. 65-86.

Harzhauser, M., Daxner-Höck, G., & Piller, W. E. (2004). An Integrated Stratigraphy of the Pannonian (Late Miocene) in the Vienna Basin. *Austrian Journal of Earth Sciences, 95/96*, pp. 6-19.

Hassinger, H. (1905a). Geomorphologische Studien aus dem Inneralpinen Wiener Becken und seinem Randgebirge. *Geographische Abhandlungen, VIII/3*, pp. 359-564.

Hassinger, H. (1905b). Zur Frage der Alten Flußterrassen bei Wien. *Mitt. k. k. Geograph. Ges. Wien, 48*, pp. 196-219.

Hinsch, R., Decker, K., & Wagreich, M. (2005). 3-D Mapping of Segmented Active Faults in the Southern Vienna Basin. *Quaternary Science Reviews, 24*, pp. 321-336.

Hilgen, F. J., Krijgsman, W., Raffi, I., Turco, E., & Zachariasse, W. J. (2000). Integrated stratigraphy and astronomical calibration of the Serravallian/Tortonian boundary section at Monte Gibliscemi, Sicily. *Marine Micropalaeontology, 38*, pp. 181-211

Hintersberger, E., Decker, K., & Lomax, J. L. (2018). Implications from Paleoseismological Investigations at the Markgrafneusied Fault (Vienna Basin, Austria) for Seismic Hazard Assessment. *Natural Hazards and Earth Systems Sciences, 18 (2)*, pp. 531-553.

Holmes, A. (1966). *Principles of Physical Geology.* London, England: Thomas Nelson and Son.

Jiricek, R. (1988). Stratigraphie, paleogeografie e mocnost sedimentu v neogénu Videnské panve. *Zem, Plyn, Nafta, 33*, pp. 529-540.

Juhasz, G. (1994): Sedimentological and stratigraphical evidences of water-level fluctuations in the Pannonian Lake. *Foldtani Kozlony*, 123, 379–398

Ke, W. T., Shaw, J. B., Mahon, R. C., & Cathcart, C. A. (2019). Distributary Channel Networks as Moving Boundaries: Causes and Morphodynamic Effects. *Journal of Geophysical Research: Earth Surface, 124 (7)*, pp. 1878-1898.

Klien, A., & Roetzel, R. (2009). Auf den Spuren der Urdonau im Raum Hollabrunn. *Eigenverlag des Vereines der Freunde des Hollabrunner Waldes* Hollabrunn 2009.

Kosi, W., Sachsenhofer, R. F., & Schreilechner, M. (2003). High Resolution Sequence Stratigraphy of Upper Sarmatian and Lower Pannonian Units in the Styrian Basin, Austria. (Piller, W. E., Ed.) *Stratigraphia Austriaca – Österr. Akad. Wiss., Schriftenr. Erdwiss. Komm., 16*, pp. 63-86.

Kovác, M., Baráth, I., Kovácová - Slamková, M., Pipík, R., Hlavatý, I., & Hudácková, N. (1998). Late Miocene Paleoenvironments and Sequence Stratigraphy: Northern Vienna Basin. *Geologica Carpathica, 49/6*, pp. 445-458.

Kováč, M., Baráth, I., Harzhauser, M., Hlavatý, I., & Hudáčková, N. (2004). Miocene Depositional Systems and Sequence Stratigraphy of the Vienna Basin. *Courier Forschungsinstitut Senckenberg, 246*, pp. 187-212.

Kreutzer, N. (1993). Das Neogen des Wiener Beckens. In Brix, F., & Schultz, O., *Erdöl und Erdgas in Österreich* (Vol. 19, pp. 232-248). Wien: Naturhistorisches Museum Wien, Berger, F., pp. 232-248.

Magyar, I., Geary, D. H., & Müller, P. (1999). Paleogeographic Evolution of the Late Miocene Lake Pannon in Central Europe. *Paleogeography, Paleoclimatology, Paleoecology, 147 (3-4)*, pp. 151-167.

Magyar, I., Radivojević, D., Sztanó, O., Synak, R., Ujszászi, K., & & Pócsik, M. (2013). Progradation of the Paleo-Danibe Shelf Margin Across the Pannonian Basin During the Late Miocene and Early Pliocene. *Global and Planetary Change, 103*, pp. 168-173.

Mitchum Jr, R. M., & Vail, P. R. (1977). Seismic Stratigraphy and Global Changes of Sea Level: Part 2. The Depositional Sequence as a Basic Unit for Stratigraphic Analysis: Section 2. Application of Seismic Reflection Configuration to Stratigraphic Interpretation. *AAPG Special Volumes*, pp. 53-62.

Moodie, A. J., Nittrouer, J. A., Carlson, B. N., Chadwick, A. J., Lamb, M. P., & Parker, G. (2019). Modeling deltaic lobe-building cycles and channel avulsions for the Yellow River delta, China. *Journal of Geophysical Research: Earth Surface, 124 (11)*, pp. 2438-2462.

Nehyba, S., & Roetzel, R. (2004). The Hollabrunn-Mistelbach Formation (Upper Miocene, Pannonian) in the Alpine-Carpathian Foredeep and the Vienna Basin in Lower Austria - An example of a coarse-grained fluvial system. *Jahrbuch der Geologischen Bundesanstalt, 144 (2)*, pp. 191-221.

Nemec, W. (1990). Deltas - remarks on terminology and classification. In Collela, A., & Prior, D. B., *Coarse-Grained Deltas.* Blackwell Scientific Publications. pp. 3-12

Olariu, C., & Bhattacharya, J. P. (2006). Terminal distributary channels and delta front architecture of river-dominated delta systems. *Journal of Sedimentary Research, 76 (2)*, pp. 212-233.

Orton, G. J. (1988). A spectrum of Middle Ordovician fan deltas and braidplain deltas, North Wales: a consequence of varying fluvial clastic input. In Nemec, W., & Steel, R. J., *Fan Deltas: Sedimentology and Tectonic Settings*. Blackie Glasgow, pp. 23- 49.

Orton, G. J., & Reading, H. G. (1993). Variability of deltaic processes in terms of sediments supply, with particular emphasize on grain size. *Sedimentology, 40 (3)*, pp. 475-512.

Papp, A. (1951). Das Pannon des Wiener Beckens. *Mitteilungen der Geologischen Gesellschaft in Wien, 39-41 (1946-1948)*, pp. 99-193.

Piller, W. E. (1999). The Neogene of the Vienna Basin. *Berichte der Geologischen Bundesanstalt, 49*, pp. 11-19.

Posamentier, H. W., & Vail, P. R. (1988). Eustatic controls on clastic deposition II - sequence and system tract models. *SEPM Special Publications, 42*, pp. 125-154.

Posamentier, H. W., & Allen, G. P. (2000). *Siliciclastic sequence stratigraphy - Concepts and Applications* (Vol. 7). Tulsa: SEPM Concepts in Sedimentology and Paleontology.

Postma, G. (1990). An Analysis of the variation in delta architecture. *Terra Nova, 2 (2)*, pp. 124-130.

Rainwater, E. H. (1966). The Geological Importance of Deltas. *Deltas in their Geological Framework*, pp. 1-15.

Rögl, F. (1999). Mediterranean and Paratethys. Facts and hypotheses of an Oligocene to Miocene paleogeography (short overview) . *Geologica Carpathica, 50 (4)*, pp. 339-349.

Royden, L. H. (1985). The Vienna Basin: a Thin-Skinned Pull-Apart Basin. In Biddle, K. T., & Christie-Blick, N., *Strike Slip Deformation, Basin Formation and Sedimentation* (Vol. 37). SEPM, Spec. Publ, pp. 319-338.

Saito, Y., Yang, Z., & Hori, K. (2001). The Huanghe (Yellow River) and Chingjiang (Yangtze River) deltas: a review on their characteristics, evolution and sediment discharge during the Holocene. *Geomorphology, 41 (2-3)*, pp. 219-231.

Schuchardt, B., Schirmer, M., Janssen, G., Nehring, S., & Leuchs, H. (1999). Estuaries and Brackish Water. *Wadden Sea Quality Status Report, 9*, pp. 175-186.

Schumm, S. A. (1985). Patterns of alluvial Rivers. *Annual Review of Earth and Planetary Sciences, 13 (1)*, pp. 5-27.

Seifert, P. (1993). DIe Waschbergzone. In Brix, F., & Schultz, O., *Erdöl und Erdgas in Österreich*. Wien: Naturhistorisches Museum Wien und F. Berger, pp. 358-359.

Siedl, W., Strauss, P., Sachsenhofer, R. F., M., H., Kuffner, T., & Kranner, M. (2020). Revised Badenian (middle Miocene) depositional systems of the Austrian Vienna Basin based on a new sequence stratigraphic framework. *Austrian Journal of Earth Sciences, 113 (1)*, pp. 87-110.

Skilling, I. P. (2002). Basaltic pahoehoe lava-fed deltas: large scale characteristics, clast generation, emplacement processes and environmental discrimination. *Geological Society, London, Special Publications, 202 (1)*, pp. 91-113.

Slingerland, R., & Smith, N. D. (2004). River avulsions and their deposits. *Annu. Rev. Earth Planet. Sci., 32*, pp. 257-285.

Smellie, J. L., Wilch, T. I., & Rocchi, S. (2013). Lava-fed deltas: a new reference tool in paleoenvironmental studies. *Geology, 41 (4)*, pp. 403-406.

Strauss, P., Harzhauser, M., Hinsch, R., & Wagreich, M. (2006). Sequence stratigraphy in a classic pull-apart basin (Neogene, Vienna Basin). A 3D seismic based integrated approach. *Geologica Carpathica-Bratislava, 57 (3)*, pp. 185-197.

Suess, E. (1866). Untersuchungen über den Charakter der österreichischen Tertiärablagerungen I. Über die Gliederung der tertiären Bildung zwischen dem Mannhart, der Donau und dem äusseren Saume des Hochgebirges. *Sitzungsberichte der Akademie der Wissenschaften mathematisch-naturwissenschaftliche Klasse, 54*, pp. 87-149.

Vespremeanu-Stroea, A., Zăinescua F., Preoteasaa, L., Tătuia F., Rotarub S., Morhanged, C., Stoicab M., Hanganue, J., Timar-Gaborf, A., Cârdanf I., Piotrowska, N. (2017). Holocene evolution of the Danube delta: An integral reconstruction and a revised chronology. *Marine Geology, 388*, pp. 38-61.

Weissl, M., Hintersberger, E., Lomax, J., Lüthgens, C., & Decker, K. (2017). Active tectonics and geomorphology of the Gaenserndorf Terrace in the Central Vienna Basin (Austria). *Quaternary International, 451*, pp. 209-222.

Wessely, G. (1988). Structure and development of the Vienna Basin in Austria. In Royden, L. H., & Horvath, F., *The Pannonian System. A study in basin evolution*. Tulsa, Oklahoma: AAPG Memoirs 45, pp. 333-346.

Wessely, G. (1993). Der Untergrund des Wiener Beckens. In Brix, F., & Schultz, O., *Erdöl und Erdgas in Österreich* (Vol. 19). Wien: Naturhistorisches Museum Wien und F. Berger, pp. 249-280.

Wessely, G. (2000). Sedimente des Wiener Beckens und seiner alpinen und subalpinen Unterlagerung. *Exkursionsführer Sediment 2000*, pp. 191-214.

Wessely, G. (2006). Wiener Becken. *Geologie der österreichischen Bundesländer – Niederösterreich*. Wien: Geologische Bundesanstalt, pp. 189-227.

Wright, L. (1977). Sediment transport and deposition at river mouths: A synthesis. *Geological Society of America Bulletin, 88 (6)*, pp. 857-868.